CIRCUIT MAP OF FRONTAL LOBE SEIZURES

Anastasia Brodovskaya

B.S. Hofstra University, 2017

A Dissertation Presented to the Graduate
Faculty of the University of Virginia
In Candidacy for the Degree of
Doctor of Philosophy

Neuroscience Graduate Program
University of Virginia
August 1, 2021

Jaideep Kapur, M.D., Ph.D.
Alev Erisir, M.D., Ph.D.
Ruth Stornetta, Ph.D.
Mark Beenhakker, Ph.D.
Howard Goodkin, M.D., Ph.D.

ABSTRACT

The central hypothesis of this dissertation is that anatomical connectivity of the seizure focus and properties of neurons drive seizure circuits. We combined novel techniques such as activity reporter TRAP2 mice, local field potential recordings, tissue clearing, viral tracing, chemogenetics, optogenetics, lesioning, and super resolution microscopy to interrogate the circuits active during frontal lobe focal motor to bilateral tonic-clonic seizures.

We found neuronal activation in the striatum, globus pallidus externus, subthalamic nucleus, substantial nigra pars reticulata, and neurons of the indirect pathway. Simultaneous LFP recordings from these structures showed that seizures activate structures via short and long latency loops, and activation of the basal ganglia modulates seizures. These studies led to the hypothesis that connectivity of excitatory neurons primarily drives long-distance seizure spread.

Seizures also preferentially activated dopamine D2 receptor-expressing neurons over D1 in the striatum, which have different projections. D2 neurons are more excitable than D1; thus, the properties of neurons also determine seizure circuits.

The D2 receptor agonist infused directly into the striatum through a bilateral cannula exerted an anticonvulsant effect. Systemic injection of the D2 agonist was also anticonvulsant in frontal lobe seizures. We found that injection of D2R agonist led to extensive activation of parvalbumin interneurons in the cortex and striatum ipsilateral to the seizure focus. D2R agonists activate PV interneurons, which in turn inhibit principal neurons, potentially explaining the anticonvulsant effect of D2R agonists.

Previous studies indicate that the thalamus is essential for seizure maintenance and generalization to the contralateral hemisphere. Surprisingly, we found that seizures spread faster to the contralateral cortex than to the contralateral thalamus. The seizure focus in the ipsilateral cortex was strongly connected to the contralateral cortex via the corpus callosum as indicated by viral track tracing, whereas the ipsilateral thalamus lacked direct monosynaptic connections to the contralateral thalamus. We propose that seizures spread from the seizure focus to the contralateral cortex by engaging the cortico-cortical commissure, corpus callosum, rather than via commissural projections

between the two thalami or through bilateral spread from the thalamus via the brainstem.

After chemogenetic inhibition of the ipsilateral thalamus, we still found contralateral seizure spread, although seizure duration decreased significantly. Anterior callosotomy, on the other hand, prevented contralateral seizure spread during initial seizures. Thus, we propose that the thalamus amplifies seizures, whereas the corpus callosum allows transmission to the contralateral hemisphere.

Recent studies also indicate that superficial layers 2/3 are recruited ahead of the deep layers 5/6 locally, but it is not known how seizures spread intracortically over a long distance. We showed that superficial layers were more activated after a seizure compared to deep layers throughout the cortex. Seizures spread faster posteriorly through the superficial layers and arrived to the posterior deep layers with a delay. AAV9 GFP injected at the seizure focus labeled posterior superficial layers stronger than posterior deep layers, suggesting more direct monosynaptic projections exist across layers 2/3 than layers 5/6. We further showed that activated cells in the posterior cortex receive direct synaptic connections from the seizure focus. However, not all neurons that received direct projections from the seizure focus became active, which might suggest that those neurons were electrophysiologically different to begin with.

TABLE OF CONTENTS

Page

Abstract……..2

Table of Contents……4

List of Figures and Tables……..…...5

Acknowledgements……6

Chapter 1……..……7

Introduction

Chapter 2……..……17

Circuits generating secondarily generalized seizures

Chapter 3……32

Activation of the basal ganglia and indirect pathway neurons during frontal lobe seizures

Chapter 4……81

Anticonvulsant D2R agonist activated inhibitory parvalbumin interneurons

Chapter 5……95

Surprising role of the thalamus and corpus callosum during focal motor to bilateral seizures

Chapter 6……...122

Long range seizure propagation through cortical layers

Chapter 7……...144

Discussion

LIST OF FIGURES AND TABLES Page

Figure 2-1……..……..20
Figure 2-2……..…..23
Figure 3-1……41
Figure 3-2……46
Figure 3-3……50
Figure 3-4……52
Figure 3-5……55
Figure 3-6……58
Figure 3-7……61
Figure 3-8……65
Figure 4-1……..……..88
Figure 4-2……..…..90
Figure 5-1……..……103
Supplementary Figure 5-1……..……105
Figure 5-2……..…108
Figure 5-3……..…110
Figure 5-4……..…113
Figure 5-5……..…116
Figure 5-6……..…117
Figure 6-1……..…129
Figure 6-2……..…132
Figure 6-3……..…134
Figure 6-4……..…137
Figure 6-5……..…139

ACKNOWLEDGEMENTS

I would first like to thank my mentor, Dr. Jaideep Kapur. No words can describe how grateful and happy I am for the chance to be his student.

I wish to thank my dissertation committee members Dr. Alev Erisir, Dr. Ruth Stornetta, Dr. Mark Beenhakker, and Dr. Howard Goodkin for their guidance and valuable comments. I thank Suchitra Joshi and John Williamson for their practical advice and technical assistance. I want to thank Shinnosuke Shiono, Tamal Batabyal, Aijaz Naik, Tanveer Singh, Huayu Sun, and the rest of the Kapur lab for interesting work and enjoyable time spent together. I would also like to thank everybody in the Neuroscience program for contributing to my graduate education at this institution.

Lastly, I dedicate this work to my parents, whom I love more than life.

CHAPTER 1

INTRODUCTION

INTRODUCTION

Frontal lobe epilepsy is the second most common type of epilepsy after temporal lobe epilepsy. However, the circuits of frontal lobe focal motor to bilateral tonic-clonic seizures, previously known as secondarily generalized (1), have not been studied in detail. Previous studies indicate that the thalamus is essential for seizure maintenance and generalization, but frontal lobe seizures also affect the motor cortex, which has extensive projections to the basal ganglia and across the corpus callosum, so the circuits might be more complex than previously thought.

This dissertation maps the circuits of frontal lobe seizures on the mesoscale and cellular levels. The central hypothesis examined is as follows:

HYPOTHESIS

Anatomical connectivity of the seizure focus and properties of neurons drive seizure circuits.

The background and the methods to test this hypothesis will be described below. Further details will be provided in the introductory comments of each chapter.

Based on the central hypothesis stated above, several corollary hypotheses can be proposed:

1. Frontal lobe seizures would extensively activate the basal ganglia, which includes the striatum, globus pallidus, subthalamic nucleus, and the substantia nigra because of extensive projections from the motor cortex, the seizure focus.
2. Indirect pathway neurons would be preferentially activated over direct because D2 receptor-expressing medium spiny neurons are more excitable than D1 receptor-expressing neurons (2,3).
3. Seizures would spread contralaterally via the corpus callosum and then to the contralateral thalamus rather than from the ipsilateral to contralateral thalamus because the two have weak monosynaptic connections.
4. Inhibition of the ipsilateral thalamus during frontal lobe motor seizures would not prevent the contralateral seizure spread.
5. Callosotomy should prevent the initial contralateral seizure spread, but new networks for generalization could be developed due to the plastic changes that exhibit neurons.

6. Superficial layers of the cortex would be more activated compared to deep layers because 80% of the callosal axons originates in the superficial layers (4).
7. Posterior superficial layers would be activated ahead of posterior deep layers because layers 2/3 have strong long-range horizontal intracortical projections, whereas layers 5/6 preferentially have subcortical projections (5).

BACKGROUND

Epilepsy is a disease characterized by an enduring predisposition to generate epileptic seizures (1,6). Seizure is a transient occurrence of signs and symptoms due to abnormal and excessive neuronal activity in the brain (6). To understand the pathophysiology of seizures, their circuits must be delineated first. How do seizures spread in the brain, and what brain structures do they affect? This dissertation will be focused on frontal lobe focal motor to bilateral tonic-clonic seizures, previously known as secondarily generalized (1), because these are the most dangerous seizures, and frontal lobe epilepsy is the second most common type of epilepsy after the temporal lobe.

METHODOLOGICAL CONSIDERATIONS

Which model to use?

An ideal animal model to investigate the circuits that underlie those seizures would cause spontaneous frontal lobe onset focal to bilateral seizures without long latency periods. The cobalt model comes the closest to the ideal model described above. This model provides reliable spontaneous seizures in more than 90% of animals. The short latency allows to obtain high fidelity LFP recordings without deterioration of electrical contacts. Other focal models such as electrical stimulation of the cortex or application of chemiconvulsants (such as 4-aminopyridine or penicillin) are the models of acute rather than spontaneous seizures and require prolonged electrical stimulation or introduce a bias toward a cortical layer in which seizures originate. Cortical freeze lesions or undercut models do not provide a reliable seizure phenotype, and the latency period spans weeks before the first seizures appear (7).

The cobalt model was initially described by Kopeloff in 1960 (8). Subsequently, it became well characterized in many species, and the model shifted from powder application to a wire (9-13). Cobalt inactivates oxygen-binding molecules within neurons, causing hypoxic injury (12).

How to visualize activated circuits?

There is much information on mapping seizure circuits (14-19). Many of those studies use techniques that allow brain-wide visualization of activated structures such as single-photon emission computed tomography that images cerebral blood flow changes, simultaneous LFP recordings from multiple structures, EEG, and 2-deoxyglucose (2-DG) mapping. Yet, many of these techniques lack cellular resolution on a whole-brain level.

Novel activity reporter TRAP2 mice allow unprecedented visualization of activated circuits on the cellular level throughout the whole brain (20,21). These mice express Cre recombinase enzyme under the control of the c-Fos promoter. Cre has a mutated estrogen receptor binding site, so that binding with 4-hyroxytamoxifen is essential for the nuclear translocation of Cre. There, the floxed tdTomato gene is relived from repression and expressed only in the activated cells.

TRAP2 technique allows only cellular spatial resolution. To gain millisecond temporal resolution, local field potential recordings were done in C7Bl/6 mice. Microelectrodes with 10 kHz sampling rate were inserted in the activated structures indicated by tdTomato expression to determine seizure onset latencies in each structure.

Inhibition or lesioning of individual structures allowed to determine their role in seizure spread. Virus labeling in TRAP2 mice also allowed to track anatomical connections and seizure spread simultaneously to further test the central hypothesis.

SUBCORTICAL SEIZURE SPREAD

Hughlings Jackson originally recognized that motor movements during seizures are caused by the spread of excessive neuronal activity to the motor cortex (22). Frontal lobe seizures affect the motor cortex, which has extensive subcortical projections to the basal ganglia (23).

Although some previous studies suggested that focal to bilateral seizures activate the basal ganglia, these studies focused on individual structures rather than on a complete circuit and lack cellular resolution (14-16). Also, it is unknown whether seizures preferentially activate direct or indirect pathways through the basal ganglia. It has been proposed that seizures spread through the indirect pathway (14); however, these studies did not show direct activation of D2 receptor-expressing medium spiny neurons over D1-expressing neurons. Graybiel showed that 75% of c-Fos positive cells expressed enkephalin, which supports preferential activation of the indirect pathway over direct (24); however, these studies were done during electrical stimulation of the motor cortex without seizure induction.

CONTRALATERAL SEIZURE SPREAD

Previous studies indicate that the thalamus is essential for seizure maintenance and generalization to the contralateral hemisphere (15, 25-28). However, seizure spread from the seizure focus to the contralateral cortex has not been previously traced. Several famous models of seizure generalization indicate that spread to the contralateral cortex occurs via commissural connections between the two thalami (17,25,26) or through bilateral spread from the thalamus via the brainstem (15,29-31). Lack of tools with good spatial and temporal resolution and the ability to inhibit specific structures made it difficult to distinguish between these models. The connectivity hypothesis predicts that seizures spread to the contralateral cortex from the seizure focus by engaging the cortico-cortical commissure, corpus callosum.

INTRACORTICAL HORIZONTAL SEIZURE SPREAD

Focal to bilateral seizures manifest in many behaviors such as altered consciousness, auras, and motor activity because they travel long distances from the onset zone. Local spread of seizures has been intensively investigated (32,33). Previous studies in the hippocampus and neocortex demonstrate that inhibition plays a strong role in seizure spread (34-36). According to the dentate gate theory, the dentate gyrus inhibits overexcitation in the hippocampal circuitry (37), whereas inhibitory surround shapes the

seizure spread in the neocortex (38-40). However, these studies do not explain how seizures spread over a long distance.

Previous studies indicate that deep cortical layer 4 is necessary for seizure generation and propagation (41,42), but the motor cortex is agranular cortex and does not contain layer 4 (43). Recent studies show that superficial layers 2/3 are recruited ahead of deep layers 5/6 during acute seizures (32,43). However, they did not investigate long-range layer recruitment during spontaneous seizures away from the seizure onset zone. The connectivity hypothesis predicts that superficial layers would be activated more and ahead of the deep layers because layers 2/3 have stronger intracortical projections (5), and 80% of the callosal axons originates from the superficial layers (4).

ORGANIZATION OF THE DISSERTATION

This dissertation is divided into several chapters that will collectively support the central hypothesis presented above. Presentation of the dissertation work begins with Chapter 2 that proposes that circuits of secondarily generalized seizures are more complex than those currently proposed. It predicts possible pathways of frontal lobe seizure spread based on the connectivity hypothesis.

The third chapter investigates the subcortical seizure circuit through the basal ganglia. It tests and supports the first and second corollary hypotheses. In addition, it tests the anticonvulsant effect of dopamine D2 receptor agonist in frontal lobe seizures. The fourth chapter arose from a fortuitous discovery that D2R agonist activates parvalbumin interneurons.

The fifth chapter maps contralateral seizure spread. It tests the third, fourth, and fifth corollary hypotheses and finds them to hold. Chapter 5 proposes that the thalamus amplifies seizures, whereas the corpus callosum allows contralateral spread. The combination of the new techniques in this chapter provides strong support for the central hypothesis.

The last sixth chapter investigates intracortical long-distance seizure propagation along the cortex. It supports the sixth and seventh corollary hypothesis and confirms that superficial layers activated more strongly and faster than deep layers.

REFERENCES FOR CHAPTER 1

1. Falco-Walter JJ, Scheffer IE, Fisher RS. The new definition and classification of seizures and epilepsy. Epilepsy Res. 2018; 139(July 2017):73–9.
2. Kreitzer AC, Malenka RC. Endocannabinoid-mediated rescue of striatal LTD and motor deficits in Parkinson's disease models. Nature. 2007; 445(7128):643–7.
3. Gertler TS, Chan CS, Surmeier DJ. Dichotomous anatomical properties of adult striatal medium spiny neurons. J Neurosci. 2008; 28(43):10814–24.
4. Fame RM, Macdonald JL, Macklis JD. Development, Specification, and Diversity of Callosal Projection Neurons.
5. Shepherd GM, Rowe TB. Neocortical Lamination: Insights from Neuron Types and Evolutionary Precursors. Front Neuroanat. 2017; 11(November):1–7.
6. Watanabe M, Forsgren L, Tomson T, et al. ILAE Official Report: A practical clinical definition of epilepsy. Epilepsia. 2014; 55(4):475–82.
7. Pitkänen A, Buckmaster PS, Galanopoulou AS, et al. Models of seizures and epilepsy. Academic Press; 2017. 1178 p.
8. Kopeloff LM. Experimental epilepsy in the mouse. Proc Soc Exp Biol Med. 1960; 104(3):500–4.
9. Henjyoji EY, Dow RS. Cobalt-induced seizures in the cat. Electroencephalogr Clin Neurophysiol. 1965; 19(2):152–61.
10. Grimm RJ, Frazee JG, Kawasaki T, et al. Cobalt epilepsy in the squirrel monkey. Electroencephalogr Clin Neurophysiol. 1970; 29(5):525–8.
11. Hartman ER, Colasanti BK, Craig CR. Epileptogenic properties of cobalt and related metals applied directly to cerebral cortex of rat. Epilepsia. 1974; 15(1):121–9.
12. Kim J, Woo J, Park Y-G, et al. Thalamic T-type Ca2+ channels mediate frontal lobe dysfunctions caused by a hypoxia-like damage in the prefrontal cortex. J Neurosci. 2011; 31(11):4063–73.
13. Singh T, Joshi S, Williamson JM, et al. Neocortical injury–induced status epilepticus. Epilepsia. 2020; 61(12).
14. Miyamoto H, Tatsukawa T, Shimohata A, et al. Impaired cortico-striatal excitatory transmission triggers epilepsy. Nat Commun. 2019; 10.

15. Blumenfeld H, Varghese GI, Purcaro MJ, et al. Cortical and subcortical networks in human secondarily generalized tonic-clonic seizures. Brain. 2009; 132:999–1012.
16. Devergnas A, Piallat B, Prabhu S, et al. The subcortical hidden side of focal motor seizures: evidence from micro-recordings and local field potentials. Brain. 2012; 135(7):2263–76.
17. Lothman EW, Collins RC. Kainic acid induced limbic seizures: metabolic, behavioral, electroencephalographic and neuropathological correlates. Brain Res. 1981; 218(1–2):299–318.
18. Engel J, Wolfson L, Brown L. Anatomical correlates of electrical and behavioral events related to amygdaloid kindling. Ann Neurol. 1978; 3(6):538–44.
19. Benabid AL, Minotti L, Koudsié A, et al. Antiepileptic effect of high-frequency stimulation of the subthalamic nucleus (corpus luysi) in a case of medically intractable epilepsy caused by focal dysplasia: A 30-month follow-up: Technical case report. Neurosurgery. 2002; 50(6):1385–92.
20. Guenthner CJ, Miyamichi K, Yang HH, et al. Permanent genetic access to transiently active neurons via TRAP: Targeted Recombination in Active Populations. Neuron. 2013; 78(5):773–84.
21. Allen WE, DeNardo LA, Chen MZ, et al. Thirst-associated preoptic neurons encode an aversive motivational drive. Science. 2017; 357(6356):1149–55.
22. York GK, Steinberg DA. Hughlings Jackson's neurological ideas. Brain. 2011; 134:3106–13.
23. Shepherd GMG. Corticostriatal connectivity and its role in disease. Nat Rev Neurosci. 2013; 14(4):278–91.
24. Parthasarathy HB, Graybiel AM. Cortically driven immediate-early gene expression reflects modular influence of sensorimotor cortex on identified striatal neurons in the squirrel monkey. J Neurosci. 1997; 17(7):2477–91.
25. Westbrook GL. Seizures and epilepsy. In: Kandel ER, Schwartz JH, Jessell TM, et al., editors. Principles of neural science. New York: McGraw-Hill; 2013. p. 1116–39.
26. Englot DJ, Morgan VL, Chang C. Impaired vigilance networks in temporal lobe

epilepsy: Mechanisms and clinical implications. Epilepsia. 2020; 61(2):189–202.

27. Paz JT, Davidson TJ, Frechette ES, et al. Closed-loop optogenetic control of thalamus as a new tool to interrupt seizures after cortical injury. Nat Neurosci. 2013; 16(1):64–70.
28. Paz JT, Huguenard JR. Microcircuits and their interactions in epilepsy: Is the focus out of focus? Nat Neurosci. 2015; 18(3):351–9.
29. Penfield W, Jasper HH. Epilepsy and the functional anatomy of the human brain. Boston: Little, Brown; 1954. 896 p.
30. Faingold CL, Penfield J. Brainstem Networks Reticulo-Cortical Synchronization in Generalized Convulsive Seizures. 2012.
31. Iadarola MJ, Gale K. Substantia nigra: site of anticonvulsant activity mediated by γ-aminobutyric acid. Science. 1982; 218(4578):1237–40.
32. Wenzel M, Hamm JP, Peterka DS, et al. Reliable and Elastic Propagation of Cortical Seizures In Vivo. Cell Rep. 2017; 19(13):2681–93.
33. Rossi LF, Wykes RC, Kullmann DM, et al. Focal cortical seizures start as standing waves and propagate respecting homotopic connectivity. Nat Commun. 2017; 8(1).
34. Schevon CA, Weiss SA, McKhann G, et al. Evidence of an inhibitory restraint of seizure activity in humans. Nat Commun. 2012; 3.
35. Prince DA, Wilder BJ. Control mechanisms in cortical epileptogenic foci. “Surround inhibition.” Arch Neurol. 1967; 16(2):194–202.
36. Sloviter RS, Zappone CA, Harvey BD, et al. Kainic acid-induced recurrent mossy fiber innervation of dentate gyrus GABAergic interneurons: a possible anatomical substrate of granule cell hyperinhibition in chronically epileptic rats. J Comp Neurol. 2006; 494(6):944–60.
37. Krook-Magnuson E, Armstrong C, Bui A, et al. In vivo evaluation of the dentate gate theory in epilepsy. J Physiol. 2015; 593(10):2379–88.
38. Trevelyan AJ, Sussillo D, Watson BO, et al. Modular Propagation of Epileptiform Activity: Evidence for an Inhibitory Veto in Neocortex. Neurobiol Dis. 2006; 26(48):12447–55.
39. Trevelyan AJ, Sussillo D, Yuste R. Feedforward Inhibition Contributes to the

Control of Epileptiform Propagation Speed. J Neurosci. 2007; 27(13):3383–7.

40. Schwartz TH, Bonhoeffer T. In vivo optical mapping of epileptic foci and surround inhibition in ferret cerebral cortex. Nat Med. 2001; 7(9):1063–7.
41. Telfeian AE, Connors BW. Layer-specific pathways for the horizontal propagation of epileptiform discharges in neocortex. Epilepsia. 1998; 39(7):700–8.
42. Connors BW, Pinto DJ, Telfeian AE. Local pathways of seizure propagation in neocortex. Int Rev Neurobiol. 2001; 45:527–46.
43. Weiler N, Wood L, Yu J, et al. Top-down laminar organization of the excitatory network in motor cortex. Nat Neurosci. 2008; 11(3):360–6.

CHAPTER 2

CIRCUITS GENERATING SECONDARILY GENERALIZED SEIZUIRES

SUMMARY AND CONCLUSIONS

1. The spread of secondarily generalized seizures is more complex than that of primarily generalized absence seizures.
2. Focal motor to bilateral tonic-clonic seizures affect the motor cortex, which has extensive subcortical projections in addition to the thalamocortical.
3. Secondarily generalized seizures could also travel through the striatum, globus pallidus, substantia nigra reticulata, and corpus callosum to the contralateral hemisphere.
4. Recruitment of principal neurons in superficial layers 2/3 of the cortex can play a critical role in corticocortical seizure spread ahead of the deep layers.

INTRODUCTION

Generalized tonic–clonic seizures (GTCSs) are very dangerous because they increase the risk of sudden unexpected death in epilepsy (SUDEP) and injuries (1). SUDEP is a sudden, unexpected, nontraumatic, and nondrowning death in patients with epilepsy, with or without evidence of seizures and excluding documented status epilepticus, in which post mortem examination does not reveal toxicologic or anatomic cause of death (2). Generalized tonic–clonic seizures or the absence of seizure freedom are the major risk factors for SUDEP. For example, people who have three GTCSs per year have a 15-fold increased risk for SUDEP (3). Forceful convulsions that are associated with GTCSs can also lead to falls and severe injuries (4). To understand the pathophysiology of generalized seizures, the circuits generating and propagating the seizures must be delineated.

During secondary generalization of seizures, focal seizures have been proposed to spread from the cortex to the thalamus and then engage the Thalamocortical circuits (5) (Figure 2-1). Thalamocortical oscillations play a critical role in generating primarily generalized seizures. However, unlike primarily generalized absence seizures, secondarily generalized tonic–clonic seizures affect the motor cortex, giving rise to convulsions. Motor cortex anatomy and the afferent and efferent connections are quite distinct from those of the somatosensory cortex, which is engaged in absence seizures. We propose that secondarily generalized tonic–clonic seizures not only engage the canonical thalamocortical circuit but also travel through the striatum, globus pallidus, substantia nigra pars reticulata, and the fibers of the corpus callosum, engaging the superficial cortical layers ahead of the deep layers.

Seizure circuits

The thalamocortical circuit underlies primarily generalized seizures

Sleep circuits mediate primarily generalized absence or petit mal seizures. During natural sleep, the thalamus generates spindle oscillations of 7 to 14 Hz, which are the result of network interactions between the reticular thalamic nucleus (RTN), thalamocortical neurons, and cortical pyramidal neurons (6). Intracellular in vivo recordings show that the burst firing of GABAergic reticular thalamic neurons induces

Figure 2-1. The canonical thalamocortical circuit. Focal seizures spread from the cortex to the thalamus, engaging the thalamocortical circuit as a mechanism for secondary generalization.

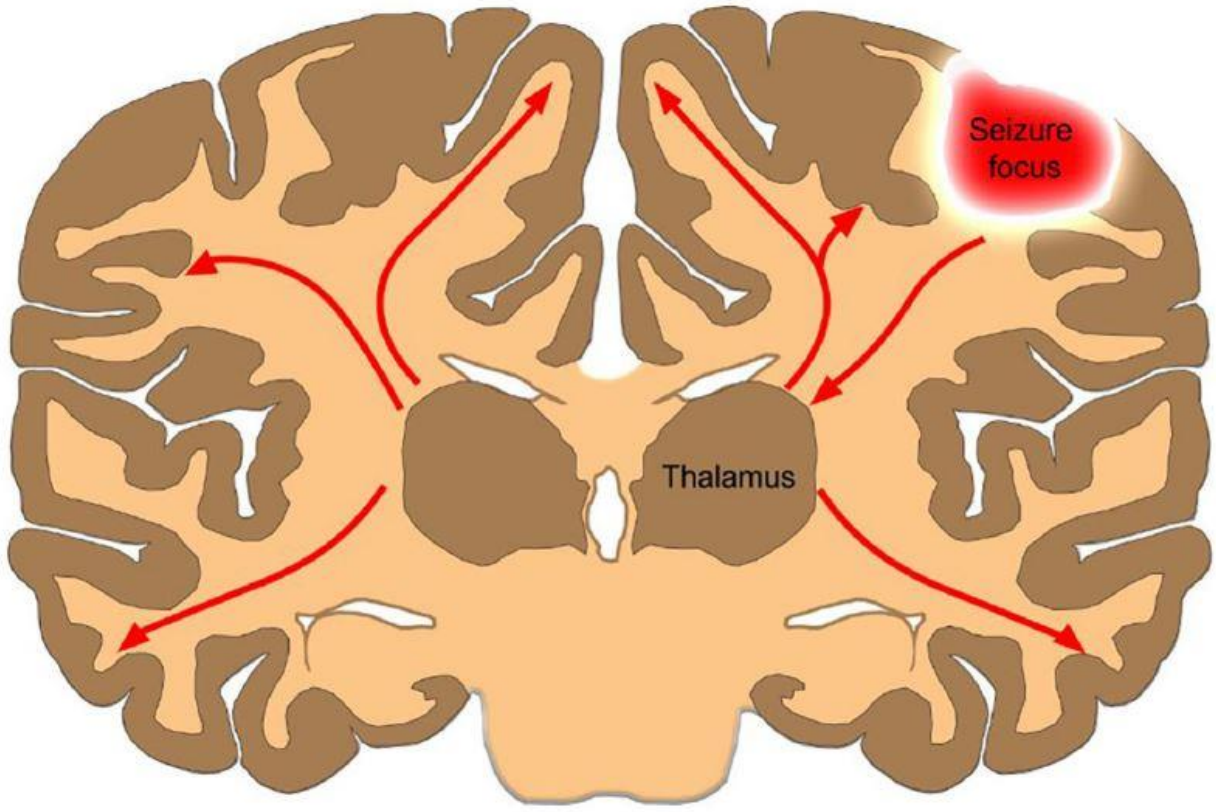

Figure 2-1

inhibitory postsynaptic potentials (IPSPs) of the thalamocortical neurons, which leads to deinactivation of the low-threshold Ca2+ current (IT) and rebound bursts in thalamocortical neurons (7). The mechanism of these natural spindle oscillations is thought to underlie the spike-and wave discharges observed in generalized absence seizures (8-11). During absence seizures, inhibitory reticular thalamic neurons drive the excitatory behavior in the ventrobasal thalamic nucleus (VB, which consists of the ventroposterior medial and lateral nuclei, VPM/VPL) and layer 4 of the somatosensory cortex, which receives projections from the VB through deinactivation of T-type Ca2+ channels. The effectiveness of GABAB antagonists to decrease seizure frequency in genetic absence epilepsy rats and drugs such as ethosuximide, T-type calcium channel blocker, in the treatment of absence seizures supports the thalamocortical mechanism of primarily generalized absence seizures (12-13).

The circuits that underlie secondarily generalized tonic–clonic seizures have not been studied in detail. Cerebral blood flow (CBF) studies in human patients during secondarily generalized tonic–clonic seizures as well as electroconvulsive therapy (ECT)-induced generalized tonic–clonic seizures in patients with refractory depression indicate that recruitment of the thalamus supports its proposed role in seizure generalization (14,15). 2-Deoxyglucose (DG) metabolic mapping studies also indicate thalamic activation; however, these studies also show activation of structures outside of the thalamocortical circuit, such as the substantia nigra (16,17).

Secondarily generalized seizures affect the motor cortex

Convulsions during secondarily generalized tonic–clonic seizures are the result of seizures affecting the motor cortex. Hughlings Jackson first recognized that convulsions are the result of seizures affecting the contralateral motor cortex (18). Unlike the somatosensory cortex, the motor cortex does not contain layer 4, and as seizures that affect the motor cortex and convulsions appear, there are no direct thalamic projections from the VPM/VPL to layer 4. The subcortical and intralaminar circuits that underlie those seizures are less clear. Motor thalamic nuclei, such as, the ventroanterior (VA), ventrolateral (VL), and ventromedial (VM) nuclei, project directly to layers 2–6 of the motor cortex (19). The motor cortex projects back to these thalamic nuclei from layers 5B and 6. The motor cortex also sends projections across the corpus callosum and to

the striatum, which in turn projects to the globus pallidus and substantia nigra reticulata (SNR) (20,21) (Figure 2-2). The canonical thalamocortical theory of seizure spread disregards the purpose of the corpus callosum during secondary generalization of seizures from one hemisphere to the other, and it does not explain why manipulation of the basal ganglia can affect seizures.

Anatomy of the motor cortex and activity spread through its subcortical connections

In the motor cortex, there are three types of principal neurons that project corticocortically as well as subcortically (19,22): IT-type neurons are intratelencephalic neurons located in all cortical layers 2/3, 5A/B, and 6. These neurons project to the identical contralateral cortex across the corpus callosum, to the striatum, and corticocortically; PT-type neurons are the pyramidal tract neurons in layer 5B. These neurons project to the brainstem and spinal cord, sending collaterals to the striatum and thalamus; CT-type neurons are corticothalamic neurons in layer 6 and send their projections to the thalamus.

The IT-type neurons of all cortical layers and the collaterals of PT type neurons of layer 5B exit the motor cortex to enter the striatum; IT-type neurons go to both the ipsilateral and contralateral striatum, whereas PT-type neurons go to the ipsilateral striatum only. The striatum is divided into ventral and dorsal parts (23). The ventral striatum consists of the nucleus accumbens and olfactory tubercle, and the dorsal striatum includes the caudate and putamen. Axons from the motor cortex enter the striatum at the dorsal part, whereas those from sensory cortical areas enter at the ventral part. Almost 90% of all striatal neurons are inhibitory GABAergic medium spiny neurons (MSNs). Two main output areas of the striatum are the globus pallidus (GP), which is subdivided into the internal (GPi) and external (GPe) segments, and the substantial nigra reticulata (SNR).

As fibers travel from the motor cortex into the striatum, they go either through the direct or indirect circuit. In the direct circuit, after passing the striatum, axons go to the GPi or to SNR, after which they enter the VA and VL nuclei in the thalamus. Medium spiny neurons in the direct path contain dopamine 1 (DRD1) receptors. In the indirect circuit, the striatum projects to the GABAergic neurons of the GPe that go to the

Figure 2-2. The proposed circuit of secondarily generalized tonic–clonic seizures. As seizures affect the motor cortex, they spread through the fibers of the corpus callosum, striatum, globus pallidus, and substantia nigra reticulata (either via the direct or indirect circuit), as well as through the thalamocortical projections.

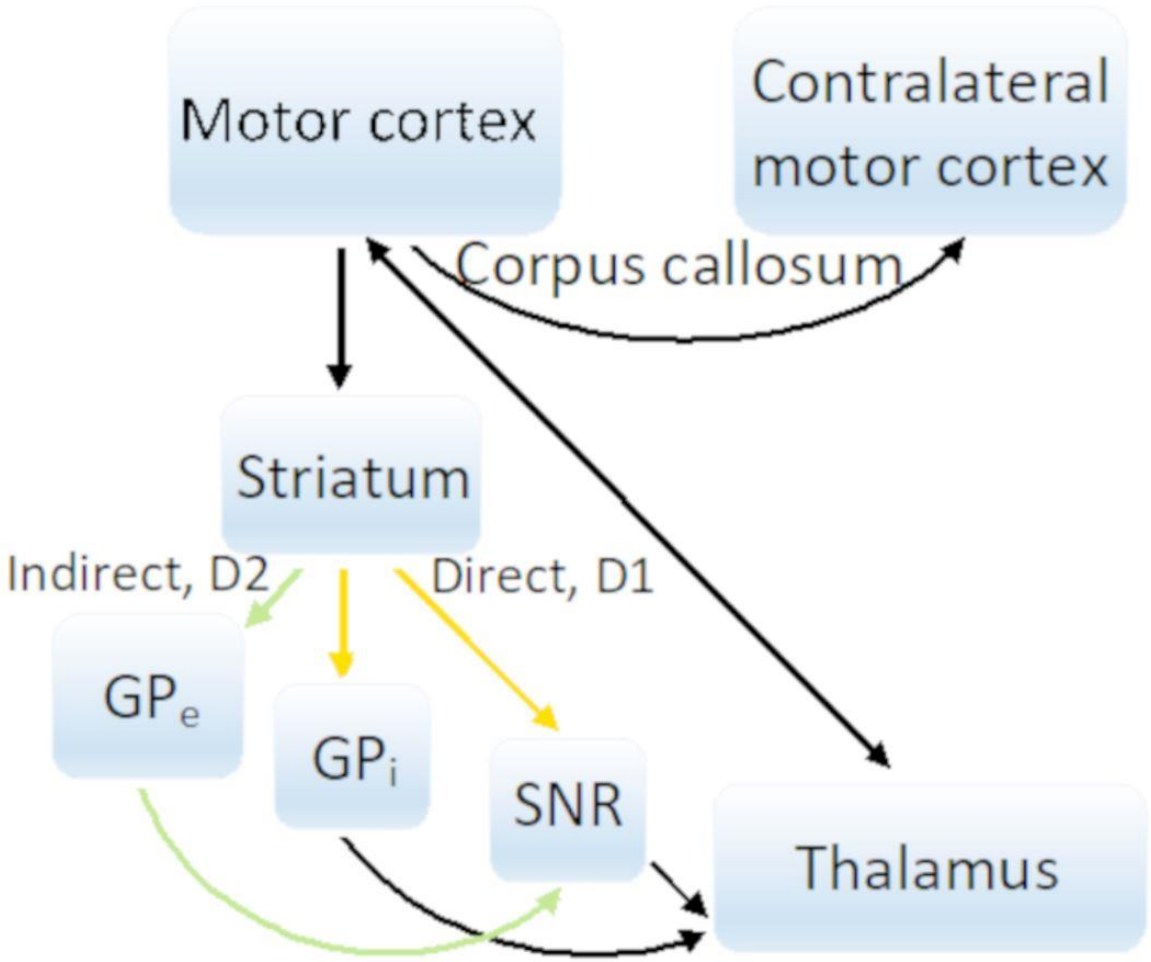

Figure 2-2

subthalamic nucleus (STN), which sends excitatory glutamatergic projections to the SNR to enter the VA/VL nuclei in the thalamus as well. Neurons in the indirect pathway are distinguished by containing dopamine type 2 (DRD2) receptors.

It would be surprising if seizure activity traveled through the sea of inhibition of the striatal GABAergic neurons after affecting the motor cortex. However, the Turski group demonstrated that application of the dopamine agonist apomorphine in the anterior parts of the striatum protects rats from pilocarpine-induced seizures (24). Specifically, these authors found that only D2 agonist LY-171555 protects animals from seizures, whereas the application of D1 agonist SKF-38393 in the striatum has no effect. The application of haloperidol, a D2 receptor antagonist, blocked the anticonvulsant actions of the D2 agonist and apomorphine.

Modulation of dopamine receptors in humans changes seizure susceptibility. Treatments with atypical antipsychotics, which are serotonin and dopamine-receptor antagonists, increase seizure risk (25,26). Groups treated with either clozapine or olanzapine, which are both dopamine, serotonin, histamine, adrenergic, and muscarinic receptor antagonists, with olanzapine having higher affinity for D2 receptors than clozapine, showed a 3.5% and 0.9% incidence of seizures, respectively, compared to placebo-treated groups during phase II-III clinical trials (27,28).

As the motor cortex projects to the striatum, one of the major output structures of the striatum is the SNR. Activation of the SNR has been found during generalized tonic–clonic seizures in 2-deoxyglucose mapping studies (16,17,29). Additionally, previous decades of research have shown that stimulation of the SNR leads to suppression of seizures, and microinfusion of bicuculine (GABAA antagonist) into the SNR has a proconvulsant effect (30).

Motor cortical pyramidal neurons also send their axons across the corpus callosum, where 80% of callosal fibers come from layer 2/3, 20% from layer 5, and a small amount from layer 6 pyramidal neurons (31). The corpus callosum is the largest commissure of the brain that connects the two hemispheres, and many studies have shown that seizures utilize it for their spread to the contralateral hemisphere (32,33). Oligodendroglioma lesions that are directly connected to the genu of the corpus callosum have been shown to be significantly more likely to cause generalized tonic–

clonic seizures than lesions in other brain regions, whereas no correlation was observed between tumor size and generalized seizure frequency (34). A corpus callosotomy study indicated that seizures were reduced by 50% in 79% of patients who underwent callosotomy (35), and in another study, two-thirds of patients experienced total cessation of generalized tonic–clonic seizures and drop attacks (36).

Intralaminar seizure propagation through the motor cortex

In previous studies, slice recordings indicated that layers 4 and 5 of the somatosensory cortex play an important role in cortical seizure initiation and corticocortical propagation (37,38), which makes intralaminar seizure spread within the motor cortex less clear. The canonical circuit indicates that excitation of the deep layers 4/5 drives the excitation in the superficial layers 2/3 (39-41). However, as seizures affect the motor cortex, the absence of layer 4 in the motor cortex suggests that seizures likely utilize different laminar circuits.

Shepherd and colleagues proposed a top-down laminar organization of the motor cortex, where layers 2/3 drive the excitation within the deep layers (42). In this study, glutamate uncaging by laser photostimulation of presynaptic neurons in one layer and electrophysiological recording of postsynaptic neurons in another layer were used to determine the layer-specific wiring of the motor cortex. The results indicated that the strongest excitatory pathway is from L2/3 descending to L5A/B. A weaker ascending pathway is also present from L5A to 2/3. The horizontal pathways are the strongest in L2, followed by those in L5A/B through L5B/6, and the weakest is in L3/5A and 6. These results indicate that the flow of excitation in the motor cortex is downwardly oriented from L2. Laminar epileptogenicity was also measured, which was expressed as a likelihood of an event per stimulus. Even under strongly excitable conditions with high stimulus intensities and unblocked NMDA receptors, a stimulus in L5B remains nonepileptogenic, with a local stimulus failing to spread through the network, whereas L2 demonstrates downward excitability and recurrent excitation.

Yuste and colleagues used two-photon microscopy to determine through which cortical layers seizures propagate in vivo (43). These investigators recorded from the somatosensory cortex using 4-AP or picrotoxin application in layer 5 to evoke ictal activity. The results indicated that ictal recruitment of layer 2/3 occurs ahead of that of

L5. Another finding was a vertical delay in the lateral spread of seizures with layer 2/3 recruitment occurring before the recruitment of layer 5.

CONCLUSIONS

More evidence now suggests that the spread of secondarily generalized seizures is more complex than that of primarily generalized absence seizures. Not only does manipulation of the basal ganglia affect seizure initiation and generalization, but corpus callosotomies also decrease the frequency of secondarily generalized seizures in patients. The canonical thalamocortical model of seizure generalization alone does not explain these findings, which indicates that the spread of secondarily generalized seizures is more complex than previously thought.

Understanding the circuit that secondarily generalized seizures affect has a potential for indicating novel targets for neuromodulation. The structures targeted by secondarily generalized seizures could also be loci of neuronal plasticity, with first seizures consolidating the circuit for future seizures. These and future studies are necessary because ignoring the complexity of the network and reducing it to simple thalamocortical oscillations provide a danger of missing novel clinical therapies for people who suffer from these devastating seizures.

REFERENCES FOR CHAPTER 2

1. Tomson T, Nashef L, Ryvlin P. Sudden unexpected death in epilepsy: current knowledge and future directions. Lancet Neurol 2008;7:1021–31.
2. Nashef L, So EL, Ryvlin P, Tomson T. Unifying the definitions of sudden unexpected death in epilepsy. Epilepsia 2012;53:227–33.
3. Harden C, Tomson T, Gloss D, et al. Practice guideline summary: sudden unexpected death in epilepsy incidence rates and risk factors. Neurology 2017;88:1674–80.
4. Asadi-Pooya AA, Nikseresht A, Yaghoubi E, Nei M. Physical injuries in patients with epilepsy and their associated risk factors. Seizure 2012;21:165–8.
5. Westbrook GL. Seizures and epilepsy. In: Kandel ER, Schwartz JH, Thomas MJ, Siegelbaum SA, Hudspeth AJ, editors. Principles of neural science. New York: McGraw-Hill; 2013. p. 1116–39.
6. SteriadeM, Mccormick DA, Sejnowski TJ. Thalamocortical oscillations in the sleeping and aroused brain. Science 1993;262:679–85.
7. Cain SM, Snutch TP. Voltage-gated calciumchannels in epilepsy. In: Noebels JL, Avoli M, Rogawski MA, et al, editors. Jasper's basic mechanisms of the epilepsies. Bethesda: National Center for Biotechnology Information (US); 2012.
8. Kellaway P. Sleep and epilepsy. Epilepsia 1985;26:S15–30.
9. Steriade M. Interneuronal epileptic discharges related to spike-and-wave cortical seizures in behaving monkeys. Electroencephalogr Clin Neurophysiol 1974;37: 247–63.
10. Kostopoulos G, Gloor P, Pellegrini A, Gotman J. A study of the transition from spindles to spike and wave discharge in feline generalized penicillin epilepsy: microphysiological features. Exp Neurol 1981;73:55–77.
11. Avoli M, Gloor P, Kostopoulos G, Gotman J. An analysis of penicillin-induced generalized spike and wave discharges using simultaneous recordings of cortical and thalamic single neurons. J Neurophysiol 1984;50:819–37.
12. Liu Z, Vergnes M, Depaulis A, Marescaux C. Involvement of intrathalamic GABAB neurotransmission in the control of absence seizures in the rat. Neuroscience 1992;48:87–93.

13. Norden AD, Blumenfeld H. The role of subcortical structures in human epilepsy. EpilepsyBehav 2002;3:219–31.
14. Blumenfeld H, Varghese GI, Purcaro MJ, Motelow JE, Enev M, McNally KA, et al. Cortical and subcortical networks in human secondarily generalized tonic-clonic seizures. Brain 2009;132:999–1012.
15. Enev M, McNally KA, Varghese G, Zubal IG, Ostroff RB, Blumenfeld H. Imaging onset and propagation of ECT-induced seizures. Epilepsia 2007;48:238–44.
16. Lothman EW, Collins RC. Kainic acid induced limbic seizures: metabolic, behavioral, electroencephalographic and neuropathological correlates. Brain Res 1981;218:299–318.
17. Engel J, Wolfson L, Brown L. Anatomical correlates of electrical and behavioral events related to amygdaloid kindling. Ann Neurol 1978;3:538–44.
18. Jackson JH. The lumleian lectures on convulsive seizures. Lancet 1890;135:685–8.
19. Hooks BM, Mao T, Gutnisky DA, Yamawaki N, Svoboda K, Shepherd GM. Organization of cortical and thalamic input to pyramidal neurons in mouse motor cortex. J Neurosci 2013;33:748–60.
20. Molyneaux BJ, Arlotta P, Menezes JR, Macklis JD. Neuronal subtype specification in the cerebral cortex. Nat Rev Neurosci 2007;8:427–37.
21. Shepherd GM. Corticostriatal connectivity and its role in disease. Nat Rev Neurosci 2013;14:278–91.
22. Shepherd GM, Rowe TB. Neocortical lamination: insights from neuron types and evolutionary precursors. Front Neuroanat 2017;11.
23. Haber SN. Corticostriatal circuitry. Dialogues Clin Neurosci 2016;18:7–21.
24. Turski L, Cavalheiro EA, Bortolotto ZA, Ikonomidou-Turski C, Kleinrok Z, Turski WA. Dopamine-sensitive anticonvulsant site in the rat striatum. J Neurosci 1988;8: 4027–37.
25. Behere RV, Anjith D, Rao NP, Venkatasubramanian G, Gangadhar BN. Olanzapine-induced clinical seizure: a case report. Clin Neuropharmacol 2009;32:297–8.
26. Uvais NA, Sreeraj VS. Seizure associated with olanzapine. J Family Med Prim Care 2018;7:1090–2.
27. Koch-Stoecker S. Antipsychotic drugs and epilepsy: indications and treatment

guidelines. Epilepsia 2002;43:19–24.
28. Alper K, Schwartz KA, Kolts RL, Khan A. Seizure incidence in psychopharmacological clinical trials: an analysis of food and drug administration (FDA) summary basis of approval reports. Biol Psychiatry 2007;62:345–54.
29. Collins RC, Santori EM, Der T, Toga AW, Lothman EW. Functionalmetabolicmapping
during forelimb movement in rat. I. Stimulation of motor cortex. J Neurosci 1986;6: 448–62.
30. Velíšková J, Moshé SL. Update on the role of substantia nigra pars reticulata in the regulation of seizures. Epilepsy Curr 2006;6:83–7.
31. Fame RM, Macdonald JL, Macklis JD. Development, specification, and diversity of callosal projection neurons. Trends Neurosci 2011;34:41–50.
32. VanWagenen WP, Herren RY. Surgical division of commissural pathways in the corpus callosum. Relation to spread of an epileptic attack. Arch NeurPsych 1940;44: 740–59.
33. Rappaport ZH, Lerman P. Corpus callosotomy in the treatment of secondary generalizing intractable epilepsy. Acta Neurochir 1988;94:10–4.
34. Wieshmann UC, Milinis K, Paniker J, Das K, Jenkinson MD, Brodbelt A, et al. The role of the corpus callosum in seizure spread: MRI lesion mapping in oligodendrogliomas. Epilepsy Res 2015;109:126–33.
35. Unterberger I, Bauer R, Walser G, Bauer G. Corpus callosum and epilepsies. Seizure 2016;37:55–60.
36. Tanriverdi T, Olivier A, Poulin N, Andermann F, Dubeau F. Long-term seizure outcome after corpus callosotomy: a retrospective analysis of 95 patients. J Neurosurg 2009;110:332–42.
37. Connors BW. Initiation of synchronized neuronal bursting in neocortex. Nature 1984;310:685–7.
38. Telfeian AE, Connors BW. Layer-specific pathways for the horizontal propagation of epileptiform discharges in neocortex. Epilepsia 1998;39:700–8.
39. Douglas RJ, Martin KA. Neuronal circuits of the neocortex. Annu Rev Neurosci 2004;27:419–51.

40. Petersen CC. The functional organization of the barrel cortex. Neuron 2007;56: 339–55.
41. Thomson AM, Lamy C. Functional maps of neocortical local circuitry. Front Neurosci 2007;1:19–42.
42. Weiler N, Wood L, Yu J, Solla SA, Shepherd GM. Top-down laminar organization of the excitatory network in motor cortex. Nat Neurosci 2008;11:360–6.
43. Wenzel M, HammJP, Peterka DS, Yuste R. Reliable and elastic propagation of cortical seizures in vivo. Cell Rep 2017;19:2681–93.

CHAPTER 3

ACTIVATION OF THE BASAL GANGLIA AND INDIRECT PATHWAY NEURONS DURING FRONTAL LOBE SEIZURES

SUMMARY AND CONCLUSIONS

1. We provide direct evidence that motor seizures activate structures that are anatomically connected to the seizure focus and between each other, suggesting that seizure spread can be predicted by connectivity.
2. We found that seizures that originate in the premotor cortex activate the striatum, globus pallidus externus, subthalamic nucleus, substantia nigra pars reticulata, and neurons of the indirect pathway.
3. 80% of all activated neurons in the striatum expressed D2 receptors. Thus, seizures preferentially activated dopamine D2 receptor-expressing neurons over D1 in the striatum, which have different projections. D2 neurons are more excitable than D1, suggesting that properties of neurons in addition to connectivity determine the pattern of neuronal activation during seizures.
3. The D2 receptor agonist infused directly into the striatum via a bilateral cannula exerted an anticonvulsant effect.
4. Seizures activate structures via short and long latency loops, and activation of the basal ganglia modulates seizures.

INTRODUCTION

Epilepsy is a disease, which afflicts more than 65 million people worldwide. Frontal lobe epilepsy is the second most common type of epilepsy after temporal lobe epilepsy. However, the neuronal circuits mediating frontal lobe seizures remain poorly understood. Focal motor to bilateral tonic-clonic seizures, previously known as secondarily generalized or partial-onset grand mal, activate the motor cortex (1). The striatum and its projections to the globus pallidus, subthalamic nucleus, and substantia nigra pars reticulata comprise the basal ganglia and are critical output structures of the motor cortex (2). Previous studies indicated that basal ganglia participate in seizures (3-5). However, these studies focused on individual structures, such as the striatum or substantia nigra, and lacked cellular resolution (6-9).

There are two types of medium spiny neurons interspersed through the striatum. Neurons that express dopamine receptors D2 (DRD2) on their surface comprise the indirect pathway and project to the globus pallidus externus (GPe), subthalamic nucleus (STN), and substantia nigra pars reticulata (SNR), inhibiting voluntary movement. Neurons that express dopamine receptors D1 (DRD1) comprise the direct pathway and project to the globus pallidus internus (GPi) and SNR, facilitating voluntary movement (10,11). Older studies described modulation of seizures by dopaminergic drugs (12), but it is unknown whether motor seizures activate the indirect or direct pathway through the striatum. We demonstrate that frontal lobe seizures preferentially activate the indirect pathway neurons of the basal ganglia, predominantly activating DRD2 neurons.

Here, we incorporated novel tools and techniques such as super-resolution and light sheet microscopy, activity reporter TRAP2 mice, tissue clearing, Cre-driven viral tracing, and local field potential (LFP) recordings from multiple structures simultaneously to map the neuronal activation circuit after frontal lobe focal motor to bilateral tonic-clonic seizures. Additionally, we suppressed seizures by infusing D2 agonists into the striatum, showing that the basal ganglia and D2 system modulate seizures.

METHODS

Animals

All studies were approved by the University of Virginia Animal Care and Use Committee. Mice expressing Cre-ER under the regulation of c-Fos promoter (Fos^{CreER}, Jackson Laboratories, #021882, or $Fos^{2A\text{-}ICreERT2}$, Jackson Laboratories, #030323) were crossed to mice expressing tdTomato from the Rosa locus (Ai9, Jackson Laboratories, #007909) to generate TRAP2 mice. TRAP2 and C57BL/6 (Charles River) mice of both sexes (7-12 weeks) were maintained on 12 hour light (6AM to 6PM)/dark (6PM to 6AM) cycle and had *ad libitum* access to food and water. For genotyping, KAPA Biosystems kit was used.

Seizure induction, EEG/LFP recordings, and virus injections

To induce seizures, TRAP2 or C57BL/6 mice were anesthetized with isoflurane, a small craniotomy was made, cobalt wire (diameter 0.5 mm, length 1 mm, 1.7 mg) was implanted in the right premotor cortex (AP +2.6 mm, ML -1.8 mm) with four subdural EEG electrodes and a reference (Figure 3-1D). Animals were continuously monitored for seizures via video/EEG. All mice developed seizures within 13-20 hours after cobalt insertion, and 4-hydroxytamoxifen (4-OHT, 50 mg/kg, s.c.) was injected at the peak of seizures within 90 minutes. Animals were perfused 5 days after 4-OHT injection to allow tdTomato expression.

Steel wire was used as a control (diameter 0.5 mm, 1.7 mg) and implanted instead of cobalt as described above. 4-OHT was injected 18 hours after steel wire implantation (average time period of seizure peak in cobalt implanted mice). Mice were monitored via continuous video/EEG for 48 hours; no seizures were observed.

Local field potentials were recorded with a custom-made array of microelectrodes (diameter 50 μm, diamel-coated nickel-chromium wire (Johnson Matthey Inc.)). Electrode length of 2 cm maintained 60-70 kΩ resistance. The data were amplified and filtered (the low cut pass 1 Hz, high cut pass 5 kHz) by 16-Channel Microelectrodes Amplifier Model 3600 (A-M Systems), digitized, and stored on a computer with PowerLab 16/35 hardware and LabChart 8 software at a sampling rate of 10 kHz. We coordinated the distance between each microelectrode's array by using non-epileptic animals with the cross-correlation to be less than 0.7 between each electrode, by

analyzing the time lag between the electrodes (in MATLAB). The cross-correlation r and delay d are defined as:

$$r = \frac{\sum_i [(x(i) - mx) * (y(i-d) - my)]}{\sqrt{\sum_i (x(i) - mx)^2} \sqrt{\sum_i (y(i-d) - my)^2}}$$

Where x(i) and y(i) are two series with i = 0, 1, 2… N-1, and mx and my are the means of the corresponding series. To record seizures, the microelectrodes were placed in the premotor cortex (AP +2.2 mm, ML -1.8 mm, DV -0.5 mm), striatum (AP +1.2 mm, ML -1.8 mm, DV -3.5 mm), VL (AP -1.3 mm, ML -1.0 mm, DV -3.75 mm), and SNR (AP -3.3 mm, ML -1.5 mm, DV -4.75 mm) together with cobalt. Seizure start was identified as a deflection of the voltage trace at least twice the baseline after visual inspection. After recordings, the electrode position was marked by applying a single burst of 40 μA, 0.75 msec monophasic square wave pulse at 50 Hz for 30 sec using a constant current stimulator (A-M Systems, Model 2100). The animals were perfused, brains were sectioned 40 μm thick on a cryostat (Leica, CM1900), and stained with DAPI (0.02% in PBS). The sections were imaged on Nikon Eclipse Ti-S, 2x/0.45 NA. If the electrode position was incorrect, the data were excluded from the analysis.

LabChart LFP data were analyzed to create spectrograms, using Fast Fourier Transform with a Cosine-Bell data window and a window size of 1024 data points (2.56 seconds), which resulted in a frequency resolution of 0.375 Hz. A window overlap of 87.5% was used to smooth the spectrogram's x-axis. We expressed power as μV2.

TRAP2 mice were injected with either AAV9-CamKII0.4.eGFP.WPRE.rBG (#105541-AAV9, Addgene) or AAV9 pCAG-FLEX-EGFP-WPRE (#51502-AAV9, Addgene) in the premotor cortex (AP +2.6 mm, ML -1.8 mm, DV -0.5 mm; 100 nl) with Hamilton syringe (#7634-01). A minimum of 2 weeks was allowed for the viral expression before proceeding with Co implantation.

Immunohistochemistry

Mice were deeply anesthetized with isoflurane and perfused intracardially with 4% paraformaldehyde (PFA) in 0.1 M phosphate buffer (PB), pH 7.2 at 4°C. Brains were fixed in PFA overnight, cryoprotected in 30% sucrose in phosphate buffered saline (PBS) for 2 days at 4°C, and sliced on a cryostat at 40 μm. Each fourth section was

placed in a blocking buffer (50 µl/ml normal goat serum (NGS), #017-000-121, Jackson ImmunoResearch, and 0.1% Triton X-100) for 2 hours. The primary antibodies (with 20 µl/ml NGS overnight at 4°C) were rabbit anti-D2R (1:250, #AB5084P, Millipore), rat anti-D1R (1:300, #D2944, Sigma), rabbit anti-NeuN (1:250, #24307, Cell Signaling), rabbit anti-GFAP (1:800, #ab7260, Abcam), mouse anti-MBP (1:500, #ab62631, Abcam), rabbit anti-enkephalin (1:2000, #20065, ImmunoStar), guinea pig anti-dynorphin (1:500, #AB5519, Millipore), rabbit anti-PV (1:500, #ab11427, Abcam), rabbit anti-preproenkephalin (1:1000, #RA14124, Neuromics). The sections were washed in 1xPBS. The secondary antibodies (1:500, Invitrogen, for 2 hours at room temperature) were 405 goat anti-rabbit, 488 goat anti-rabbit, 488 goat anti-guinea pig, 488 goat anti-mouse, 488 goat anti-rat, 633 goat anti-rat.

Processing, image acquisition, drug treatment, and analysis

Mice were perfused with 4% PFA and 4% acrylamide in 0.1 M PB to clarify tissue. Brains were fixed in the same solution overnight at 4°C. 200 µm thick sections were sliced on a vibratome (Leica VT3200) and incubated in 1% acrylamide in PBS with 0.25% VA-044 (#27776-21-2, Wako Chemicals) in the dark overnight at 4°C. The sections were degassed in nitrogen for 1-5 min, polymerized at 37°C for 3 hours, washed in PBS, and incubated with 8% sodium dodecyl sulfate (SDS, BIO-RAD) in PBS at 37°C for 24-36 hours covered in parafilm until transparent. For whole brain clearing, SDS was changed every day for 2 weeks until the whole brain became transparent. The sections were then washed in PBS with 0.1% Triton X-100 and mounted in RIMS (40 g histodenz in 30 ml 0.2 M PB, 0.1% Tween-20, 0.01% sodium azide, pH 7.5).

Confocal images were done on Nikon Eclipse Ti-U at 10x/0.45 NA or 20x/0.95 NA, 1024x1024 frame size. Images were tiled as stacks with 5 µm z-interval and stitched using NIS Elements software. Imaris 9.3.0 (Bitplane) was used for visualization and Adobe Photoshop CC for cropping an original image and figure display. DRD2 or DRD1 were imaged on Zeiss LSM 980 Multiphoton Airyscan 2 at 63x/1.40 NA, oil, or Leica SP8 STED at 93x/1.30 NA, glycerol. One third of the whole clarified brain was imaged on Zeiss Z.1 Light Sheet microscope with objective lens 5x/0.1 NA, detection

objective lens 5x/0.16 NA, and arivis Vision4D software. Excitation lasers were 405, 488, 561, and 633 nm.

For sumanirole vs artificial cerebrospinal fluid (aCSF) treatment, C57BL/6 mice were implanted with cobalt, four surface EEG electrodes, a reference, and a bilateral guide cannula (PlasticsOne, C235G-2.7/SPC, 26 GA, 2.1 mm below pedestal) at AP +1.02 mm, ML ±1.35 mm, DV -1.75 mm into the striatum and stabilized with dental cement. An internal bilateral cannula (PlasticsOne, C235I/SPC, 33GA, 1 mm projection) was connected to two 5 µl Hamilton syringes prefilled with either sumanirole maleate (10 µg/injection per lobe in aCSF) or aCSF (in mM, 127 NaCl, 2 KCl, 1.5 MgSO4, 25.7 NaHCO3, 10 dextrose, and 1.5 CaCl2; 300 mOsm) as a control, and injected by a blinded experimenter slowly over 75 s at 18 hours after cobalt insertion. The blinded experimenter counted seizures before the injections (15-18 hrs after Co) to determine the baseline, following the injections (18-20.5 hrs after Co) because sumanirole has a sustained effect for at least 2 hours, and after the injections (20.5-23.5 hrs after Co) to determine return to the baseline.

To count the number of tdTomato positive cells in cobalt vs steel implanted mice, Imaris Spots detection or ImageJ were used and confirmed manually by a blinded investigator. A region of interest was drawn, background was subtracted, and the threshold was adjusted. The number of cells was counted on a 40 µm cryostat section in a structure and averaged across sequential sections in a mouse. Each point on a graph is the average value for a separate mouse. At least three sections were analyzed per lobe per animal. In the steel wire implanted mice, left and right lobe data were combined and averaged in each animal.

To determine whether DRD2/DRD1 or ENK/DYN positive cells colocalized with tdTomato positive cells, tdTomato cells were tagged using Imaris Spots detection tool on 20x confocal images. Colocalization was manually checked based on whether approximately 50% of the surface colocalized with the marker of interest. The number of tdTomato positive cells that colocalized with either DRD2 or DRD1 (ENK or DYN) was divided by the total number of all tdTomato positive cells, which allowed to determine % of tdTomato cells expressing the marker.

Statistics

All statistical analysis was performed in Prism 8. Unpaired t-test was used for normally distributed and the Kolmogorov-Smirnov test for data not normally distributed. Data are presented as mean ± SEM, where n is the number of animals or the number of seizures followed by the number of animals. Results were considered statistically significant for $p < 0.05$.

RESULTS

Frontal lobe seizures activate the striatum

To visualize neuronal activation during seizures, we used TRAP mice, modified to a new generation TRAP2 that utilizes the activity of immediate early gene c-Fos to drive Cre expression (13,14). 4-hydroxytamoxifen (4-OHT) injection translocates Cre inside the nucleus that relieves the repression from tdTomato, which labels activated cells. Non-active cells are not labeled with tdTomato because they do not express Cre. To initiate frontal lobe focal motor to bilateral tonic-clonic seizures, we used well-characterized cobalt (Co) model (15-18). Cobalt inactivates oxygen-binding molecules within neurons, causing hypoxic injury (19). Cobalt wire (1.7 mg) was inserted into the right premotor cortex of a TRAP mouse with five subdural EEG electrodes on both hemispheres (Figure 3-1D). The mice were monitored for seizures via continuous video/EEG. Interictal spike-wave discharges appeared in the EEG within hours after recovery from surgery and became more frequent and bilateral. Spontaneous focal and focal to bilateral tonic-clonic seizures repeatedly occurred over the next 6-36 hrs and lasted 10-180 seconds (Figure 3-1C). Animals were injected with 4-OHT (50 mg/kg, s.c.) 90 minutes after focal to bilateral seizures to cause recombinant expression of tdTomato in activated neurons. In a separate experiment, we found that tdTomato expression peaks when 4-OHT is administered 90 minutes following a seizure. This time course is consistent with c-Fos mRNA expression after a seizure (20-23). After five days of tdTomato protein accumulation, the whole brain was serially sectioned into 40 μm sections and imaged on a confocal microscope to analyze the pattern of tdTomato expression.

Secondarily generalized tonic-clonic seizures led to cortical activation in both hemispheres, as seen on bilateral EEG (Figure 3-1D) and in increased tdTomato signal (Figure 3-1A,B). The ipsilateral hemisphere of mice with seizures had more tdTomato signal than the contralateral (Figure 3-1A,B), where % activation is the total tdTomato fluorescence in the cortex divided by the total cortical area. Observed cortical activation could be a result of motor activity, cortical injury, or seizures. We implanted steel wire instead of cobalt and injected 4-OHT 18 hours after the surgery. The control steel wire

Figure 3-1. Frontal lobe seizures activate the striatum. A) % Activation in the ipsilateral (red) and contralateral (blue) cortex in mice with seizures compared to the ipsilateral (green) and contralateral (dark green) cortex of the control steel wire implanted mice without seizures across the whole brain from the anterior (3.5 mm bregma) to the posterior cortex (-4.5 mm bregma), KS test, n = 4-6 mice. B) Representative tdTomato expression in the ipsilateral (red) and contralateral (blue) cortex in mice with seizures compared to the steel wire control mice without seizures (green), quantification in A. Boxed insets: enlarged images from the middle areas. C) After Co implantation, TRAP mice developed spontaneous repeated focal seizures (blue) and focal motor to bilateral tonic-clonic seizures (red). 4-OHT was injected at the peak of secondarily generalized tonic-clonic seizures within 90 min of the last seizure (red arrow). Points indicate mean and shaded regions SEM (n = 8 mice). D) A schematic of the cobalt placement and EEG electrodes (red), and a representative EEG recording from each electrode during focal motor to bilateral seizure in a TRAP mouse. E) Left: tdTomato (red) expression in the striatum immunolabeled for NeuN (green). Dotted lines indicate the striatum. Right: magnified view of the striatum. Boxed inset: tdTomato positive neurons colocalized with NeuN. F) Left: steel wire control showed minimal tdTomato expression in the striatum. Right: magnified view of the striatum. G) Cobalt implanted mice had more tdTomato positive cells in the ipsilateral and contralateral striatum compared to the steel wire implanted mice (each point is the average number of cells in a 40 μm section across sequential striatal sections in a mouse) (ipsilateral: 1036 ± 229.4 cells, n = 9 mice, KS test; contralateral: 349.8 ± 115.2 cells, n = 9 mice, KS test; control: 20.90 ± 5.909 cells, n = 5 mice). The ipsilateral striatum had more tdTomato positive cells than the contralateral in mice with seizures (KS test). H) Left: striosomes immunolabeled for MOR (green) and tdTomato expression in the striatum. Middle: striosome that did not express tdTomato. Right: striosome that was tdTomato positive. (I) An astrocyte immunolabeled for GFAP (green) expressed tdTomato in the striatum. J) Left: SP8 super-resolution

Lightning microscopy image of tdTomato positive myelinated axons immunolabeled for myelin basic protein (MBP) (green) in the ipsilateral striatum. Right: magnified view of myelinated tdTomato positive axons. K) Cross-section of myelinated axons containing tdTomato indicated by the thin white rectangle in J. Data are mean ± SEM, KS test (Kolmogorov-Smirnov test), **** $p < 0.0001$. Also see Supplementary Video 1.

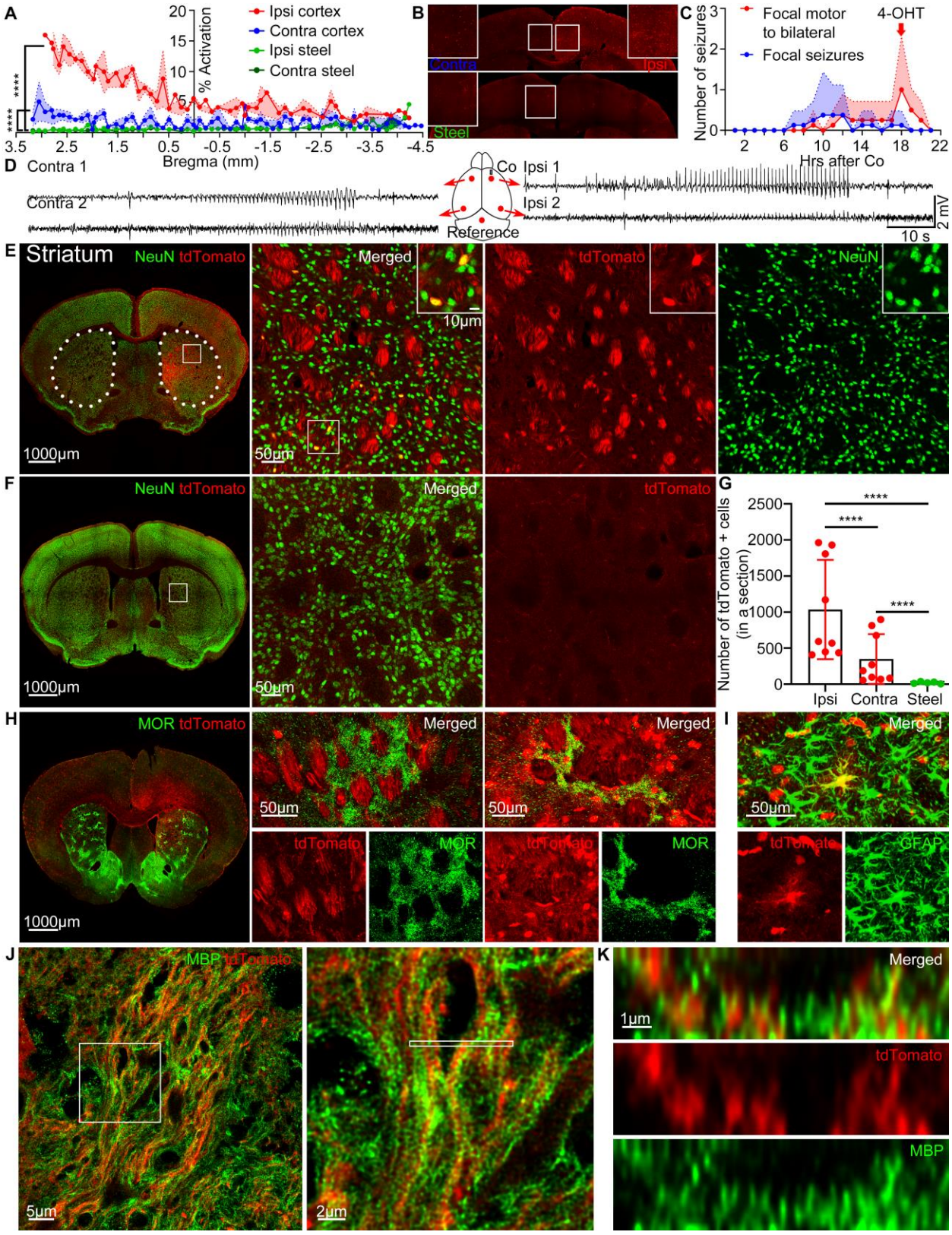
A
Ipsi cortex
Contra cortex
Ipsi steel
Contra steel
% Activation
Bregma (mm)
B
Contra
Ipsi
Steel
C
Focal motor to bilateral
Focal seizures
4-OHT
Number of seizures
Hrs after Co
D
Contra 1
Contra 2
Co
Ipsi 1
Ipsi 2
Reference
2 mV
10 s
E
Striatum
NeuN tdTomato
Merged
tdTomato
NeuN
10µm
1000µm
50µm
F
NeuN tdTomato
Merged
tdTomato
1000µm
50µm
G
Number of tdTomato + cells (in a section)
Ipsi
Contra
Steel
H
MOR tdTomato
Merged
tdTomato
MOR
1000µm
50µm
I
Merged
tdTomate
GFAP
50µm
J
MBP tdTomato
5µm
2µm
K
Merged
tdTomato
MBP
1µm

Figure 3-1

mice had no seizures and showed minimal cortical tdTomato expression (Figure 3-1A,B).

The dorsal striatum strongly expressed tdTomato (Figure 3-1E). The ipsilateral striatum to the seizure focus expressed more tdTomato positive cells than contralateral (Figure 3-1E,G). The graph (Figure 3-1G) represents the average number of tdTomato positive cells on a 40 μm section across sequential striatal sections in a mouse, where each point is the average value for a separate mouse. The striatum of the control mice had fewer tdTomato positive cells compared to both the ipsilateral and contralateral striatum of the mice with seizures (Figure 3-1F,G). tdTomato was observed throughout the whole striatum from the anterior to the posterior sections. Neurons in the striatum expressed tdTomato; however, not all neuronal somas were tdTomato positive. We will demonstrate below the electrographic activation of the striatum, which is the result of the neuronal firing. Striatal fiber bundles also expressed tdTomato (Figure 3-1E). Myelinated axon fibers course through the striatum, and our previous studies have suggested that tdTomato can fill axons. We tested whether the fiber bundles were myelinated axons filled with tdTomato, using an antibody against myelin basic protein (MBP) (Figure 3-1J). SP8 super-resolution Lightning microscopy revealed myelin spiraling and wrapping around the tdTomato expressing axons (Figure 3-1J and Supplementary Video 1). The cross-sectional view demonstrated that myelin surrounded each axon containing tdTomato (Figure 3-1K). Additionally, the striatum is made up of the striosomes (also called patches), which express μ opioid receptors (MOR), and the surrounding matrix (24). Both limbic and sensorimotor cortical areas project to the striosomes and matrix, but the striosomes receive more inputs from limbic cortical regions (25). The striosomes did not express tdTomato (Figure 3-1H). Only rare occasional striosomes close to the midline were tdTomato positive (Figure 3-1H). We also found a few tdTomato positive cells that did not colocalize with NeuN. Astrocytes are known to play a role in ictogenesis (26). To visualize astrocytes, we used the anti-GFAP antibody and found few astrocytes that expressed tdTomato (Figure 3-1I).

Seizures activate the indirect basal ganglia pathway neurons

We conducted a series of experiments to investigate whether focal motor to bilateral tonic-clonic seizures activate the indirect (dopamine receptor D2-expressing) or direct

(dopamine receptor D1-expressing) pathway. D2 agonists exert anticonvulsant action and suppress pilocarpine and kindled seizures (12,27), whereas D1 agonists and D2 antagonists are pro-convulsant (28). Patients taking high-affinity D2 antagonists for schizophrenia or psychosis have a higher risk of seizures (29-32). However, these studies demonstrate D2 receptor modulation of seizures and do not report activation of the striatum or activation of the medium spiny neurons during seizures.

We used a highly selective full D2 agonist, sumanirole, to determine if modulation of the indirect pathway would be protective against Co-induced seizures. Sumanirole has more than 200-fold selectivity for the D2 receptors over other dopamine receptor subtypes and a sustained effect for at least 2 hours with onset starting around 30 min post-injection in rodents (33-37). Because dopamine receptors D2 are also highly expressed in the cortex in addition to the medium spiny neurons of the indirect pathway, we injected sumanirole directly into the anterior striatum via a bilateral cannula. After implanting C57BL/6 mice with cobalt, they received one blinded injection of either sumanirole (10 µg/injection per lobe in aCSF) or aCSF 18 hours after cobalt insertion via a bilateral cannula and were monitored via video/EEG for another 10 hours (Figure 3-2A,D). After the injection, both groups of mice did not have a noticeable behavioral or electrographic change and continued having spike-wave discharges after cobalt insertion (Figure 3-2B). None of the sumanirole injected mice experienced seizures during 2.5 hours following the injection as determined by a blinded investigator, whereas the aCSF injected mice had more seizures (Figure 3-2C), which indicates that the D2 receptor agonist is anticonvulsant in cobalt-induced seizures.

It is unknown whether seizures activate the indirect or direct pathway. We wanted to quantitatively assess whether the tdTomato positive medium spiny neurons expressed either D2 or D1 receptors in the striatum. The entire striatum of TRAP mice after a seizure was serially sectioned and immunolabeled for D2 and D1 receptors (Figure 3- 2E,F) (38). Around 80% of all activated neurons in the striatum expressed DRD2 in the ipsilateral and contralateral striatum and not DRD1 (Figure 3-2I). The proportion of activated DRD2 versus DRD1 positive neurons remained constant throughout the striatum from the anterior to posterior sections, suggesting no rostrocaudal gradient (Figure 3-2J).

Figure 3-2. Seizures activate the indirect basal ganglia pathway neurons. A) C57BL/6 mice were implanted with cobalt and a bilateral cannula. Sumanirole or aCSF was injected via a bilateral cannula into the striatum at 18 hrs after Co (red arrow). The number of seizures was counted by a blinded experimenter before the injection (15-18 hrs after Co), following (18-20.5 hrs after Co), and after the injection (20.5-23.5 hrs after Co). B) A representative EEG 20 min after bilateral sumanirole injection into the striatum. C) The effect of either sumanirole (red) or aCSF (green) injection (red arrow) on the number of seizures before the injection (15-18 hrs after Co) (sum per mouse, n = 5 mice): D2 agonist: 2.2 ± 0.58, aCSF: 2.4 ± 0.87, (KS test), following the injection (18-20.5 hrs after Co): D2 agonist: 0.0 ± 0.0, aCSF: 1.4 ± 0.68 ($p = 0.0476$, KS test), and after the injection (20.5-25.5 hrs after Co): D2 agonist: 2.2 ± 0.37, aCSF: 2.0 ± 0.45 (unpaired t-test). D) Light microscope image of the traces left from the bilateral cannula targeting dorsal anterior striatum (red arrows). E) DRD2 (green) and tdTomato (red) expression in the striatum. (F) DRD1 (green) and tdTomato expression in the striatum. G) ENK (green) and tdTomato expression in the striatum. Boxed inset: tdTomato positive neurons colocalized with ENK. H) DYN (green) and tdTomato expression in the striatum. Boxed inset: the majority of tdTomato positive neurons did not colocalize with DYN. I) % Colocalization of tdTomato positive cells with either DRD2 or DRD1 in the striatum. Colocalization of tdTomato with: DRD2 in the ipsilateral striatum (red): 79.71 ± 1.857%; DRD2 in the contralateral striatum (blue): 78.40 ± 2.542%; DRD1 in the ipsilateral striatum (green): 10.93 ± 1.085%; DRD1 in the contralateral striatum (black): 11.55 ± 1.736%, (n = 4-5 mice). J) Point line graph of the data in (I) across bregma from the anterior (1.6 mm) to posterior (-0.8 mm) striatum. K) % Colocalization of tdTomato positive cells with either ENK or DYN in the striatum. Colocalization of tdTomato with: ENK in the ipsilateral striatum (red): 79.46 ± 1.158 %; ENK in the contralateral striatum (blue): 75.09 ± 2.092 %; DYN in the ipsilateral striatum (green): 15.43 ± 1.170 %; DYN in the contralateral striatum (black): 21.12 ± 0.3507 %, (n = 3 mice).

Data are mean ± SEM, KS test (Kolmogorov-Smirnov test), n.s. non-significant, * $p < 0.05$.

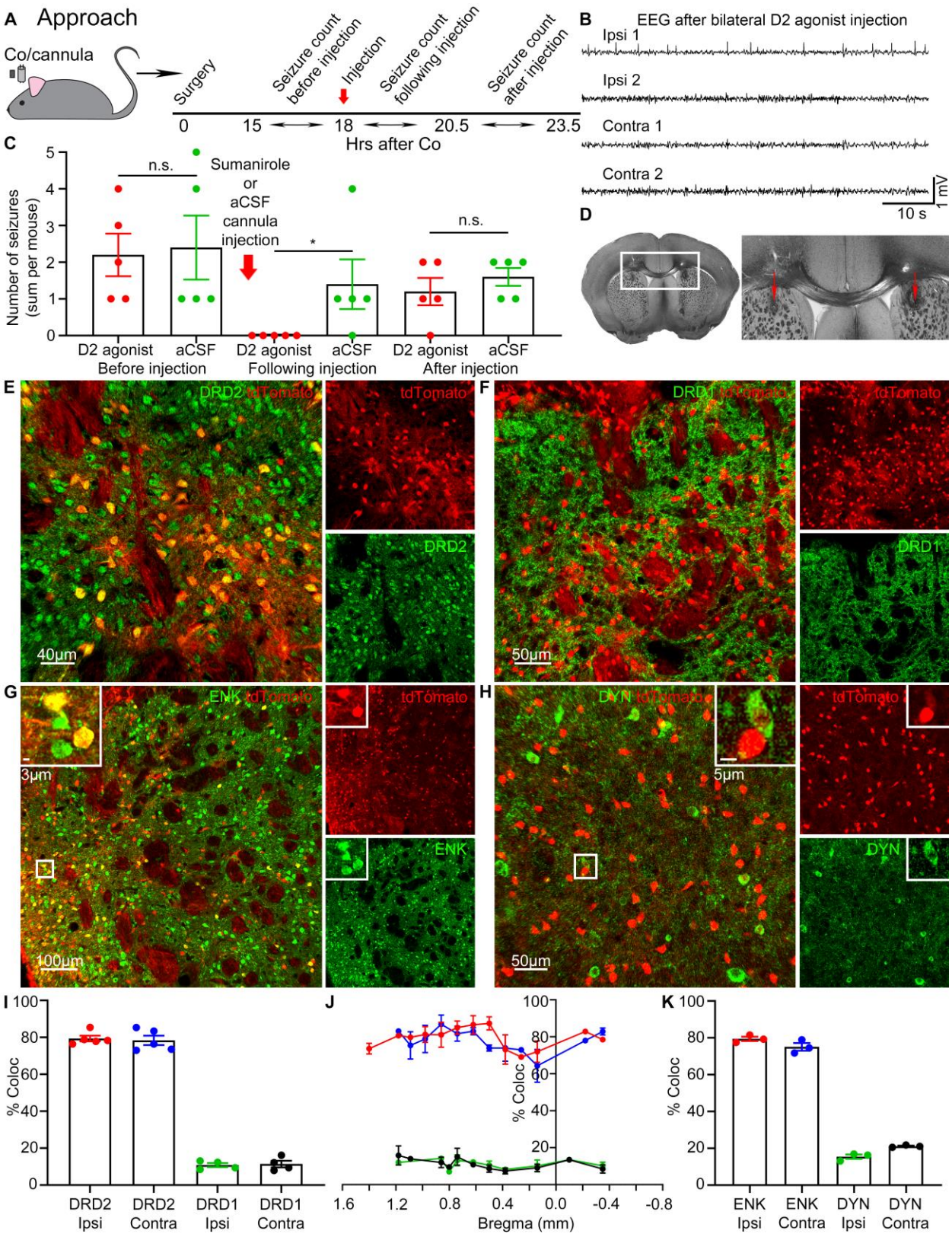
A Approach
Co/cannula
Surgery
Seizure count before injection
Injection
Seizure count following injection
Seizure count after injection
0
15
18
20.5
23.5
Hrs after Co
B
EEG after bilateral D2 agonist injection
Ipsi 1
Ipsi 2
Contra 1
Contra 2
1 mV
10 s
C
Number of seizures (sum per mouse)
n.s.
Sumanirole or aCSF cannula injection
*
n.s.
D2 agonist
aCSF
Before injection
Following injection
After injection
D
E
DRD2 tdTomato
tdTomato
DRD2
40µm
F
DRD1 tdTomato
tdTomato
DRD1
50µm
G
ENK tdTomato
tdTomato
ENK
3µm
100µm
H
DYN tdTomato
tdTomato
DYN
5µm
50µm
I
% Coloc
DRD2 Ipsi
DRD2 Contra
DRD1 Ipsi
DRD1 Contra
J
% Coloc
Bregma (mm)
K
% Coloc
ENK Ipsi
ENK Contra
DYN Ipsi
DYN Contra

Figure 3-2

We performed confirmatory experiments by immunolabeling for enkephalin and dynorphin (Figure 3-2G,H). The majority of indirect pathway neurons express enkephalin (ENK), whereas the majority of the direct pathway medium spiny neurons express substance P and dynorphin (DYN) (39,40). Similarly, around 80% of all activated neurons in the striatum expressed ENK and not DYN, which indicates preferential activation of the indirect pathway neurons (Figure 3-2K).

Dopamine receptors are expressed on the neuronal membrane, and tdTomato expression is intracellular (41). False positives are possible due to other labeled cells lying on top within a 40 μm section. To counter this problem, we carried out SP8 super-resolution STED microscopy imaging of triple labeled sections with anti-DRD2 and anti-DRD1 antibodies. Super-resolution microscopy confirmed that tdTomato positive cells express DRD2 and not DRD1 (Figure 3-3). We also found examples of membranous, nuclear, and cytoplasmic expression of DRD2 (Figure 3-3A-C).

Activation of the GPe, STN, and SNR in addition to the thalamus

Next, we investigated the activity of the striatal projection targets. The indirect pathway D2 medium spiny neurons project to the globus pallidus externus (GPe), subthalamic nucleus (STN), and substantia nigra pars reticulata (SNR), whereas the direct pathway D1 medium spiny neurons project to the globus pallidus internus (GPi) and SNR. The direct and indirect pathways are segregated (10,29,42-49).

The Paxinos Brain Atlas does not distinguish between the external and internal segments of the globus pallidus in a mouse brain (50). Therefore, we adopted the online Allen Brain Reference Atlas distinction between GPe and GPi, which shows the GPe located medial to the posterior striatum and lateral to the septum and internal capsule. The GPi is posterior relative to the GPe, where the hippocampus first appears, medial to the GPe, and lateral to the reticular thalamic nucleus and internal capsule. Parvalbumin (PV) immunolabeling allowed easy visualization of the location of the reticular thalamic nucleus and GPe (up to 59% of all GPe neurons express PV) (51-54).

The GPe, a part of the indirect pathway, strongly expressed tdTomato (Figure 3-4A,C). Neurons expressed tdTomato in the ipsilateral GPe to the seizure focus, which had more tdTomato positive cells than the contralateral (Figure 3-4A,E). The GPe of the control mice had fewer tdTomato positive cells compared to both the ipsilateral and

Figure 3-3. Activated cells in the striatum express DRD2 but not DRD1. A) SP8 super-resolution STED image shows tdTomato positive cells (red) express DRD2 (green) but not DRD1 (blue) on the neuronal membrane in the striatum. B) STED image shows tdTomato positive cells express DRD2 (green) but not DRD1 (blue) inside the nucleus in the striatum. C) Left: LSM 980 Airyscan 2 image shows tdTomato positive cells express DRD2 (green) in the striatum. Right: magnified view of cytoplasmic DRD2.

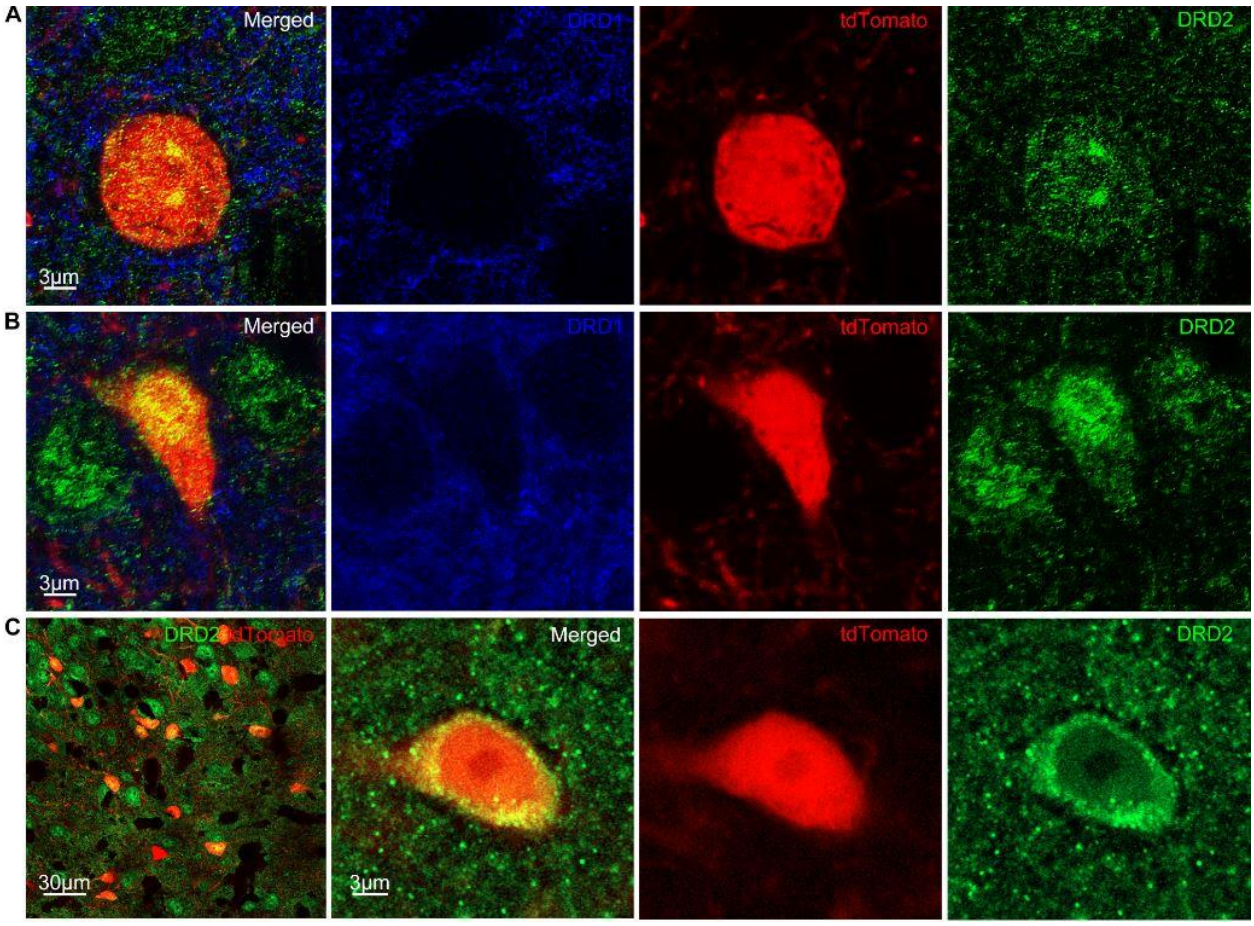
A
Merged
DRD1
tdTomato
DRD2
3μm
B
Merged
DRD1
tdTomato
DRD2
3μm
C
DRD2tdTomato
Merged
tdTomato
DRD2
30μm
3μm

Figure 3-3

Figure 3-4. Activation of the GPe of the indirect pathway but not GPi of the direct pathway. (A) tdTomato (red) expression in the globus pallidus externus (GPe) immunolabeled for NeuN (green) and its magnified view. Boxed inset: tdTomato positive neurons colocalized with NeuN. (B) tdTomato expression in arkypallidal GPe neurons immunolabeled for preproenkephalin (ppENK, green). (C) tdTomato expression in the GPe immunolabeled for PV (green) and its magnified view. Dotted lines indicate nuclear boundaries: str, striatum; RTN, reticular thalamic nucleus; int, internal capsule. (D) Left: steel wire control showed minimal tdTomato expression in the GPe. Right: magnified view of the GPe. (E) Cobalt implanted mice had more tdTomato positive cells in both the ipsilateral and contralateral GPe compared to the steel wire implanted mice (each point is the average number of cells in a 40 μm section across sequential GPe sections in a mouse) (ipsilateral: 17.81 ± 2.778 cells, unpaired t-test; contralateral: 9.329 ± 2.553 cells, $p = 0.0109$, unpaired t-test; control: 7.118 ± 2.550 cells; n = 5 mice). The ipsilateral GPe had more tdTomato positive cells than the contralateral in mice with seizures (unpaired t-test). (F) Left: minimal tdTomato expression in the globus pallidus internus (GPi) during seizures immunolabeled for PV (green). Right: magnified view of the GPi. Dotted lines indicate nuclear boundaries. (G) Left: steel wire control showed minimal tdTomato expression in the GPi. Right: magnified view of the GPi. (H) Cobalt implanted mice had similar tdTomato expression in both the ipsilateral and contralateral GPi as the control mice (each point is the average number of cells in a 40 μm section across sequential GPi sections in a mouse) (ipsilateral: 3.400 ± 1.439 cells, unpaired t-test; contralateral: 2.033 ± 1.096 cells, unpaired t-test; control: 2.448 ± 0.8656 cells; n = 5 mice). The number of tdTomato positive cells in the ipsilateral and contralateral GPi was similar (unpaired t-test). Data are mean ± SEM, n.s. non-significant, * $p < 0.05$, **** $p < 0.0001$.

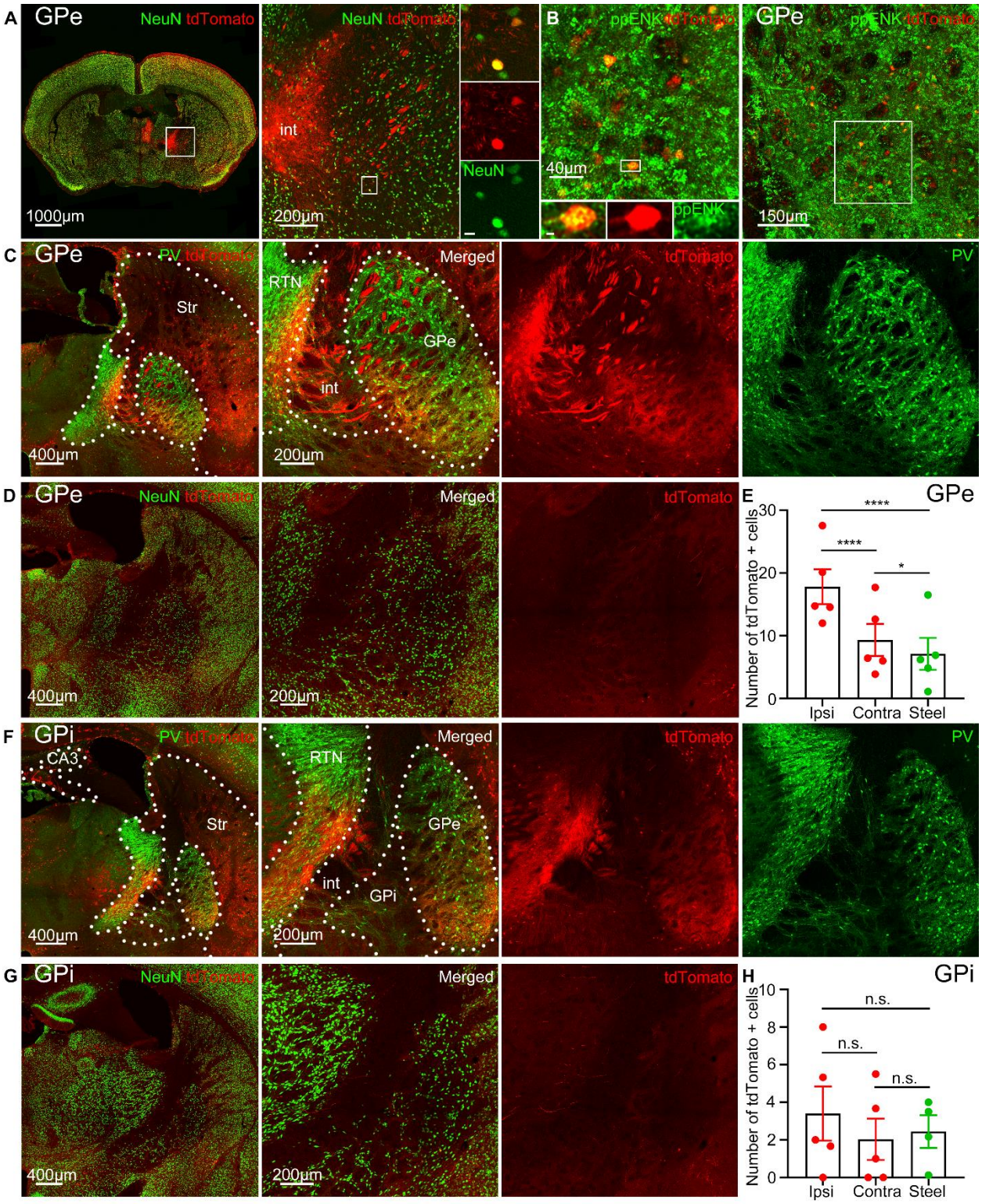
A
GPe
NeuN tdTomato
1000μm
NeuN tdTomato
int
200μm
NeuN
B
ppENK tdTomato
40μm
ppENK
GPe
ppENK tdTomato
150μm
C
GPe
PV tdTomato
Str
400μm
Merged
RTN
GPe
int
200μm
tdTomato
PV
D
GPe
NeuN tdTomato
400μm
Merged
200μm
tdTomato
E
GPe
Number of tdTomato + cells
****
****
*
Ipsi
Contra
Steel
F
GPi
PV tdTomato
CA3
Str
400μm
Merged
RTN
GPe
int
GPi
200μm
tdTomato
PV
G
GPi
NeuN tdTomato
400μm
Merged
200μm
tdTomato
H
GPi
Number of tdTomato + cells
n.s.
n.s.
n.s.
Ipsi
Contra
Steel

Figure 3-4

contralateral GPe of the mice with seizures (Figure 3-4D,E). Not only neurons but also axonal fibers in the GPe were tdTomato positive (Figure 3-4A,C). There are two types of GPe neurons, prototypic (PV positive that project to the STN) and arkypallidal (FoxP2 and preproenkephalin positive that project to the striatum) (55). Prototypic cells inhibit arkypallidal, and the STN is reciprocally connected and provides excitatory input to both cell types. We found that almost none of the PV neurons in the GPe expressed tdTomato (Figure 3-4C), suggesting that seizures do not activate prototypic GPe cells. We immunolabeled GPe for arkypallidal neurons with anti-preproenkephalin antibody and found that almost all of the tdTomato cells in GPe were arkypallidal (Figure 3-4B). It was recently reported that activation of the indirect (D2) medium spiny neurons inhibits prototypic cells, disinhibiting the STN and arkypallidal cells (55). However, it is possible that GPe arkypallidal neurons were activated directly from the cortex.

The GPi, a part of the direct pathway, had similar tdTomato expression as the background activity of the controls (Figure 3-4F-H). Both the ipsilateral and contralateral GPi in mice with seizures had a similar number of tdTomato-expressing cells as the GPi of the controls. The number of tdTomato positive cells was also similar in the ipsilateral and contralateral GPi.

The subthalamic nucleus strongly expressed tdTomato in both hemispheres (Figure 3- 5A). The STN is a lens-shaped nucleus that lies below the posterior and ventrobasal thalamic nuclei above the cerebral peduncle and receives GABAergic projections from the GPe as a part of the indirect pathway. Both the ipsilateral and contralateral STN of mice with focal motor to bilateral tonic-clonic seizures had more tdTomato-expressing cells than the STN of the controls (Figure 3-5B,C). The number of tdTomato positive cells in the ipsilateral STN was similar to that in the contralateral STN (Figure 3-5C).

The substantia nigra pars reticulata also expressed tdTomato (Figure 3-5D). Located laterally to the mammillary nuclei, SNR receives GABAergic projections from the striatum via the direct pathway and glutamatergic projections from the STN via the indirect pathway, while sending GABAergic projections to the motor thalamic nuclei such as the ventrolateral and ventromedial (56). Both the ipsilateral and contralateral SNR had more tdTomato expressing neurons than the SNR of the controls (Figure 3-

Figure 3-5. Seizures activate the subthalamic nucleus and substantia nigra pars reticulata. A) tdTomato expression in the subthalamic nucleus (STN) immunolabeled for NeuN (green) and its magnified view. Boxed inset: tdTomato positive neurons colocalized with NeuN. Dotted lines indicate the STN boundaries. B) Left: steel wire control showed minimal tdTomato expression in the STN. Right: magnified view of the STN. C) Cobalt implanted mice had more tdTomato positive cells in the ipsilateral and contralateral STN compared to the steel wire control mice (each point is the average number of cells in a 40 μm section across sequential STN sections in a mouse) (ipsilateral: 89.90 ± 22.49 cells, unpaired t-test; contralateral: 78.11 ± 25.15 cells, unpaired t-test; control: 2.030 ± 0.5463 cells; n = 5 mice). The number of tdTomato positive cells in the ipsilateral STN was similar to that in the contralateral (unpaired t-test). D) tdTomato expression in the substantia nigra pars reticulata (SNR) immunolabeled for NeuN (green) and its magnified view. Boxed inset: tdTomato positive neurons colocalized with NeuN. Dotted lines indicate the SNR boundaries. E) Left: steel wire control showed minimal tdTomato expression in the SNR. Right: magnified view of the SNR. F) Cobalt implanted mice had more tdTomato positive cells in both ipsilateral and contralateral SNR compared to the steel wire implanted mice (each point is the average number of cells in a 40 μm section across sequential SNR sections in a mouse) (ipsilateral: 20.65 ± 4.580 cells, $p = 0.0005$, unpaired t-test; contralateral: 10.36 ± 1.704 cells, $p = 0.0029$, unpaired t-test; control: 4.688 ± 1.985 cells; n = 4 mice). The ipsilateral SNR had more tdTomato positive cells than the contralateral in mice with seizures ($p = 0.0010$, unpaired t-test). Data are mean ± SEM, n.s. non-significant, ** $p < 0.01$, *** $p < 0.001$, **** $p < 0.0001$.

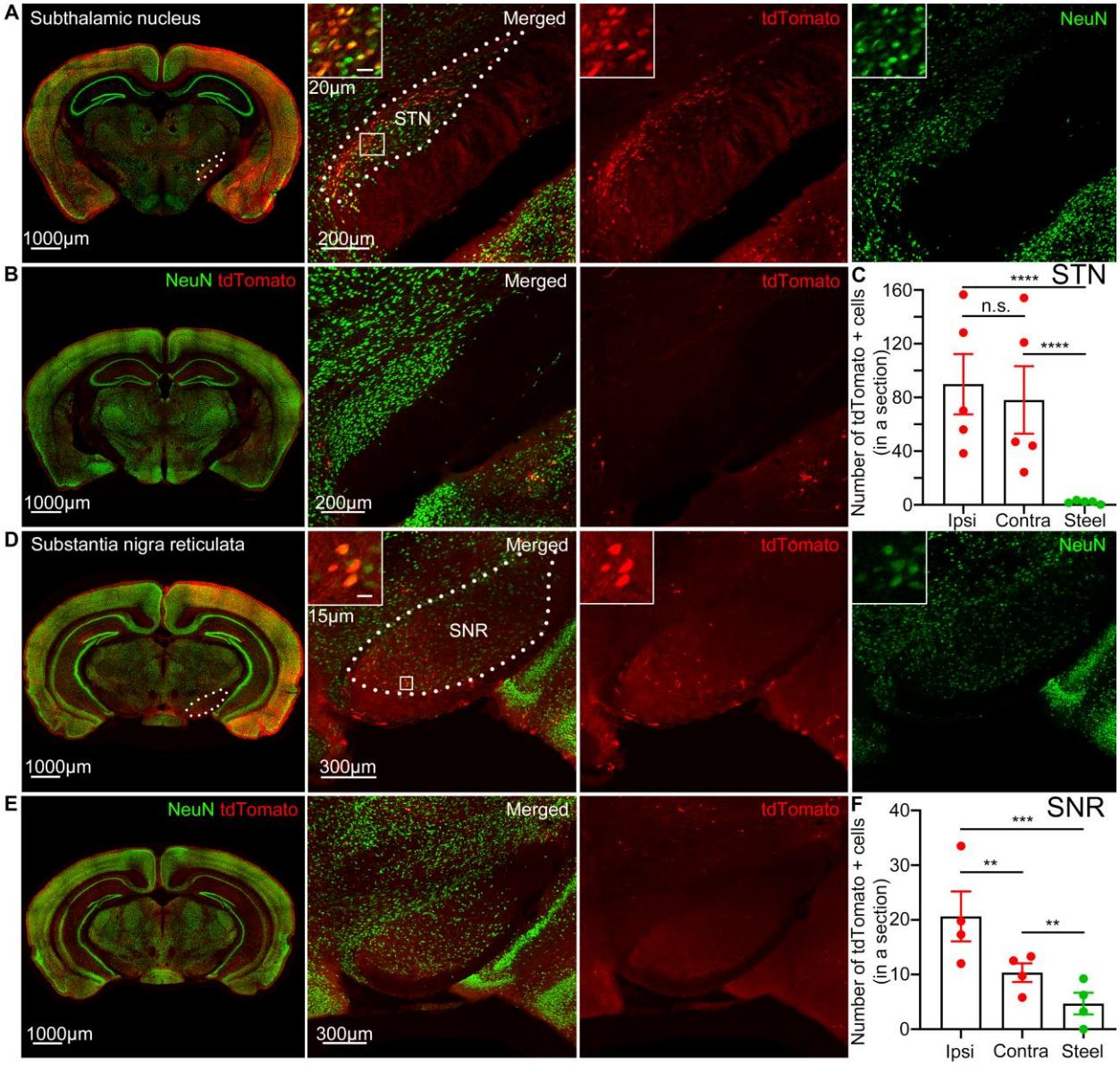
A
Subthalamic nucleus
1000μm
Merged
20μm
STN
200μm
tdTomato
NeuN
B
NeuN tdTomato
1000μm
Merged
200μm
tdTomato
C
STN
Number of tdTomato + cells (in a section)
160
120
80
40
0
****
n.s.
****
Ipsi
Contra
Steel
D
Substantia nigra reticulata
1000μm
Merged
15μm
SNR
300μm
tdTomato
NeuN
E
NeuN tdTomato
1000μm
Merged
300μm
tdTomato
F
SNR
Number of tdTomato + cells (in a section)
40
30
20
10
0
***
**
**
Ipsi
Contra
Steel

Figure 3-5

5D-F). The ipsilateral SNR had more tdTomato expressing cells than the contralateral (Figure 3-5F).

Motor thalamic nuclei also expressed tdTomato (Figure 3-6A). The motor thalamus consists of the ventroanterior/ventrolateral (VA/VL) and ventromedial (VM) nuclei. These nuclei receive reciprocal projections from the motor cortex and GABAergic inhibitory projections from the SNR (56,57). Motor thalamic nuclei VL/VM ipsilateral to the seizures focus were active and expressed more tdTomato positive cells than the contralateral or VL/VM of the control mice without seizures (Figure 3-6A-D). Ipsilateral centromedian (CM) (58), mediodorsal (MD), and anterior reticular thalamic (RTN) nuclei were tdTomato positive as well (Figure 3-6A,E,F and 4F).

Electrographic activation of the basal ganglia during seizures

The TRAP technique has limited temporal resolution, so we recorded local field potentials (LFP) from the premotor cortex, motor thalamic nucleus VL, striatum, and substantia nigra pars reticulata simultaneously. We selected the VL because of its larger size compared to other motor thalamic nuclei and, thus, easier electrode targeting. Custom made array of microelectrodes recorded local field potentials at a 10 kHz sampling rate, which allowed us to detect seizure spread with millisecond precision (Figure 3-7A). To establish that the source of electrical activity recorded from one microelectrode was independent of that from a neighboring microelectrode, we analyzed the cross-correlation of activities recorded from two neighboring electrodes. The cross-correlation has to be less than 0.7 for the activities to be considered independent. Microelectrodes with 60-75 kΩ resistance and 2 cm length yielded recording without significant cross-contamination (less than 0.7) (Figure 3-7B). The location of the electrodes was marked by applying a single burst of 40 μA, 0.75 ms monophasic square wave pulse at 50 Hz for 30 s after the recordings were complete. The data were analyzed only if the electrode tip location was correct (Figure 3-7C).

Simultaneous LFP recordings from the premotor cortex, VL, striatum, and SNR ipsilateral to the seizure focus confirmed that focal motor to bilateral tonic-clonic seizures indeed activate these structures (Figure 3-7D). Seizures, consisting of rhythmic spike-wave discharges mixed with low amplitude fast (gamma) activity, were recorded from each of these structures. Next, we compared seizure onset time in each structure

Figure 3-6. Seizures activate motor thalamic nuclei. A) Top: tdTomato expression in the thalamus immunolabeled for NeuN (green). Bottom: magnified view of the thalamus. Boxed inset (white arrow): tdTomato positive neurons colocalized with NeuN. Dotted lines indicate nuclear boundaries: CM, centromedian; MD, mediodorsal; VM, ventromedial; VL, ventrolateral; RTN, reticular thalamic nucleus; ZI, zona incerta. (B) Top: steel wire control showed minimal tdTomato expression in the thalamus. Bottom: magnified view of the thalamus. (C to F) Number of tdTomato positive cells in cobalt implanted mice (red) compared to the steel wire implanted mice (green) in the thalamic nuclei VL, VM, MD, and CM (either on the ipsilateral (Ipsi) or contralateral (Contra) side to the seizure focus or, in the case of the CM, in the whole nucleus (Seizure)), (each point is the average number of cells in a 40 μm section across sequential nuclear sections in a mouse) (VL: ipsilateral: 54.77 ± 17.17 cells, p = 0.0006, unpaired t-test; contralateral: 9.667 ± 6.850 cells, unpaired t-test; control: 5.183 ± 1.417 cells; n = 5 mice; the ipsilateral VL had more tdTomato positive cells than the contralateral (p = 0.0194, unpaired ttest); VM: ipsilateral: 29.55 ± 8.469 cells, p = 0.0008, KS test; contralateral: 1.833 ± 0.7472 cells, KS test; control: 1.508 ± 0.7932 cells; n = 5 mice; the ipsilateral VM had more tdTomato positive cells than the contralateral (p = 0.0033, unpaired t-test); MD: ipsilateral: 211.6 ± 58.51 cells, p = 0.0006, KS test; contralateral: 22.65 ± 7.437 cells, p = 0.0006, KS test; control: 2.749 ± 0.8787 cells; n = 5 mice; the ipsilateral MD had more tdTomato positive cells than the contralateral (unpaired t-test); CM: whole nucleus (Seizure): 91.97 ± 13.07 cells, p = 0.0002, unpaired t-test; control: 7.778 ± 2.338 cells; n = 5 mice). Data are mean ± SEM, KS test (Kolmogorov-Smirnov test), n.s. non-significant, * $p < 0.05$, ** $p < 0.01$, *** $p < 0.001$, **** $p < 0.0001$.

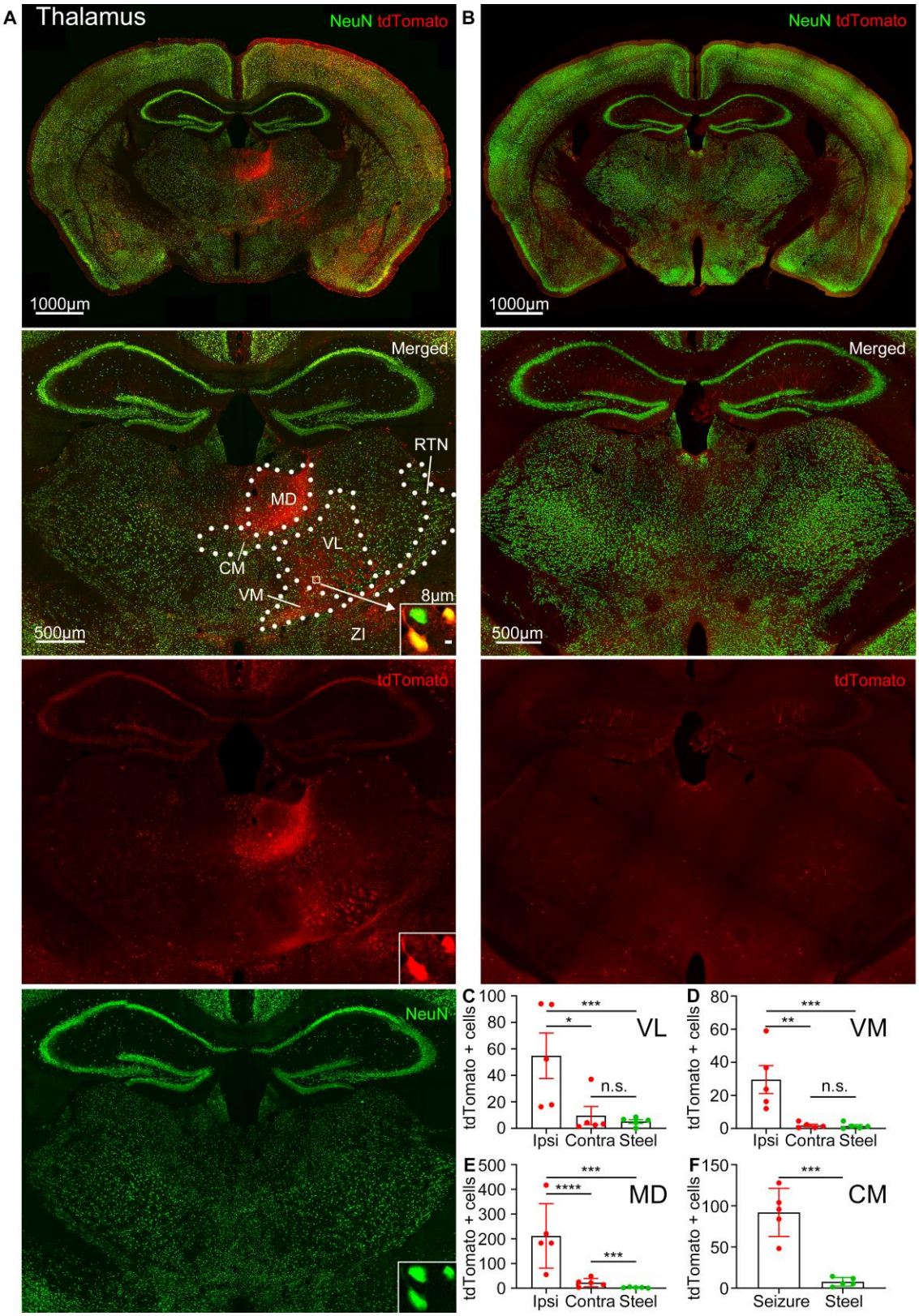
A
Thalamus
NeuN tdTomato
1000μm
B
NeuN tdTomato
1000μm
Merged
RTN
MD
VL
CM
VM
ZI
8μm
500μm
Merged
500μm
tdTomato
tdTomato
NeuN
C
VL
tdTomato + cells
***
*
n.s.
Ipsi Contra Steel
D
VM
tdTomato + cells
***
**
n.s.
Ipsi Contra Steel
E
MD
tdTomato + cells
***
****
***
Ipsi Contra Steel
F
CM
tdTomato + cells
***
Seizure Steel

Figure 3-6

to the onset time at the seizure focus in the premotor cortex. Surprisingly, some seizures required several hundred milliseconds to arrive at the striatum or SNR; in contrast, other seizures took several seconds to appear in these structures, suggesting two populations based on latency, fast (< 200 ms) and slow (> 200 ms). In recordings from the striatum, 70% of seizures were short latency, and the rest took longer (Figure 3-7F). In the SNR, similarly, 48% of seizures were short latency, and remaining seizures had longer latency (Figure 3-7G). However, all of the seizures required less than 200 ms to arrive at the VL (Figure 3-7E). We found that some seizures required up to around 10 seconds to appear in the striatum or SNR, which suggests that internal inhibition exists within these structures during some seizures, which prevents immediate ictal onset within them.

We also discovered that after seizure invaded the SNR, spike frequency in the cortex and thalamus decreased by half (Figure 3-7H,I). Spike frequency was defined as the number of spikes per second (Figure 3-7I). In long latency seizures during onset delay in the SNR, faster cortical and thalamic spikes were detected, whereas after seizure started in the SNR, cortical and thalamic spike frequency dropped (Figure 3-7D,H), which could be a delayed hyper-synchronized activity in the cortex/thalamus, which is even measurable from the SNR. In short-latency seizures, where seizures started almost simultaneously in the cortex, thalamus, and SNR, no such spike frequency change was noticed, and spike frequency was slower to begin with (Supplementary Figure 3-1). Thus, activation of the basal ganglia circuit modulates seizures. In particular, activation of the SNR exerts an inhibitory effect on thalamocortical projections, inhibiting ongoing movement (59).

Anatomical connections of the seizure focus determine seizure circuit

We hypothesized that anatomical projections of the seizure focus influence seizure propagation, so we tracked both in a single experiment. To trace the efferent connections from the seizure focus, we injected AAV9 GFP virus (AAV9-CamKII0.4.eGFP.WPRE.rBG) in TRAP2 mice at the same coordinates in the premotor cortex two weeks before the cobalt insertion surgery. We injected 4-OHT 90 min after focal to bilateral seizures and clarified either anterior 1/3rd of the whole brain and

Figure 3-7. Activation of the basal ganglia modulates seizures. A) Custom made arrays of LFP microelectrodes that record from the ipsilateral premotor cortex, striatum, VL, and SNR and their dimensions for stereotaxic surgery. (B) A correlation matrix plots the correlation coefficients (from 1.0 to 0) for each pair of structures, which were calculated based on the LFP time lags between the microelectrodes with the dimensions from (A) and 60-75 kΩ resistance. (C) Lesions that were done after the recordings to mark the locations of the microelectrode tips that targeted the VL and SNR (red arrows). (D) Representative simultaneous LFP recordings from the premotor cortex, VL, striatum, and SNR and their corresponding power spectrums. The seizure focus was in the premotor cortex. Red arrows indicate seizure onset time (twice the baseline). Red bars in the striatum and SNR indicate the delay of seizure onset. (E) Seizure onset times (ms) in the ipsilateral VL after the beginning of seizures in the premotor cortex. Pie chart: 100% of seizures required < 200 ms to arrive to the VL from the premotor cortex (blue): 33.0095 ± 3.1550 ms, n = 63 seizures from 16 mice. (F) Seizure onset times (ms or s) in the ipsilateral striatum after the beginning of seizures in the premotor cortex. Pie chart: 70% of seizures required < 200 ms to arrive to the striatum from the premotor cortex (blue): 19.6643 ± 3.5197 ms, n = 28 seizures from 8 mice, and 30% of seizures required > 200 ms (red): 5.7125 ± 1.1929 s, n = 12 seizures from 4 mice. (G) Seizure onset times (ms or s) in the ipsilateral SNR after the beginning of seizures in the premotor cortex. Pie chart: 48% of seizures required < 200 ms to arrive to the SNR from the premotor cortex: 41.8526 ± 5.4110 ms, n = 31 seizures from 12 mice, and 52% of seizures required > 200 ms (red): 6.9970 ± 0.6562 s, n = 33 seizures from 11 mice. (H) Simultaneous LFP recordings from the ipsilateral premotor cortex, VL, and SNR. Spike frequency drops in the premotor cortex and VL after seizure appears in the SNR (red bar and dashed vertical lines). Red arrows indicate seizure onset time. (I) Spike frequency quantification (spikes/sec) in the premotor cortex and VL before

seizure in the SNR (black) and during seizure in the SNR (red) (premotor cortex before seizure in SNR: 2.682 ± 0.1699 spikes/sec; premotor cortex during seizure in SNR: 1.756 ± 0.1782 spikes/sec; $p = 0.0055$, unpaired t test; VL before: 2.866 ± 0.1656 spikes/sec; VL during: 1.687 ± 0.1563 spikes/sec; $p = 0.0079$, KS test; n = 12 seizures from 4 mice). Data are mean ± SEM, ** $p < 0.01$.

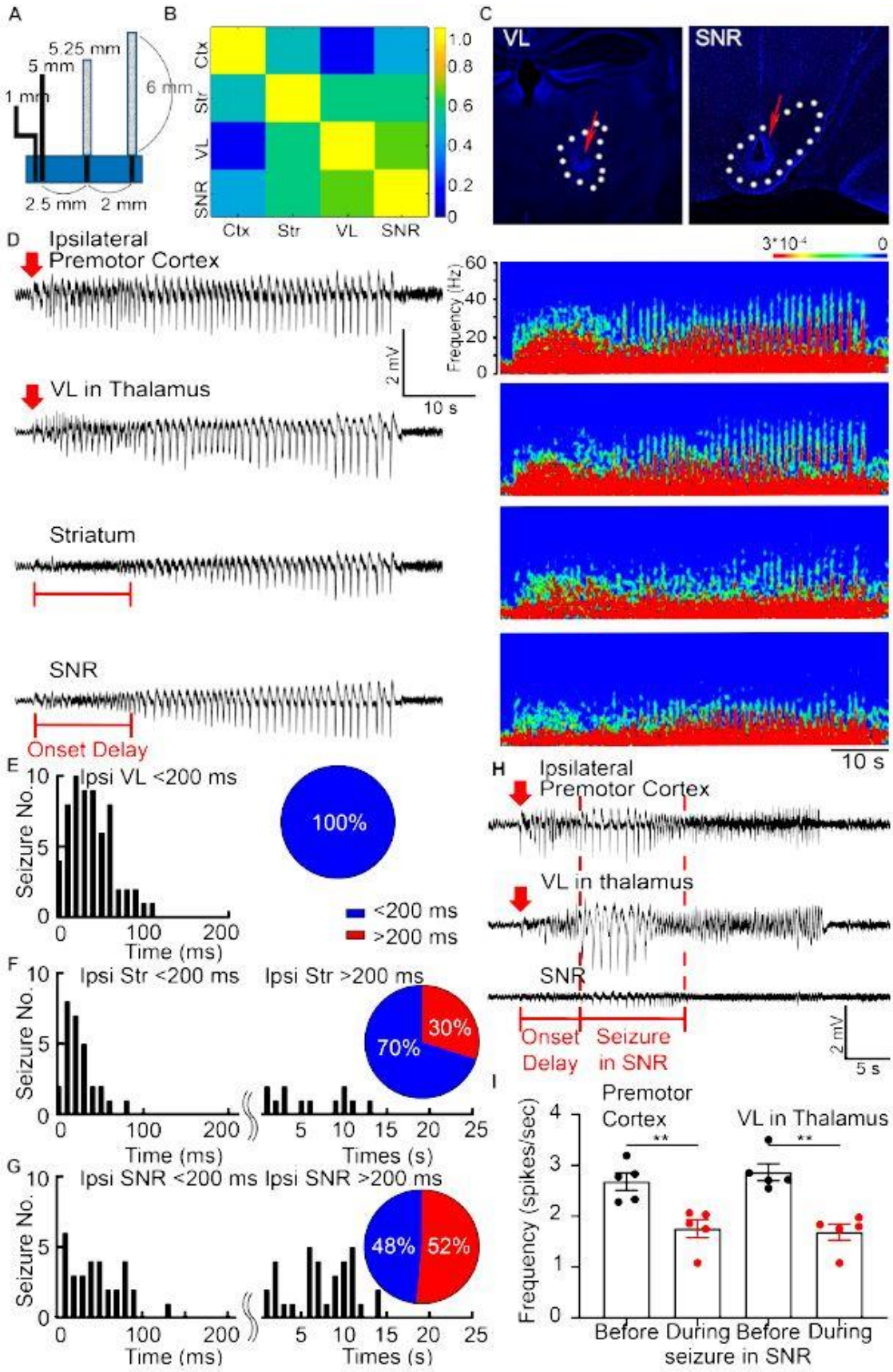
A
5.25 mm
5 mm
1 mm
6 mm
2.5 mm
2 mm
B
Ctx
Str
VL
SNR
1.0
0.8
0.6
0.4
0.2
0
C
VL
SNR
3*10-4
0
D
Ipsilateral
Premotor Cortex
VL in Thalamus
Striatum
SNR
Onset Delay
2 mV
10 s
Frequency (Hz)
60
40
20
0
10 s
E
Ipsi VL <200 ms
Seizure No.
Time (ms)
100%
<200 ms
>200 ms
F
Ipsi Str <200 ms
Ipsi Str >200 ms
70%
30%
Time (ms)
Times (s)
G
Ipsi SNR <200 ms
Ipsi SNR >200 ms
48%
52%
Time (ms)
Times (s)
H
Ipsilateral
Premotor Cortex
VL in thalamus
SNR
Onset Delay
Seizure in SNR
2 mV
5 s
I
Premotor Cortex
VL in Thalamus
**
**
Frequency (spikes/sec)
Before During Before During
seizure in SNR

Figure 3-7

imaged it using a light sheet microscope or clarified 200 μm thick sections, imaged them in tiles, and reconstructed into whole slice images on a confocal microscope (60).

GFP and tdTomato extensively colocalized in the striatum, indicating that seizures followed anatomical projections from the seizure focus (Figure 3-8A). To gain better resolution of the axons expressing both tdTomato and the virus, we used SP8 super-resolution Lightening microscopy to image a single axonal bundle from a horizontal section in the striatum. tdTomato positive axons expressed AAV9-GFP (Figure 3-8B and Supplementary Video 2). Thick 200 μm clarified sections revealed how GFP and tdTomato positive axons traverse from the ipsilateral anterior to posterior striatum (Figure 3-8D). Not all tdTomato positive axons expressed AAV9-GFP because seizures can travel multiple synapses, whereas this Cre-independent virus has not been reported to transport trans-synaptically (61). Additionally, cortico-cortical spread allowed seizure to reach the striatum from a different cortical location that was not labeled by the virus, and not all of the neurons at the seizure focus could be labeled with AAV9. During focal seizures, LFP recordings indicate that the ipsilateral striatum was also active and synchronized with the cortex because the motor cortex projects directly to the striatum (Supplementary Figure 3-2).

Light-sheet microscopy allowed us to visualize viral spread in a whole unsliced brain of a TRAP mouse after secondarily generalized seizures. Three-dimensional rendering of the brain revealed the structure of AAV9-GFP positive axons that ran posteriorly through the striatum (Figure 3-8C and Supplementary Video 3). GFP and tdTomato also colocalized throughout the ipsilateral GPe (Figure 3-8E). tdTomato positive fibers expressed GFP as they ran dorsally in the GPe, a part of the indirect pathway. AAV9 Cre-independent virus does not cross more than one synapse (61), which means parallel projections exist directly from the motor cortex to the GPe in addition to the striatal projections to the GPe. Previous literature supports that the direct cortico-pallidal projections exist (62-64).

Next, we injected Cre-driven AAV9 pCAG-FLEX-EGFP-WPRE in TRAP2 mice at the seizure focus, so that the virus would only be expressed in activated neurons and axons. We found GFP and tdTomato colocalization in the striatum and GPe (Figure 3-

Figure 3-8. Anatomical connections of the seizure focus influence seizure circuit. A) Left: a horizontal section shows AAV9-CamKII0.4.eGFP.WPRE.Rbg virus (green) labeling anatomical projections of the seizure focus in the premotor cortex and tdTomato expression (red) after focal motor to bilateral tonic-clonic seizure. Right: magnified view of the viral expression in the striatum ipsilateral to the seizure focus. Boxed inset: colocalization of tdTomato positive axons and AAV9-GFP. B) Left: SP8 super-resolution Lightning microscopy image of a horizontal axonal bundle in the striatum that expresses AAV9-GFP and tdTomato. Right: magnified view of the axonal bundle. Boxed insets: colocalization of tdTomato positive axons and AAV9-GFP. C) Light sheet microscopy 3D image of one-third of clarified brain that expresses AAV9-GFP from the seizure focus and tdTomato. White arrow indicates striatal axons that run posteriorly from the seizure focus. D) Left: clarified 200 μm section of the striatum that expresses AAV9-GFP and tdTomato in the striatum. Right: magnified view of the striatum. Boxed insets: tdTomato positive axons colocalized with AAV9-GFP. E) Clarified 200 μm section of the GPe that expresses AAV9-GFP and tdTomato. Boxed insets: tdTomato positive fibers colocalized with AAV9-GFP. F) Cre-driven AAV9 (pCAG-FLEX-EGFP-WPRE) was injected in TRAP2 mice at the seizure focus in the premotor cortex. The striatum and GPe expressed Cre-driven virus as well as the cerebral peduncle (cp) and zona incerta (ZI) near STN and SNR. Also see Supplementary Video 2 and 3.

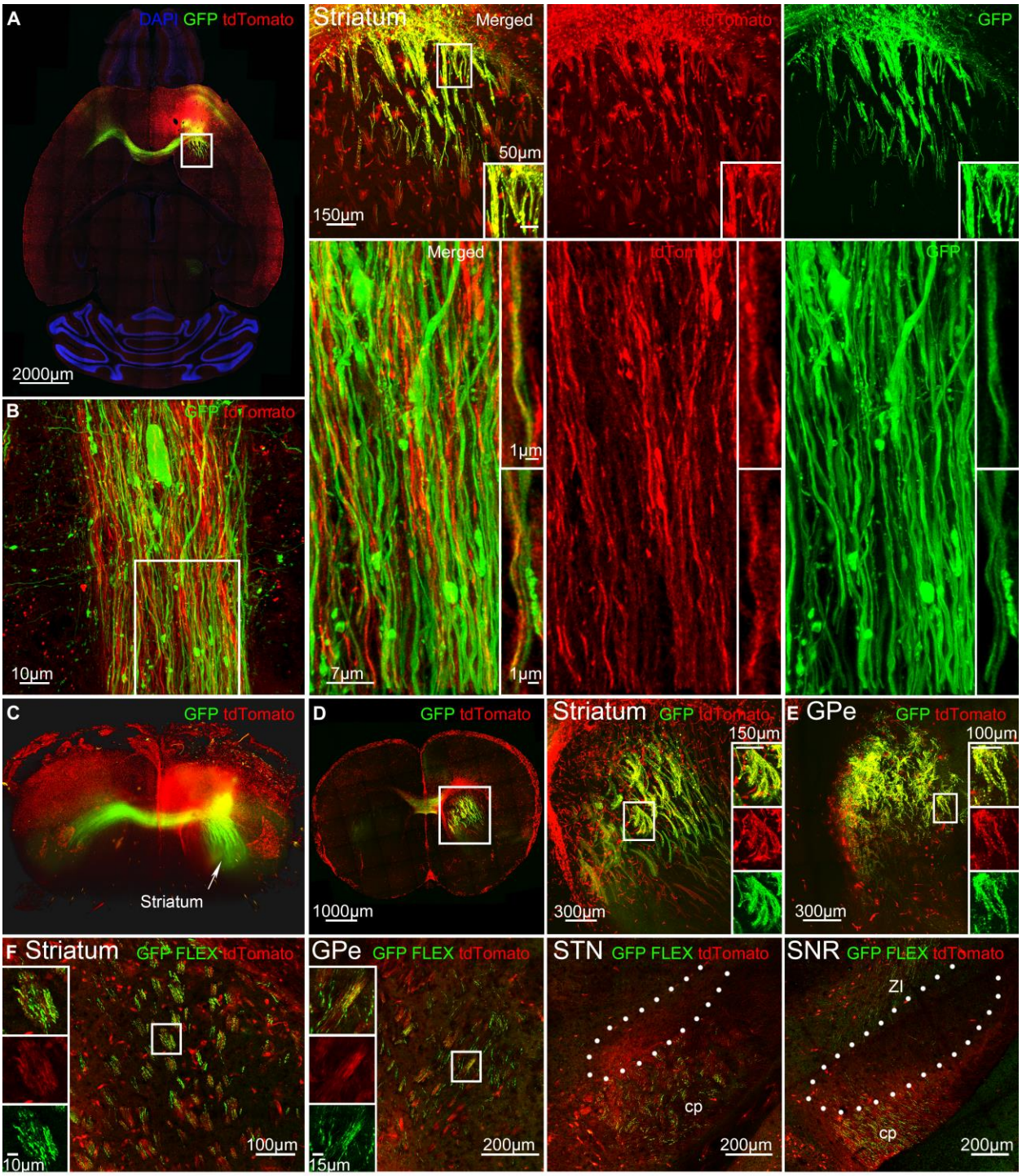
A
DAPI GFP tdTomato
2000µm
Striatum
Merged
50µm
150µm
tdTomato
GFP
Merged
1µm
7µm
1µm
GFP
B
GFP tdTomato
10µm
C
GFP tdTomato
Striatum
D
GFP tdTomato
1000µm
Striatum GFP tdTomato
150µm
300µm
E GPe
GFP tdTomato
100µm
300µm
F Striatum
GFP FLEX tdTomato
100µm
10µm
GPe GFP FLEX tdTomato
200µm
15µm
STN GFP FLEX tdTomato
cp
200µm
SNR GFP FLEX tdTomato
ZI
cp
200µm

Figure 3-8

8F). We did not find viral expression in the GPi, and cerebral peduncle (cp) and zona incerta (ZI) expressed the virus in close proximity to the STN and SNR (Figure 3-8F).

DISCUSSION

Our studies, for the first time, map neuronal activation of the basal ganglia during frontal lobe focal motor to bilateral seizures with unprecedented spatial resolution. This map suggests at least two possibilities that seizures either activate structures of the basal ganglia and indirect pathway neurons directly from the cortex or propagate along the indirect pathway sequentially. Our studies could not distinguish between these two possibilities, so future experiments with calcium imaging, chemogenetics, and other techniques will be necessary to distinguish these possibilities.

We show that seizures originating in the premotor cortex activate anatomically connected structures on the mesoscale and cellular levels: striatum, globus pallidus, subthalamic nucleus, substantia nigra, and the thalamus, which suggests that neuronal connections play a role in seizure spread. We show striatal activation during frontal lobe secondarily generalized tonic-clonic seizures. Furthermore, around 80% of all activated neurons in the striatum during focal to bilateral seizures expressed D2 receptors, and the D2 agonist exerted an anticonvulsant effect. These findings indicate that the indirect system modulates seizures similar to how the physiological activation of the indirect pathway suppresses motor movement (48). The TRAP technique lacks temporal resolution and represents the activity of neurons over approximately 90 min, but seizures occur over 10-180 seconds, a much shorter time scale. Physiological brain activity causes TRAPing of neurons, and the rate of activation of c-Fos can vary from region to region. To complement TRAP spatial resolution and gain temporal resolution, we recorded local field potentials and found that seizures activate structures via short and long latency loops, and activation of the basal ganglia modulates seizures. Seizures originating in the frontal lobe, the second most common site of seizure foci after the temporal lobe, follow the anatomical connections of the motor cortex, so anatomical projections of the epileptic focus influence the seizure circuit.

Hughlings Jackson originally proposed that the motor cortex generates seizures (1), and seminal studies of Jasper and Penfield demonstrated seizure-induced reorganization of the motor cortex (65). The striatum is the key output structure of the motor cortex. Studies in the 1980s suggested that basal ganglia participate in seizures (4,66,67), and dopaminergic drugs modulate them (12). Previous studies also reported

electrographic activation of the striatum during focal and absence seizures (7,8,68) and hyperactivity of striatal neurons after amygdala kindled temporal lobe seizures (69). However, these studies did not provide spatial and temporal resolution of the current study (6,9).

We used the cobalt model to induce frontal lobe secondarily generalized seizures (15-17,19). We selected this model over others for several reasons. The cobalt model provides reliable, spontaneous seizures in more than 90% of animals. The short latency allows us to obtain high fidelity LFP recordings because electrical contacts do not deteriorate. These seizures are consistently associated with focal onset electrographic spike-wave discharges and beta-gamma bursts of activity. Anticonvulsant drugs such as carbamazepine and phenytoin suppress these seizures as they do in human focal motor seizures (70). Although electrical stimulation of the cortex or application of chemiconvulsants (e.g. 4-aminopyridine or penicillin) are also models of focal seizures, these are the models of acute rather than spontaneous seizures and require prolonged electrical stimulation or introduce a bias toward a cortical layer in which seizures originate. Cortical freeze lesion or undercut models do not provide a reliable seizure phenotype, and latency period spans weeks before first seizures appear (71). However, the cobalt model has limitations as well: it creates a lesion near cobalt implantation, seizures stop in 2-3 days, and it is not a model of epileptogenesis. The current study did not investigate epileptogenesis but studied seizure circuits.

We provide direct evidence that motor seizures activate the structures that are anatomically connected to the seizure focus and between each other, suggesting that subcortical seizure spread is influenced by connectivity. Our findings are similar to a previous study that mapped the effects of artificial electrical stimulation of the motor cortex without inducing seizures. Graybiel and colleagues found c-Fos expression in the striatum, GPe, STN, and the reticular thalamic nucleus, but not in the GPi. They found that out of all c-Fos positive cells in the striatum, 75% of them expressed enkephalin, suggesting preferential activation of the indirect pathway over the direct during sensorimotor cortical stimulation without seizures (72).

A recent study of seizure spread from the visual cortex, combining in vivo imaging and electrophysiology, demonstrated that seizures follow anatomical

connections of the visual cortex (73,74). Our studies show that seizures originating in the premotor cortex activate anatomically connected subcortical basal ganglia structures, preferentially activating DRD2 neurons. D2-expressing medium spiny neurons (MSNs) of the indirect pathway are more excitable than D1 MSNs (75). D2 MSNs have a smaller surface area and dendritic trees and a less hyperpolarized resting membrane potential compared to those of D1 MSNs, which explains higher responsiveness of D2 MSNs to current injections (75,76) and, as we find, easier and greater activation of D2 MSNs during seizures. Higher excitability of D2 neurons also suggests that properties of neurons in addition to connectivity determine the pattern of neuronal activation during seizures.

We found strong tdTomato expression in the GPe, yet the striatum sends GABAergic projections and inhibits it. Similarly, motor thalamic nuclei VM/VL expressed tdTomato, but the SNR inhibits VM/VL (56). The activation of the GPe and VM/VL could be explained by the existence of direct, parallel cortico-pallidal and cortico-thalamic projections as indicated by the viral expression in the GPe (Figure 3-8E) and previous studies (57,64). Although activation of the indirect pathway neurons inhibits prototypic GPe neurons, disinhibiting STN and arkypallidal GPe neurons (55) (Figure 3-4B), our study could not distinguish whether the observed activation of these basal ganglia structures is a result of the direct cortical excitation or a sequential flow of excitation through the indirect pathway. Future experimnets will be necessary to address this.

The canonical circuit posits that focal seizures engage the thalamocortical circuit, which leads to secondarily generalized tonic-clonic seizures (77-84). Even though we studied secondarily generalized seizures, we did not investigate the mechanism behind secondary generalization (or bilateral spread). We observed profound activation of the motor and MD thalamic nuclei, which might play a key role in generalized seizures. Here, we report basal ganglia activation on the cellular level in addition to the thalamus, which suggests that seizure circuit might be more complex and driven by the properties of neurons and connectivity with multiple, parallel pathways active.

It is essential to understand the neural circuits supporting these seizures because frontal lobe epilepsy is the second most common type of epilepsy. Repeated generalized tonic-clonic seizures are the leading risk factor for sudden unexpected

death in epilepsy (SUDEP) (85) and lead to fractures and soft tissue injuries (86). Understanding the neuronal circuits that generate and propagate these seizures will allow for the development of novel therapeutic approaches. Injection of an excitatory amino acid derivative N-Methyl-D-aspartate (NMDA) into the striatum protects against limbic pilocarpine seizures, whereas striatal lesioning worsens seizures (87). Low-frequency striatal stimulation had an antiepileptic effect in 57 patients with pharmaco-resistant temporal lobe epilepsy (88,89). Previous studies also suggest that the substantia nigra pars reticulata is critically involved in seizure generalization (5). 14C-2-deoxyglucose metabolic mapping studies found involvement of the SNR in motor seizures (4,67). Infusion of muscimol, GABA receptor agonist, into the SNR produces anticonvulsant effect (66,90), and SNR lesions are anticonvulsant too (91). High-frequency stimulation of the STN also led to a reduction in seizure frequency in patients with drug-resistant epilepsy (92). STN high-frequency stimulation decreases the activity of the SNR and induces its functional inhibition (93,94). Low concentrations of dopamine in the striatum have been shown to produce depolarization and increased frequency of spontaneous firing, whereas high concentrations inhibited spontaneous firing (12). Despite this complex dual effect, D2 agonist or the release of dopamine is thought to reduce activity along the indirect pathway and reduce SNR activity (59), potentially explaining anticonvulsant effect of D2 agonists. During seizures, however, we find activation the STN and SNR.

Our study generates new targets for modulation of seizures by deep brain stimulation (DBS). Currently, patients with refractory epilepsy are treated with the anterior thalamic nucleus and responsive neurostimulation (95). In the future, multiple subcortical structures could be targeted for modulation, stimulation, resection, or medications. Overall, our studies provide the precise neuronal activity map of frontal lobe focal to bilateral tonic-clonic seizures, revealing a richly complex circuit subject to modulation by the basal ganglia.

REFERENCES FOR CHAPTER 3

1. Hughlings Jackson J. The Lumleian Lectures on convulsive seizures. Lancet. 1890; 135(3476):785–8.
2. Shepherd GMG. Corticostriatal connectivity and its role in disease. Nat Rev Neurosci. 2013; 14(4):278–91.
3. Engel J, Wolfson L, Brown L. Anatomical correlates of electrical and behavioral events related to amygdaloid kindling. Ann Neurol. 1978; 3(6):538–44.
4. Lothman EW, Collins RC. Kainic acid induced limbic seizures: metabolic, behavioral, electroencephalographic and neuropathological correlates. Brain Res. 1981; 218(1–2):299–318.
5. Velíšková J, Moshé SL. Update on the role of substantia nigra pars reticulata in the regulation of seizures. Epilepsy Curr. 2006; 6(3):83–7.
6. Blumenfeld H, Varghese GI, Purcaro MJ, et al. Cortical and subcortical networks in human secondarily generalized tonic-clonic seizures. Brain. 2009; 132:999–1012.
7. Devergnas A, Piallat B, Prabhu S, et al. The subcortical hidden side of focal motor seizures: evidence from micro-recordings and local field potentials. Brain. 2012; 135(7):2263–76.
8. Miyamoto H, Tatsukawa T, Shimohata A, et al. Impaired cortico-striatal excitatory transmission triggers epilepsy. Nat Commun. 2019; 10.
9. He X, Chaitanya G, Asma B, et al. Disrupted basal ganglia-thalamocortical loops in focal to bilateral tonic-clonic seizures. Brain. 2020; 143(1):175–90.
10. Gerfen CR, Surmeier DJ. Modulation of striatal projection systems by dopamine. Annu Rev Neurosci. 2011; 34:441–66.
11. Calabresi P, Picconi B, Tozzi A, et al. Direct and indirect pathways of basal ganglia: a critical reappraisal. Nat Neurosci. 2014; 17(2):1022–30.
12. Turski L, Cavalheiro EA, Bortolotto ZA, et al. Dopamine-sensitive anticonvulsant site in the rat striatum. J Neurosci. 1988; 8(11):4027–37.
13. Guenthner CJ, Miyamichi K, Yang HH, et al. Permanent genetic access to transiently active neurons via TRAP: Targeted Recombination in Active Populations. Neuron. 2013; 78(5):773–84.

14. Allen WE, DeNardo LA, Chen MZ, et al. Thirst-associated preoptic neurons encode an aversive motivational drive. Science. 2017; 357(6356):1149–55.
15. Henjyoji EY, Dow RS. Cobalt-induced seizures in the cat. Electroencephalogr Clin Neurophysiol. 1965; 19(2):152–61.
16. Grimm RJ, Frazee JG, Kawasaki T, et al. Cobalt epilepsy in the squirrel monkey. Electroencephalogr Clin Neurophysiol. 1970; 29(5):525–8.
17. Hartman ER, Colasanti BK, Craig CR. Epileptogenic properties of cobalt and related metals applied directly to cerebral cortex of rat. Epilepsia. 1974; 15(1):121–9.
18. Singh T, Joshi S, Williamson JM, et al. Neocortical injury–induced status epilepticus. Epilepsia. 2020; 61(12).
19. Kim J, Woo J, Park Y-G, et al. Thalamic T-type Ca2+ channels mediate frontal lobe dysfunctions caused by a hypoxia-like damage in the prefrontal cortex. J Neurosci. 2011; 31(11):4063–73.
20. Morgan JI, Cohen DR, Hempstead JL, et al. Mapping patterns of c-fos expression in the central nervous system after seizure. Science. 1987; 237(4811):192–7.
21. Labiner DM, Butler LS, Cao Z, et al. Induction of c-fos mRNA by kindled seizures: complex relationship with neuronal burst firing. J Neurosci. 1993; 13(2):744–51.
22. André V, Pineau N, Motte JE, et al. Mapping of neuronal networks underlying generalized seizures induced by increasing doses of pentylenetetrazol in the immature and adult rat: a c-Fos immunohistochemical study. Eur J Neurosci. 1998; 10(6):2094–106.
23. Peng Z, Houser CR. Temporal patterns of Fos expression in the dentate gyrus after spontaneous seizures in a mouse model of temporal lobe epilepsy. Neurobiol Dis. 2005; 25(31):7210–20.
24. Graybiel AM, Ragsdale CW. Histochemically distinct compartments in the striatum of human, monkey, and cat demonstrated by acetylthiocholinesterase staining. Proc Nati Acad Sci USA. 1978; 75(11):5723–6.
25. Smith JB, Klug JR, Ross DL, et al. Genetic-based dissection unveils the inputs and outputs of striatal patch and matrix compartments. Neuron. 2016; 91(5):1069–84.

26. Clasadonte J, Haydon PG. Astrocytes and Epilepsy. In: Noebels JL, Avoli M, Rogawski MA, editors. Jasper's basic mechanisms of the epilepsies. 4th editio. National Center for Biotechnology Information (US); 2012. p. 591–605.
27. Wahnschaffe U, Löscher W. Anticonvulsant effects of ipsilateral but not contralateral microinjections of the dopamine D2 agonist LY 171555 into the nucleus accumbens of amygdala-kindled rats. Brain Res. 1991; 553(2):181–7.
28. Turski WA, Cavalheiro EA, Ikonomidou C, et al. Dopamine control of seizure propagation: intranigral dopamine D1 agonist SKF-38393 enhances susceptibility to seizures. Synapse. 1990; 5(2):113–9.
29. Koch-Stoecker S. Antipsychotic drugs and epilepsy: indications and treatment guidelines. Epilepsia. 2002; 43(2):19–24.
30. Alper K, Schwartz KA, Kolts RL, et al. Seizure incidence in psychopharmacological clinical trials: an analysis of Food and Drug Administration (FDA) summary basis of approval reports. Biol Psychiatry. 2007; 62(4):345–54.
31. Behere R V., Anjith D, Rao NP, et al. Olanzapine-induced clinical seizure: a case report. Clin Neuropharmacol. 2009; 32(5):297–8.
32. Uvais NA, Sreeraj VS. Seizure associated with olanzapine. J Fam Med Prim care. 2018; 7(5):1090–2.
33. Durham RA, Eaton MJ, Moore KE, et al. Effects of selective activation of dopamine D2 and D3 receptors on prolactin secretion and the activity of tuberoinfundibular dopamine neurons. Eur J Pharmacol. 1997; 335(1):37–42.
34. Sethy VH, Ellerbrock BR, Wu H. U-95666E: A potential anti-Parkinsonian drug with anxiolytic activity. Prog Neuro-Psychopharmacol & Biol Psychiat. 1997; 21:873–83.
35. McCall RB, Lookingland KJ, Bédard PJ, et al. Sumanirole, a highly dopamine D2-selective receptor agonist: in vitro and in vivo pharmacological characterization and efficacy in animal models of Parkinson's disease. J Pharmacol Exp Ther. 2005; 314(3):1248–56.
36. Barone P, Lamb J, Ellis A, et al. Sumanirole versus placebo or ropinirole for the adjunctive treatment of patients with advanced Parkinson's disease. Mov Disord.

2007; 22(4):483–9.

37. Singer C, Lamb J, Ellis A, et al. A comparison of sumanirole versus placebo or ropinirole for the treatment of patients with early Parkinson's disease. Mov Disord. 2007; 22(4):476–82.
38. Stojanovic T, Orlova M, Sialana FJ, et al. Validation of dopamine receptor DRD1 and DRD2 antibodies using receptor deficient mice. Amino Acids. 2017; 49(6):1101–9.
39. Gerfen CR, Engber TM, Mahan LC, et al. D1 and D2 dopamine receptor-regulated gene expression of striatonigral and striatopallidal neurons. Science. 1990; 250(4986):1429–32.
40. Curran EJ, Watson SJ. Dopamine receptor mRNA expression patterns by opioid peptide cells in the nucleus accumbens of the rat: A double in situ hybridization study. J Comp Neurol. 1995; 361(1):57–76.
41. Deng YP, Lei WL, Reiner A. Differential perikaryal localization in rats of D1 and D2 dopamine receptors on striatal projection neuron types identified by retrograde labeling. J Chem Neuroanat. 2006; 32(2–4):101–16.
42. Harrison MB, Wiley RG, Wooten GF. Selective localization of striatal D1 receptors to striatonigral neurons. Brain Res. 1990; 528(2):317–22.
43. Le Moine C, Normand E, Guitteny AF, et al. Dopamine receptor gene expression by enkephalin neurons in rat forebrain. Proc Natl Acad Sci USA. 1990; 87:230–4.
44. Pollack AE, Harrison MB, Wooten GF, et al. Differential localization of A2a adenosine receptor mRNA with D1 and D2 dopamine receptor mRNA in striatal output pathways following a selective lesion of striatonigral neurons. Brain Res. 1993; 631(1):161–6.
45. Hersch SM, Ciliax BJ, Gutekunst C-A, et al. Electron Microscopic Analysis of Dl and D2 Dopamine Receptor Proteins in the Dorsal Striatum and Their Synaptic Relationships with Motor Corticostriatal Afferents. J Neurosci. 1995; 75(7):5222–37.
46. Le Moine C, Bloch B. D1 and D2 dopamine receptor gene expression in the rat striatum: sensitive cRNA probes demonstrate prominent segregation of D1 and D2 mRNAs in distinct neuronal populations of the dorsal and ventral striatum. J

Comp Neurol. 1995; 355(3):418–26.

47. Gong S, Zheng C, Doughty ML, et al. A gene expression atlas of the central nervous system based on bacterial artificial chromosomes. Nature. 2003; 425(6961):917–25.
48. Kravitz A V., Freeze BS, Parker PRL, et al. Regulation of parkinsonian motor behaviours by optogenetic control of basal ganglia circuitry. Nature. 2010; 466(7306):622–6.
49. Lee HJ, Weitz AJ, Bernal-Casas D, et al. Activation of Direct and Indirect Pathway Medium Spiny Neurons Drives Distinct Brain-wide Responses. Neuron. 2016; 91:412–24.
50. Franklin KBJ, Paxinos G. Paxinos and Franklin's the mouse brain in stereotaxic coordinates. 4th Editio. Academic Press; 2012. 360 p.
51. Boley AM, Perez SM, Lodge DJ. A fundamental role for hippocampal parvalbumin in the dopamine hyperfunction associated with schizophrenia. Schizophr Res. 2014; 157(1–3):238–43.
52. Abdi A, Mallet N, Mohamed FY, et al. Prototypic and arkypallidal neurons in the dopamine-intact external globus pallidus. J Neurosci. 2015; 35(17):6667–88.
53. Dodson PD, Larvin JT, Duffell JM, et al. Distinct Developmental Origins Manifest in the Specialized Encoding of Movement by Adult Neurons of the External Globus Pallidus. Neuron. 2015; 86:501–13.
54. Saunders A, Huang KW, Sabatini BL. Globus pallidus externus neurons expressing parvalbumin interconnect the subthalamic nucleus and striatal interneurons. PLoS One. 2016; 11(2).
55. Ketzef M, Silberberg G. Differential Synaptic Input to External Globus Pallidus Neuronal Subpopulations In Vivo. Neuron. 2020; :1–14.
56. Solomon IC, Halat TJ, El-Maghrabi R, et al. Projections from the substantia nigra pars reticulata to the motor thalamus of the rat: Single axon reconstructions and immunohistochemical study. J Comp Neurol. 2001; 440(1):20–30.
57. Hooks BM, Mao T, Gutnisky DA, et al. Organization of cortical and thalamic input to pyramidal neurons in mouse motor cortex. J Neurosci. 2013; 33(2):748–60.
58. Terlau J, Yang J, Khastkhodaei Z, et al. Spike-wave discharges in absence

epilepsy: segregation of electrographic components reveals distinct pathways of seizure activity. J Physiol. 2020; 598(12):2397–414.

59. DeLong MR, Wichmann T. Circuits and circuit disorders of the basal ganglia. Arch Neurol. 2007; 64(1):20–4.
60. Yang B, Treweek JB, Kulkarni RP, et al. Single-cell phenotyping within transparent intact tissue through whole-body clearing. Cell. 2014; 158(4):945–58.
61. Zingg B, Chou X-L, Zhang Z-G, et al. AAV-mediated anterograde transsynaptic tagging: mapping corticocollicular input-defined neural pathways for defense behaviors. Neuron. 2017; 93(1):33–47.
62. Chen MC, Ferrari L, Sacchet MD, et al. Identification of a direct GABAergic pallidocortical pathway in rodents. Eur J Neurosci. 2015; 41(6):748–59.
63. Grewal SS, Holanda VM, Middlebrooks EH. Corticopallidal connectome of the globus pallidus externus in humans: an exploratory study of structural connectivity using probabilistic diffusion tractography. Am J Neuroradiol. 2018; 39(11):2120–5.
64. Karube F, Takahashi S, Kobayashi K, et al. Motor cortex can directly drive the globus pallidus neurons in a projection neuron type-dependent manner in the rat. Elife. 2019; 8:1–25.
65. Penfield W, Jasper HH. Epilepsy and the functional anatomy of the human brain. Boston: Little, Brown; 1954. 896 p.
66. Iadarola MJ, Gale K. Substantia nigra: site of anticonvulsant activity mediated by γ-aminobutyric acid. Science. 1982; 218(4578):1237–40.
67. Velíšková J, Miller AM, Nunes ML, et al. Regional neural activity within the substantia nigra during peri-ictal flurothyl generalized seizure stages. Neurobiol Dis. 2005; 20(3):752–9.
68. Aupy J, Wendling F, Taylor K, et al. Cortico-striatal synchronization in human focal seizures. Brain. 2019; 142:1282–95.
69. Kücker S, Töllner K, Piechotta M, et al. Kindling as a model of temporal lobe epilepsy induces bilateral changes in spontaneous striatal activity. Neurobiol Dis. 2010; 37(3):661–72.
70. Chang JH, Yang X-F, Zempel JM, et al. The unilateral cobalt wire model of neocortical epilepsy: a method of producing subacute focal seizures in rodents.

Epilepsy Res. 2004; 61:153–60.

71. Pitkänen A, Buckmaster PS, Galanopoulou AS, et al. Models of seizures and epilepsy. Academic Press; 2017. 1178 p.
72. Parthasarathy HB, Graybiel AM. Cortically driven immediate-early gene expression reflects modular influence of sensorimotor cortex on identified striatal neurons in the squirrel monkey. J Neurosci. 1997; 17(7):2477–91.
73. Rossi LF, Wykes RC, Kullmann DM, et al. Focal cortical seizures start as standing waves and propagate respecting homotopic connectivity. Nat Commun. 2017; 8(1).
74. Tobin WF, Weston MC. Focusing on the big picture: Induced focal seizures propagate along synaptic pathways. Epilepsy Curr. 2018; 18(1):47–8.
75. Gertler TS, Chan CS, Surmeier DJ. Dichotomous anatomical properties of adult striatal medium spiny neurons. J Neurosci. 2008; 28(43):10814–24.
76. Kreitzer AC, Malenka RC. Endocannabinoid-mediated rescue of striatal LTD and motor deficits in Parkinson's disease models. Nature. 2007; 445(7128):643–7.
77. Connors BW. Initiation of synchronized neuronal bursting in neocortex. Nature. 1984; 310(5979):685–7.
78. Detre JA, Alsop DC, Aguirre GK, et al. Coupling of cortical and thalamic ictal activity in human partial epilepsy: Demonstration by functional magnetic resonance imaging. Epilepsia. 1996; 37(7):657–61.
79. Redecker C, Bruehl C, Hagemann G, et al. Coupling of cortical and thalamic metabolism in experimentally induced visual and somatosensory focal epilepsy. Epilepsy Res. 1997; 27(2):127–37.
80. Blumenfeld H. The thalamus and seizures. Arch Neurol. 2002; 59(1):135–7.
81. Cain SM, Snutch TP. Voltage-gated calcium channels in epilepsy. In: Noebels JL, Avoli M, Rogawski MA, editors. Jasper's basic mechanisms of the epilepsies. 4th editio. National Center for Biotechnology Information (US); 2012.
82. Paz JT, Davidson TJ, Frechette ES, et al. Closed-loop optogenetic control of thalamus as a new tool to interrupt seizures after cortical injury. Nat Neurosci. 2013; 16(1):64–70.
83. Westbrook GL. Seizures and epilepsy. In: Kandel ER, Schwartz JH, Jessell TM,

et al., editors. Principles of neural science. New York: McGraw-Hill; 2013. p. 1116–39.

84. Englot DJ, Morgan VL, Chang C. Impaired vigilance networks in temporal lobe epilepsy: Mechanisms and clinical implications. Epilepsia. 2020; 61(2):189–202.
85. Harden C, Tomson T, Gloss D, et al. Practice guideline summary: Sudden unexpected death in epilepsy incidence rates and risk factors. Neurology. 2017; 88(17):1674–80.
86. Asadi-Pooya AA, Nikseresht A, Yaghoubi E, et al. Physical injuries in patients with epilepsy and their associated risk factors. Seizure. 2012; 21(3):165–8.
87. Turski L, Meldrum BS, Cavalheiro EA, et al. Paradoxical anticonvulsant activity of the excitatory amino acid N-methyl-D-aspartate in the rat caudate-putamen. Proc Natl Acad Sci U S A. 1987; 84(6):1689–93.
88. Chkhenkeli SA. The inhibitory influence of the nucleus caudatus electrostimulation on the human's amygdalar and hippocampal activity at temporal lobe epilepsy. In: Bull Georgian Acad Sci. Stereotact Funct Neurosurg; 1978. p. 406–11.
89. Chkhenkeli SA, Chkhenkeli IS. Effects of therapeutic stimulation of nucleus caudatus on epileptic electrical activity of brain in patients with intractable epilepsy. In: Stereotactic and Functional Neurosurgery. Stereotact Funct Neurosurg; 1997. p. 221–4.
90. Velíšková J, Claudio OI, Galanopoulou AS, et al. Developmental aspects of the basal ganglia and therapeutic perspectives. Epileptic Disord. 2002; 4(Suppl.3).
91. Garant DS, Gale K. Lesions of substantia nigra protect against experimentally induced seizures. Brain Res. 1983; 273:156–61.
92. Chabardès S, Kahane P, Minotti L, et al. Deep brain stimulation in epilepsy with particular reference to the subthalamic nucleus. Epileptic Disord. 2002; 4 Suppl 3:S83-93.
93. Benazzouz A, Piallat B, Pollak P, et al. Responses of substantia nigra pars reticulata and globus pallidus complex to high frequency stimulation of the subthalamic nucleus in rats: electrophysiological data. Neurosci Lett. 1995; 189(2):77–80.
94. Benabid AL, Minotti L, Koudsié A, et al. Antiepileptic effect of high-frequency

stimulation of the subthalamic nucleus (corpus luysi) in a case of medically intractable epilepsy caused by focal dysplasia: A 30-month follow-up: Technical case report. Neurosurgery. 2002; 50(6):1385–92.

95. Zangiabadi N, Ladino LD, Sina F, et al. Deep brain stimulation and drug-resistant epilepsy: a review of the literature. Front Neurol. 2019; 10:601.

CHAPTER 4

ANTICONVULSANT D2R AGONIST ACTIVATED INHIBITORY PARVALBUMIN INTERNEURONS

SUMMARY AND CONCLUSIONS

1. We find that systemic injection of a D2R agonist sumanirole suppresses frontal lobe seizures.
2. Injection of D2R agonist led to extensive activation of parvalbumin interneurons in the cortex and striatum ipsilateral to the seizure focus.
3. D2R agonists activate PV interneurons, which in turn inhibit principal neurons, potentially explaining their anticonvulsant effect.

INTRODUCTION

Dopamine receptor modulation changes susceptibility to seizures. Dopamine type 2 receptor (D2R) agonists are anticonvulsants and suppress pilocarpine and kindled seizures (1,2), whereas D2R antagonists are proconvulsant (3). According to the FDA package insert and series of carefully performed studies, patients taking high-affinity D2R antagonists such as haloperidol, clozapine, and olanzapine for schizophrenia or psychosis have a higher risk of seizures (4,5). D2R agonists are anticonvulsants in limbic seizures, but their effectiveness in frontal lobe seizures was not tested (1,2). We previously found that D2R agonist injected through a bilateral cannula directly into the striatum stopped frontal lobe seizures for 2.5 hrs following the injection (6). Here, we wanted to determine whether systemic injection would also be anticonvulsant. Also, the mechanism behind dopamine receptor modulation of seizures is not fully understood. Thus, we tested whether D2R agonists activate inhibitory PV interneurons to suppress seizures.

METHODS

Animals

University of Virginia Animal Care and Use Committee approved the experimental protocol. Transient Recombination of Activated Populations, second-generation (TRAP2) mice were generated by crossing $Fos^{2A\text{-}ICreERT2}$ (#030323) and Ai9 mice (#007909, Jackson Laboratories). We studied TRAP2 and C57Bl/6 mice of both sexes (6-12 weeks old), gave them *ad libitum* food and water, and maintained on 12 hr light/12 hr dark cycle. KAPA Biosystems kit was used for genotyping.

Seizure induction and drug injections

We placed 1.7 mg cobalt wire in the right premotor cortex (AP +2.6 mm, ML -1.8 mm) of C57Bl/6 mice with four bilateral EEG electrodes under isoflurane anesthesia and continuously monitored for seizures via video/EEG (7). All mice developed seizures before any injections were made. In the first cohort, Co-implanted C57Bl/6 and TRAP2 mice were injected once with sumanirole (5 mg/kg, i.p.) at 18 hrs (or another group at 20 hrs) after Co. In the second cohort, we injected sumanirole or normosol as control i.p. consecutively three times at 18, 20, and 22 hrs after Co placement. A blinded investigator counted the number of seizures 2 hrs before the injections (16-18 hrs after Co) to determine the baseline, 2 hrs following each injection (18-20, 20-22, 22-24 hrs after Co) because sumanirole has a sustained effect for at least 2 hours, and 2 hrs after the injections (24-26 hrs after Co) to determine return to the baseline (Figure 4-1A).

To label activated cells after D2 agonist injection, cobalt-implanted TRAP2 mice were injected with sumanirole at 18 hrs after Co and with 4-hydroxytamoxifen (4-OHT, 50 mg/kg, s.c.) within 90 min after sumanirole. Co-implanted control TRAP2 mice were injected with 4-OHT within 90 min after a secondarily generalized tonic-clonic seizure. Animals were perfused 5 days after 4-OHT injection to allow tdTomato expression.

Immunohistochemistry, microscopy, and analysis

TRAP2 mice were perfused with 4% PFA, sliced on a cryostat at 40 µm, immunolabeled with rabbit anti-NeuN (1:500, #24307, Cell Signaling) and rabbit anti-PV (1:500, #ab11427, Abcam), and imaged on a confocal microscope at 10x/0.45 NA or 20x/0.95 NA as described previously (6).

We used ImageJ and Imaris Spots detection tools to count tdTomato positive cells in D2R agonist injected vs. non-injected mice. We subtracted background and adjusted the threshold to count cells.

The fraction of activated PV cells was detected using the Imaris Spots tool. The number of cells expressing both tdTomato and PV was divided by the total number of PV positive cells in the right (ipsilateral to the focus) and left cortex and the striatum.

Statistics

We analyzed data using Prism 8 for all statistical tests and presented them as mean ± SEM, where n is the number of animals. We used an unpaired t-test for normally distributed data and the Kolmogorov-Smirnov (KS) test if not distributed normally to compare means of two groups. Results were considered statistically significant for $p < 0.05$.

RESULTS

Systemic administration of D2 receptor agonist is anticonvulsant during frontal lobe seizures

We placed cobalt in the right premotor cortex to cause frontal lobe focal motor to bilateral tonic-clonic seizures (7). Mice always had only behavioral seizures, and none of the seizures were only electrographic. To determine if systemic D2R agonist injection was anticonvulsant, we administered full selective D2R agonist sumanirole i.p. (5 mg/kg) or normosol as a control. Because sumanirole has a sustained effect for at least two hours (6), we had two injection cohorts. In the first cohort, we compared seizure number before and after a single sumanirole injection at 18 hours after cobalt insertion at the peak of seizures. In the second cohort, we did three consecutive injections at 18, 20, and 22 hours after cobalt insertion to determine if the anticonvulsant effect could be prolonger and maintained (Figure 4-1A). After a single sumanirole injection at 18 hours after cobalt, animals had fewer seizures following than before the treatment (Figure 4-1C) (Before: 2.17 ± 0.60; Following: 0.67 ± 0.67 ($p = 0.0152$, KS test); After: 1.50 ± 0.67). During three consecutive injections, D2R agonist-injected mice had fewer seizures after the first injection than the control mice (Figure 4-1B). However, seizures continued after the second and third injections (Figure 4-1B) (Before: D2 agonist 2.00 ± 0.37, normosol 1.20 ± 0.49, KS test; Following 1^{st}: D2 agonist 0.00 ± 0.00, normosol 1.20 ± 0.58 ($p = 0.0486$); Following 2^{nd}: D2 agonist 1.00 ± 0.52, normosol 1.00 ± 0.55; Following 3^{rd}: D2 agonist 0.50 ± 0.34, normosol 0.80 ± 0.20, KS test; After: D2 agonist 1.67 ± 0.67, normosol 0.40 ± 0.25, KS test). We wanted to determine whether the lack of effect after the second and third D2 agonist injections was due to tachyphylaxis or due to a rundown of the seizure burden. Therefore, we did a single sumanirole injection at 20 hours after cobalt and found a similar number of seizures before and following the treatment (Figure 4-1D) (Before: 3.00 ± 0.71; Following: 1.50 ± 1.19; After: 3.25 ± 1.25). We could not notice the anticonvulsant effect due to the natural decline in seizure frequency in our model and not due to tachyphylaxis. Animals exhibited no change in EEG/behavior, and D2 agonist treatment did not modify seizure severity pattern, although hypoactivity was possible in some mice.

Next, we visualized activated neurons after a single D2R agonist injection using TRAP2 mice that express Cre under the c-Fos promoter regulation. We injected TRAP2 mice with sumanirole (5 mg/kg, i.p.) at 18 hours after cobalt insertion, followed by 4-OHT injection within 90 minutes after sumanirole to translocate Cre inside the nucleus and relieve repression from tdTomato to labeled activated cells (Figure 4-1E,K, L). For controls, we injected TRAP2 mice with 4-OHT 90 minutes after a seizure (Figure 4-1F). All mice were injected with 4-OHT after equivalently severe seizures. D2 agonist injected and seizure control mice had a similar number of activated tdTomato positive neurons in the right and left cortex and striatum (Figure 4-1G-J).

Increased activation of PV interneurons in the ipsilateral cortex and striatum after D2R agonist injection

PV interneurons express D2Rs (8). We compared PV interneuron activation in cobalt-implanted TRAP2 mice that received systemic D2R agonist injection (Figure 4-2A,C) versus those with only a seizure (Figure 4-2B,D). We found more tdTomato positive PV interneurons in the right (ipsilateral) cortex and striatum of D2R agonist-injected mice than in those of mice with seizures (Figure 4-2E,G) (Ipsi cortex: D2R agonist 57.86 ± 10.41%, seizure 29.49 ± 3.32% ($p = 0.0241$); Ipsi striatum: D2R agonist 80.69 ± 6.00%, seizure 44.07 ± 6.94% ($p = 0.0062$)). In contrast, the contralateral cortex and striatum of D2R agonist-injected mice and mice with seizures had a similar fraction of activated PV cells (Figure 2F, H) (Contra cortex: D2R agonist 44.61 ± 15.48%, seizure 18.83 ± 4.04%; Contra striatum: D2R agonist 60.25 ± 16.95%, seizure 22.61 ± 8.04%). We next plotted % of activated PV interneurons across bregma from anterior to posterior cortex and striatum, where each black line is a simple linear regression for a separate mouse (Figure 4-2G-J). Only in the ipsilateral cortex all D2 agonist injected mice and mice with seizures had positive slopes, meaning the closer to the seizure focus (in the anterior premotor cortex), the more PV cells were active (Figure 4-2G). Whereas in the striatum, PV interneurons were on average uniformly active with no anterior to posterior activation pattern.

Figure 4-1. Systemic injection of D2 agonist is anticonvulsant in frontal lobe seizures. A) Approach in B: cobalt-implanted mice were i.p. injected with either sumanirole or normosol at 18, 20, 22 hrs after Co (red arrows), and seizure number was counted in the time periods indicated by black horizontal arrows. B) The effect of sumanirole (green) or normosol (red) on seizure number before the 1st injection (16-18 hours after Co), following 1st, 2nd, and 3rd injections (18-20, 20-22, 22-24 hours after Co), and after the 3rd injection (24-26 hours after Co) (n = 5-6 mice). C) Approach in D: Co-implanted mice were i.p. injected with sumanirole (red arrow) at 18 hrs after Co. D) The effect of single sumanirole injection on seizure number before the injection (16-18 hours after Co), following the injection (18-20 hours after Co), and after the injection (20-22 hours after Co) (n = 6 mice). E) tdTomato expression in Co-implanted TRAP2 mice after D2 agonist injection. F, tdTomato expression after a seizure. G-J) cell number in the right (ipsilateral) and left (contralateral) cortex and striatum to the seizure focus in D2 agonist injected TRAP2 mice (green) versus TRAP2 mice after a seizure (red) (n = 4-5 mice). Each point on the graph represents mean cell number in the structure on a slice at a specific distance from bregma for either D2 agonist or seizure mouse groups ± SEM. Unpaired t test or KS test were done to compare means of the two groups. K, L, Activation of the cortex and striatum in D2 agonist injected TRAP2 mice. Data are mean ± SEM, unpaired t test unless specified, n.s. non-significant, * $p < 0.05$.

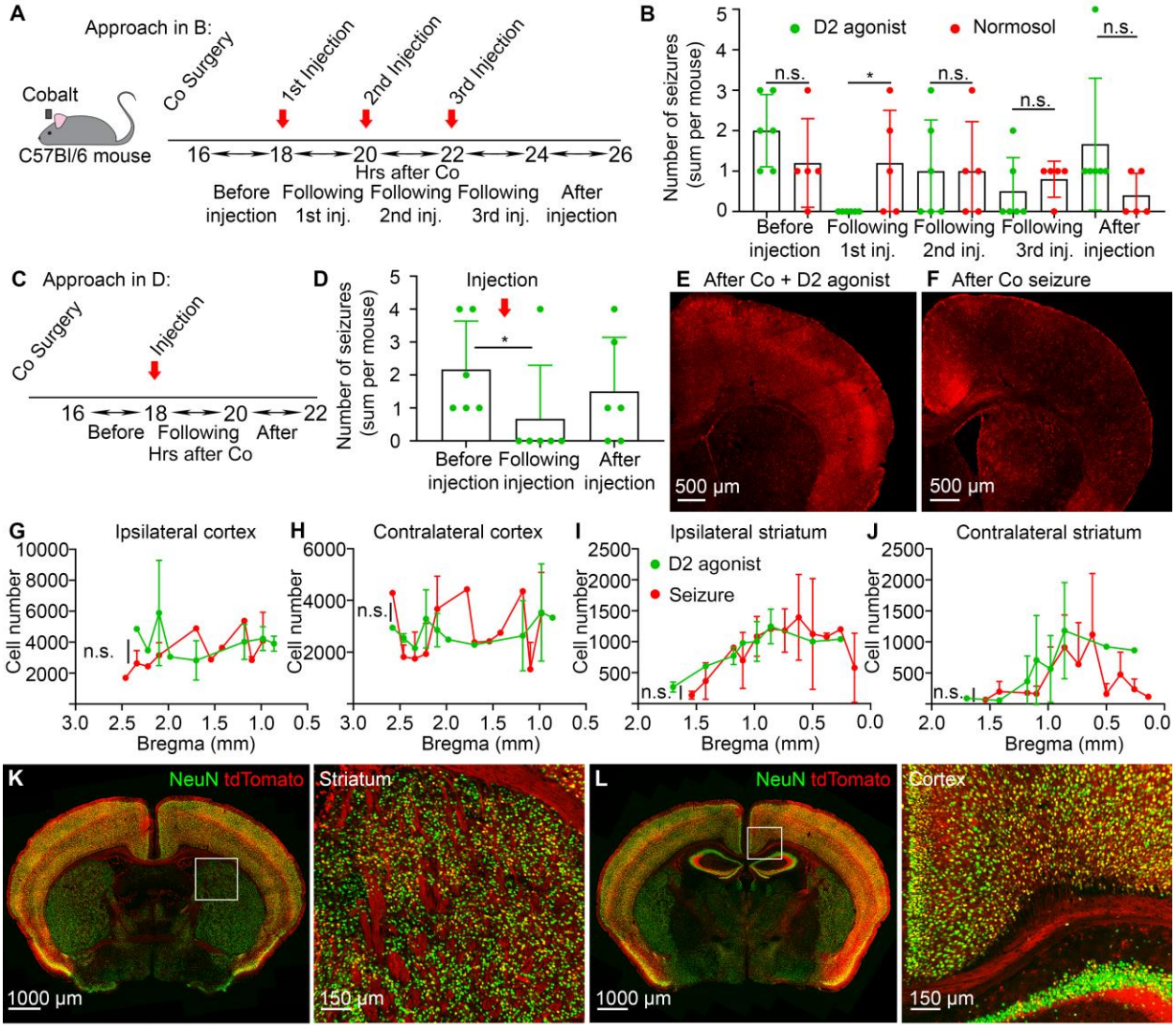
A
Approach in B:
Co Surgery
1st Injection
2nd Injection
3rd Injection
Cobalt
C57Bl/6 mouse
16 18 20 22 24 26
Hrs after Co
Before injection
Following 1st inj.
Following 2nd inj.
Following 3rd inj.
After injection
B
D2 agonist
Normosol
Number of seizures (sum per mouse)
n.s.
*
C Approach in D:
Co Surgery
Injection
16 18 20 22
Before Following After
Hrs after Co
D
Injection
E After Co + D2 agonist
F After Co seizure
500 µm
G Ipsilateral cortex
H Contralateral cortex
I Ipsilateral striatum
J Contralateral striatum
Cell number
Bregma (mm)
D2 agonist
Seizure
K
NeuN tdTomato
Striatum
1000 µm
150 µm
L
Cortex

Figure 4-1

Figure 4-2. D2 agonist increases the number of activated PV interneurons in the right (ipsilateral) cortex and striatum. tdTomato expression (red) in PV interneurons (green) A) in the cortex after D2 agonist injection, B) in the cortex after seizures, C) in the striatum after D2R agonist injection, D) in the striatum after seizures. E-H) % of activated PV interneurons in Co-implanted TRAP2 mice after D2R agonist injection (green) or after seizure (red) (tdTomato positive PV interneurons divided by the total number of PV interneurons in the specified structure, n = 4-5 mice). G-J) % of activated PV cells from anterior to posterior cortex and striatum across bregma. Black lines indicate simple linear regressions for separate D2 agonist injected mice (green) and mice with seizures (red). Data are mean ± SEM, unpaired t-test, n.s. non-significant, * $p < 0.05$, ** $p < 0.01$.

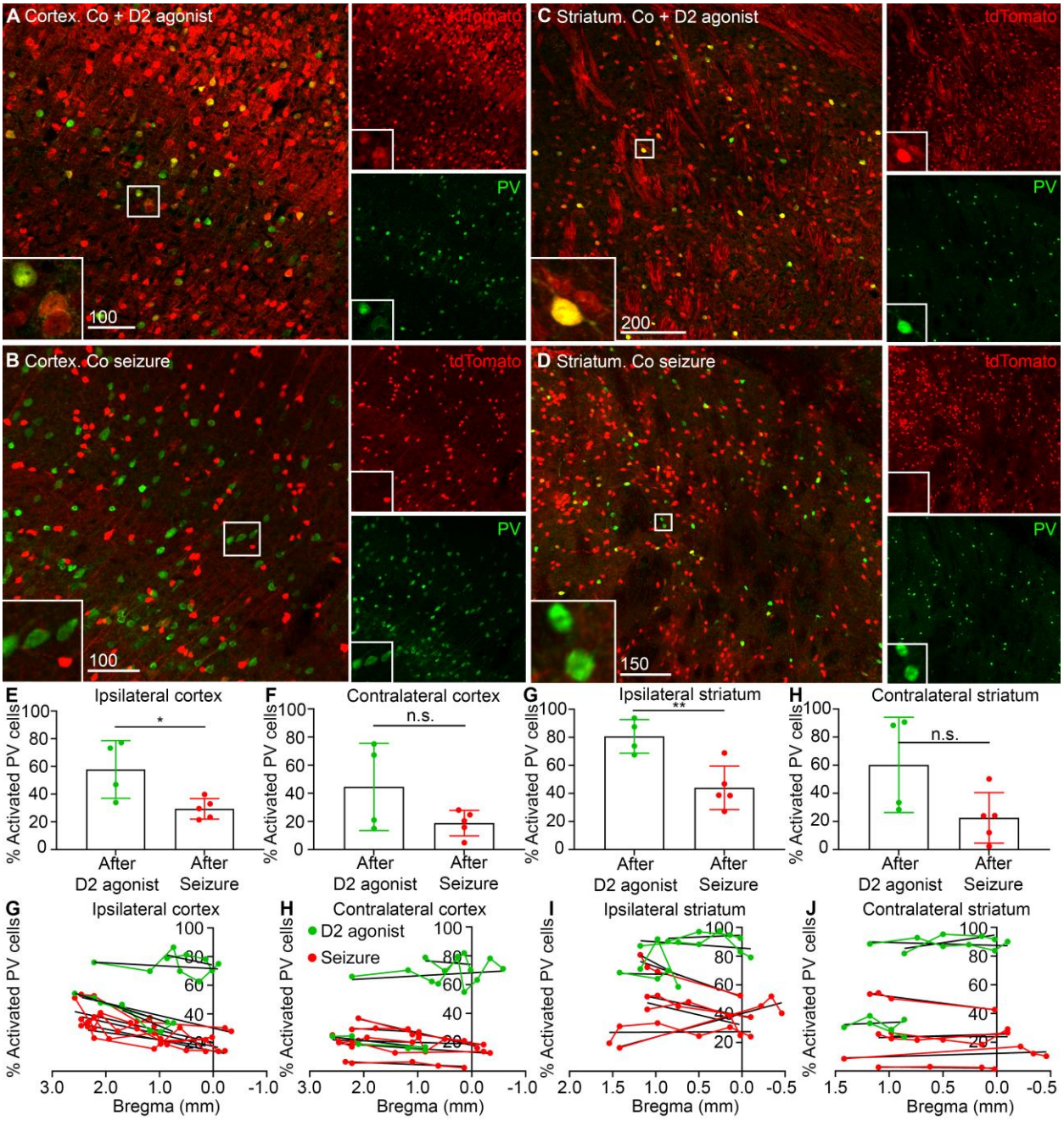
A Cortex. Co + D2 agonist
tdTomato
PV
100
C Striatum. Co + D2 agonist
tdTomato
PV
200
B Cortex. Co seizure
tdTomato
PV
100
D Striatum. Co seizure
tdTomato
PV
150
E
Ipsilateral cortex
% Activated PV cells
*
After D2 agonist
After Seizure
F
Contralateral cortex
n.s.
G
Ipsilateral striatum
**
H
Contralateral striatum
n.s.
G
Ipsilateral cortex
H
Contralateral cortex
D2 agonist
Seizure
I
Ipsilateral striatum
J
Contralateral striatum
Bregma (mm)

Figure 4-2

DISCUSSION

Systemic D2R agonist injection is anticonvulsant in frontal lobe focal motor to bilateral tonic-clonic seizures. D2R activation increased PV interneuron activity in the cortex and striatum ipsilateral to the seizure focus. Previous studies report increased D2 receptor density in the nucleus accumbens ipsilateral but not contralateral to the stimulating electrode in the amygdala or hippocampus (2). We hypothesize that stronger ipsilateral activation of PV interneurons is due to the stronger impact of seizures on the side of the focus, and possibly, increased number of D2Rs, compared to the contralateral side. PV interneurons express both D2 and D1 receptors (8). D2 agonists increase the excitability of fast-spiking PV interneurons (8) and decrease EPSPs of pyramidal cortical neurons, whereas D1 agonists do not affect pyramidal neuron EPSPs (9).

We previously showed that frontal lobe focal motor to bilateral tonic-clonic seizures preferentially activate the indirect pathway of the basal ganglia (6). D2 agonists reduce activity along the indirect pathway and of the substantia nigra reticulata (10), which could also potentially explain the anticonvulsant effect of D2 agonists. All D2 receptors activate G protein-regulated inwardly rectifying K^+ channels (GIRK) and decrease Ca^{2+} currents (11). Thus, D2 receptor stimulation decreases the excitability of striatal medium spiny neurons by increasing K^+ currents, inducing hyperpolarization. On the other hand, D2 agonists affect PV interneurons indirectly by depressing GABA inhibitory synaptic input to them (12).

Although it is uncertain whether increased ipsilateral cortical or striatal inhibition leads to decreased seizures, and while other interneurons could also play a role in increased inhibition after D2R agonist treatment, GABAergic parvalbumin interneurons are important regulators of excitatory projection pyramidal neurons, and PV interneuron dysfunction leads to seizures (13-16). Thus, enhanced activity of parvalbumin interneurons after D2 receptor activation may explain the anticonvulsant effect of D2R agonists.

REFERENCES FOR CHAPTER 4

1. Turski L, Cavalheiro EA, Bortolotto ZA, et al. Dopamine-sensitive anticonvulsant site in the rat striatum. J Neurosci. 1988; 8(11):4027–37.
2. Wahnschaffe U, Löscher W. Anticonvulsant effects of ipsilateral but not contralateral microinjections of the dopamine D2 agonist LY 171555 into the nucleus accumbens of amygdala-kindled rats. Brain Res. 1991; 553(2):181–7.
3. Turski WA, Cavalheiro EA, Ikonomidou C, et al. Dopamine control of seizure propagation: intranigral dopamine D1 agonist SKF-38393 enhances susceptibility to seizures. Synapse. 1990; 5(2):113–9.
4. Koch-Stoecker S. Antipsychotic drugs and epilepsy: indications and treatment guidelines. Epilepsia. 2002; 43(2):19–24.
5. Alper K, Schwartz KA, Kolts RL, et al. Seizure incidence in psychopharmacological clinical trials: an analysis of Food and Drug Administration (FDA) summary basis of approval reports. Biol Psychiatry. 2007; 62(4):345–54.
6. Brodovskaya A, Shiono S, Kapur J. Activation of the basal ganglia and indirect pathway neurons during frontal lobe seizures. Brain. 2021; .
7. Singh T, Joshi S, Williamson JM, et al. Neocortical injury–induced status epilepticus. Epilepsia. 2020; 61(12).
8. Tseng KY, Mallet N, Toreson KL, et al. Excitatory response of prefrontal cortical fast-spiking interneurons to ventral tegmental area stimulation in vivo. Synapse. 2006; 59(7):412–7.
9. Tseng KY, O'Donnell P. D2 dopamine receptors recruit a GABA component for their attenuation of excitatory synaptic transmission in the adult rat prefrontal cortex. Synapse. 2007; 61(10):843–50.
10. Centonze D, Grande C, Usiello A, et al. Receptor subtypes involved in the presynaptic and postsynaptic actions of dopamine on striatal interneurons. J Neurosci. 2003; 23(15):6245–54.
11. DeLong MR, Wichmann T. Circuits and circuit disorders of the basal ganglia. Arch Neurol. 2007; 64(1):20–4.
12. Neve KA, Seamans JK, Trantham-Davidson H. Dopamine receptor signaling. J

Recept Signal Transduct. 2004; 24(3):165–205.

13. Miyamoto H, Tatsukawa T, Shimohata A, et al. Impaired cortico-striatal excitatory transmission triggers epilepsy. Nat Commun. 2019; 10.
14. Li KX, Lu YM, Xu ZH, et al. Neuregulin 1 regulates excitability of fast-spiking neurons through Kv1.1 and acts in epilepsy. Nat Neurosci. 2012; 15(2):267–73.
15. Hu H, Gan J, Jonas P. Fast-spiking, parvalbumin+ GABAergic interneurons: from cellular design to microcircuit function. Science (80-). 2014; 345(6196).
16. Jiang X, Lachance M, Rossignol E. Involvement of cortical fast-spiking parvalbumin-positive basket cells in epilepsy. Prog Brain Res. 2016; 226:81–126.

CHAPTER 5

SURPRISING ROLE OF THE THALAMUS AND CORPUS CALLOSUM DURING FOCAL MOTOR TO BILATERAL SEIZURES

SUMMARY AND CONCLUSIONS

1. We propose that the thalamus amplifies seizures, whereas the corpus callosum allows the transmission to the contralateral hemisphere.
2. Seizures spread faster to the contralateral cortex than to the contralateral thalamus.
3. Ipsilateral thalamus is very weakly connected to the contralateral via direct monosynaptic projections.
4. After chemogenetic inhibition of the ipsilateral thalamus, seizures still spread to the contralateral cortex, but seizure duration decreases.
5. Anterior callosotomy prevents contralateral seizure spread during initial seizures.
6. Our findings support the model in which seizure spread to the contralateral cortex occurs via the corpus callosum rather than through commissural connections between the two thalami or through bilateral spread from the thalamus via the brainstem.

INTRODUCTION

Focal motor to bilateral tonic-clonic seizures, previously known as secondarily generalized (1), are among the most dangerous seizures and manifest in many behaviors, including sensory auras, motor activity, and altered consciousness because they can travel long distances in the brain from the onset zone. Previous studies showed that the thalamus plays a central role in seizure spread (2-4), and inhibition of the ipsilateral thalamus stops seizures in the ipsilateral and contralateral cortex (5). However, seizure spread from the seizure focus to the contralateral cortex has not been previously traced. We propose that seizures spread from the ipsilateral thalamus to the contralateral by engaging the cortico-cortical commissure, corpus callosum (Figure 5-1a).

In several models, the thalamus is essential for seizure maintenance and secondary generalization to the contralateral hemisphere (2,4,5). Focal cortical seizures spread to the ipsilateral thalamus and, inhibiting specific thalamic nuclei, suppress seizures (5). These studies demonstrate that the thalamus is a seizure choke point (6). However, these models do not explain the role of the thalamus in bilateral seizure spread. In some famous illustrations of seizure generalization, two thalami are fused into single thalamus projecting to both cerebral hemispheres (Figure 5-1B) (2,4,7). This model would suggest commissural connections between two thalamic nuclei participating in seizures. Others have suggested bilateral spread from the thalamus via the brainstem (Figure 5-1C) (3,8-10). Penfield and Jasper proposed that seizure generalization occurs via the centrencephalon, which includes brainstem reticular formation (8,9).

Lack of tools with good spatial and temporal resolution and inability to inhibit specific structures precisely made it difficult to distinguish between these models. We used activity reporter mice, local field potential recordings, viral tracing, chemogenetics, optogenetics, and callosotomy lesioning experiments to investigate the role of the thalamus and corpus callosum in the spread of frontal lobe focal motor to bilateral tonic-clonic seizures. We propose that the thalamus amplifies seizures, whereas the corpus callosum allows the transmission to the contralateral hemisphere.

METHODS

Animals

University of Virginia Animal Care and Use Committee approved all protocols. Transient Recombination in Active Populations, second-generation (TRAP2) mice were generated by crossing $Fos^{2A\text{-}ICreERT2}$ (#030323) to Ai9 mice (#007909, Jackson Laboratories) (11,12). TRAP2 and C57Bl/6 (Charles River) mice (7-12 weeks) of both sexes were maintained on 12 hr light/12 hr dark cycle and had *ad libitum* food and water. For genotyping, KAPA Biosystems kit was used.

Seizure induction, EEG and LFP electrophysiology, and viral injections

To induce seizures, we used a well-established cobalt model and implanted 1.7 mg cobalt (Co) wire in the right premotor cortex of either TRAP2 or C57Bl/6 mice with four bilateral EEG electrodes and a reference under isoflurane anesthesia (13). Mice were continuously monitored via video/EEG, and all of them developed seizures within 13-20 hours after cobalt insertion. 4-hydroxytamoxifen (4-OHT, 50 mg/kg s.c.) was injected within 90 of a focal motor to bilateral tonic-clonic seizure, and mice were perfused 5 days after to allow tdTomato expression.

We recorded local field potentials (LFPs) with a custom-made array of microelectrodes and analyzed LabChart 8.0 LFP data with Fast Fourier Transform as previously described (14). 2 cm electrodes maintained 60-70 kΩ resistance and sampled at 10 kHz. The signal was amplified and filtered using a band pass filter (1 Hz low pass, 5kHz high pass) and a notch filter. To record seizures, microelectrodes were placed in the bilateral premotor cortex (AP -2.2 mm, ML ±1.8 mm) and bilateral VL (AP -1.3 mm, ML ±1.0 mm, DV -3.75 mm) with cobalt and cerebellar reference. Seizure start was defined as a deflection of voltage trace at least twice the baseline. After recordings, the electrode position was marked by a single 40 µA, 0.75 msec pulse at 50 Hz for 30 sec. The brains were sectioned at 40 µm, stained with DAPI, and imaged on Nikon Eclipse Ti-S, 2x/0.45 NA. If the electrode position was incorrect, the data were excluded.

We injected AAV9 CamKII0.4.eGFP.WPRE.rBG (#105541-AAV9, Addgene) or Cre-driven AAV9 pCAG-FLEX-EGFP-WPRE (#51502-AAV9, Addgene) in the right premotor cortex of TRAP2 or C57Bl/6 mice (AP +2.6 mm, ML -1.8 mm, DV -0.5 mm;

100 nl) or in the right (ipsilateral) VL (AP -1.05 mm, ML -1.0 mm, DV -3.15 mm) with Hamilton syringe (#7634-01) and allowed 2 weeks for the viral expression.

Immunohistochemistry and imaging

Mice were perfused with 4% PFA, sliced on a cryostat at 40 µm, and immunolabeled with rabbit anti-NeuN (1:500, #24307, Cell Signaling) or mouse anti-MBP (1:500, #ab62631, Abcam) as previously described[14]. Confocal images were taken on Nikon Eclipse Ti-U at 10x/0.45 NA or 20x/0.95 NA, 1024x1024 or 512x512 frame size, 5 µm z-interval. Myelinated axons were imaged on Leica SP8 STED at 93x/1.3 NA, glycerol. GFP FLEX callosum fibers were imaged on CSU-W1 SoRa Yokogawa Spinning Disk Confocal, Nikon at 100x/1.35 NA, silicon, or 60x/1.49 NA, oil, 2304x2304, 0.5 µm step size. Excitation lasers were 405, 488, and 561. Imaris.3.0 (Bitplane) was used for visualization and Adobe Photoshop CC for figure display.

Chemogenetics and whole-cell electrophysiology

We mixed AAV8 hSyn-dF-HA-KORD-IRES-mCitrine (#65417-AAV8, Addgene, 60 nl) and AAV9 CamKII.HI.GFP-Cre.WPRE.SV40 (#105551-AAV9, Addgene 60 nl) in 1:1 ratio and injected into the ipsilateral VL (AP -1.3 mm, ML -1.0 mm, DV -3.7 mm, 120 nl) of C57Bl/6 mice and allowed 2 weeks for expression. We placed LFP microelectrodes in the bilateral premotor cortex and bilateral VL along with cobalt and recorded for 48 hours. Mice were injected either with salvinorin B (SALB, 10 mg/kg in DMSO), saline, or DMSO s.c. at 20 hours after Co implantation at the peak of seizures. A blinded investigator counted the number of seizures and duration.

We confirmed the ability of KORD to generate SALB-induced hyperpolarization using whole-cell electrophysiology. The brains of C57Bl/6 KORD injected mice were immersed in ice-cold oxygenated dissection buffer (4 °C, 95% O_2, and 5% CO_2) containing (in mM) 65.5 NaCl, 2 KCl, 5 $MgSO_4$, 1.1 KH_2PO_4, 1 $CaCl_2$, 10 dextrose, and 113 sucrose (300 mOsm), and coronal thalamic slices (300 µm) were prepared with a vibratome (VT1200s, Leica). The slices were then placed in an interface chamber containing oxygenated artificial cerebrospinal fluid (aCSF) at 25 °C and allowed to equilibrate for 30 min. The aCSF contained (in mM) 124 NaCl, 4 KCl, 1 $MgCl_2$, 25.7 $NaHCO_3$, 1.1 KH_2PO_4, 10 dextrose, and 2.5 $CaCl_2$ (300 mOsm). The patch electrode was filled with an internal solution containing (in mM) 115 cesium methane sulfonate, 20

CsCl, 10 KCl, 10 HEPES, 0.5 sodium-EGTA, 2.5 $MgCl_2$, 5 Mg-ATP and 5 lidocaine, pH 7.3, 285 mOsm. mCitrine fluorescence positive neurons were current-clamped. 100 nM SALB in DMSO or just DMSO control was bath applied for 10 min, and we tested the resting membrane potential to determine hyperpolarization.

Closed loop optogenetics

We injected C57Bl/6 mice with AAV9 CamKII-ArchT-GFP (#99039, Addgene, 120 nl) or AAV9 CamKII0.4.eGFP.WPRE.rBG (#105541-AAV9, Addgene) in the ipsilateral VL and allowed 2 weeks for expression. Mice were then implanted with LFP microelectrodes in the bilateral premotor cortex and bilateral VL, cobalt, and optic fiber in the ipsilateral VL. Our optogenetics setup consisted of fiber coupled LED light source (540 nm, 8 mW, 5 pulses in 500 ms (each pulse is 50 ms ON/50 ms OFF)) and polymer optical fiber 1000 µm core, which was coupled to polymer optical fiber 500 µm core via rotary joint (Prizmatix). The LED was externally triggered by a USB-TTL interface based on Arduino UNO Rev3 board. The timing of pulses was controlled from MATLAB (2020a). The LFP signals were recorded using LabChart software (ADInstruments). We accessed LabChart functions from MATLAB and fetched LFP recording data in online mode. We developed a deep convolutional neural network-based automated seizure detection model in MATLAB, which accepted single channel LFP measurements (in our case, from the ipsilateral cortex). The neural net continuously accessed data for 500 ms (5000 samples, 10kHz sampling frequency) in addition to 500 ms of the most recent data. Before feeding the data to the net, the data was preprocessed in multiple stages to discard high-frequency noise. The net output a scalar number, which was used to discriminate a seizure spike from the rest of the recording, using a manually set threshold. Once a seizure spike was detected, a signal from the USB-TTL interface was promptly dispatched to activate TTL pulses.

Callosotomy

We used a custom-made knife to cut the corpus callosum of C57Bl/6 mice. A small craniotomy was made at the posterior contralateral cortex (AP -3.5 mm, ML 0.5 mm), avoiding damaging the superior sagittal sinus. The knife was slowly advanced at an entrance angle 52° for 5 mm. The withdrawal angle was 54° for 2.5 mm and changed

back to 52° for another 2.5 mm. Mice were also implanted with Co, four bilateral EEG electrodes, a reference, and were monitored for seizures via continuous video/EEG.

Statistics

We analyzed data using Prism 8 and presented them as mean ± SEM, where n is the number of animals or the number of seizures followed by the number of animals. We used an unpaired t-test for normally distributed data and Kolmogorov-Smirnov test if not distributed normally. Results were considered statistically significant for $p < 0.05$.

RESULTS

Focal motor to bilateral tonic-clonic seizures activate the corpus callosum and thalamus

To initiate focal motor to bilateral tonic-clonic seizures, we placed 1.7 mg of cobalt in the right premotor cortex of TRAP2 mice with four bilateral EEG electrodes and monitored mice continuously via video/EEG as previously described (13) (Figure 5-1D). To labels cells active during a seizure, we used TRAP2 mice, which express Cre under the immediate early gene promoter c-Fos. 4-hydroxytamoxifen (4-OHT) was injected within 90 min after focal motor to bilateral tonic-clonic seizure, bringing Cre into a nucleus and relieving repression from tdTomato. Non-active cells were not labeled with tdTomato because they did not express Cre. We serially sectioned the brain into 40 µm to analyze the pattern of tdTomato expression.

The whole corpus callosum strongly expressed tdTomato from anterior to posterior sections (Figure 5-1E). To verify that these were axons, we used an antibody against myelin basic protein (MBP). SP8 super-resolution Lightning microscopy revealed myelin spiraling around the corpus callosum axons (Figure 5-1F and Supplementary Video 1). To confirm that activation of the corpus callosum was not the result of motor activity or cortical injury, we implanted steel wire instead of cobalt and injected 4-OHT 18 hours after surgery. These mice did not develop seizures and had no callosal activation (Supplementary Figure 5-1A).

The ipsilateral thalamus also strongly expressed tdTomato during focal motor to bilateral tonic-clonic seizures (Figure 5-1G). Motor thalamic ventromedial (VM) and ventrolateral (VL) nuclei as well as centromedian (CM) and mediodorsal (MD) nuclei were tdTomato positive, activation of which we quantified on the cellular level previously (14). Control steel wire-implanted mice without seizures did not show thalamic activation (Supplementary Figure 5-1B).

Seizures spread faster to the contralateral cortex than to the contralateral thalamus

Because the TRAP technique provides spatial but not temporal resolution, we recorded local field potentials (LFPs) from the ipsilateral and contralateral premotor cortex and ipsilateral and contralateral thalamic nucleus VL simultaneously. Custom made array of microelectrodes with 10 kHz sampling rate allowed us to record with millisecond precision. We selected the motor thalamic nucleus VL because of its larger size and

Figure 5-1. Cellular activation in the corpus callosum and thalamus. A-C) Schematics of three models of focal to bilateral seizure spread (red arrows) from the seizure focus to the contralateral cortex. D) A schematic of cobalt placement and EEG electrodes (red), and a representative focal to bilateral tonic-clonic seizure. E) Left: tdTomato expression in the corpus callosum at 0.86 mm bregma immunolabeled for NeuN (green) and its magnified view. Right: tdTomato expression in the posterior corpus callosum at 0.02 and -2.18 mm bregma. F) Left: SP8 super-resolution Lightning microscopy shows myelinated axons in the corpus callosum immunolabeled for myelin basic protein (MBP, green). Right and boxed inset: the magnified image of myelinated axons. G) Left: tdTomato expression in the thalamus immunolabeled for NeuN and its magnified view. Dotted lines indicate nuclear boundaries; MD, mediodorsal; VM, ventromedial; VL, ventrolateral. Also, see Supplementary Figure 1.

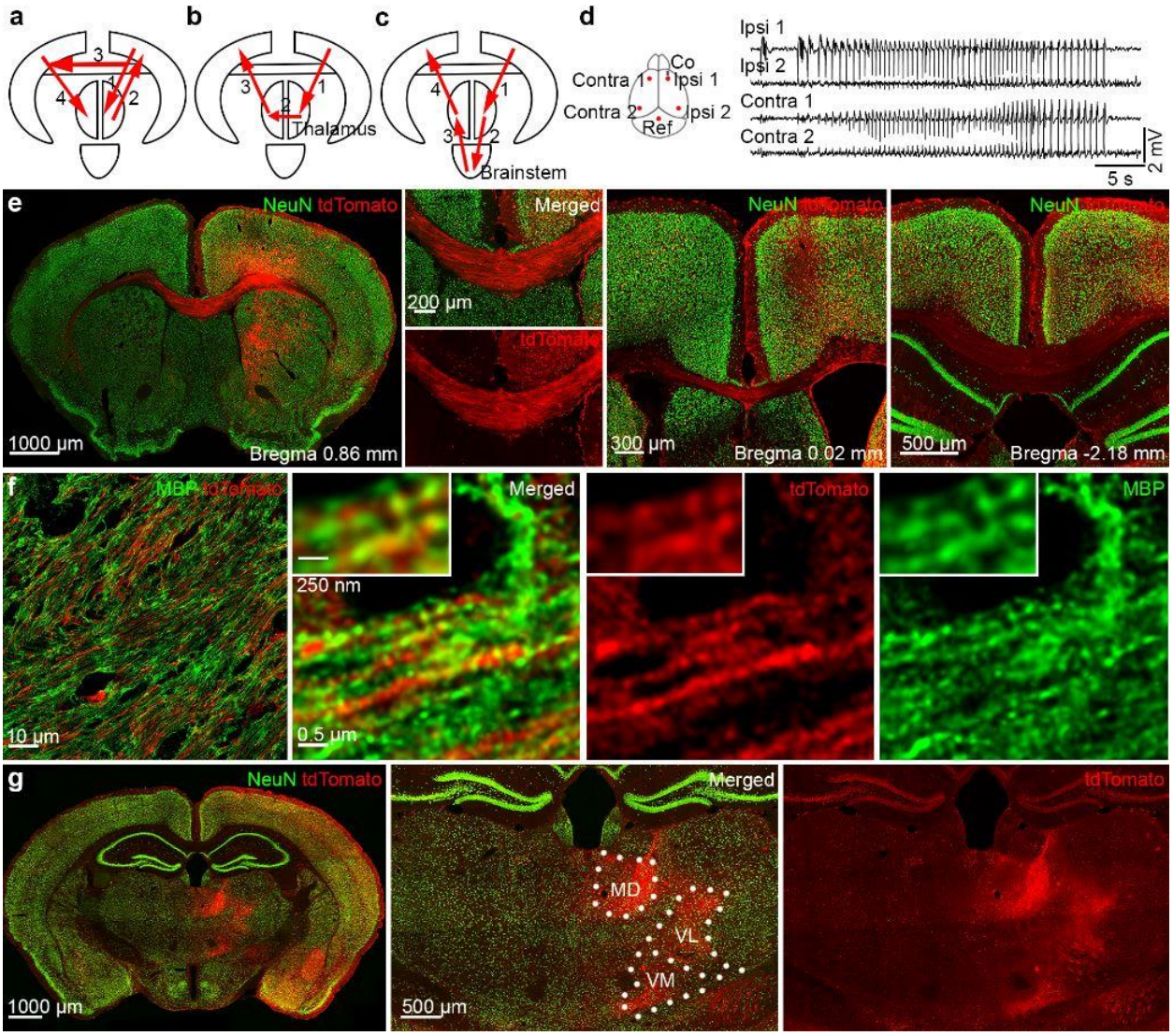
a
b
c
d
Thalamus
Brainstem
Co
Contra 1
Ipsi 1
Contra 2
Ipsi 2
Ref
Ipsi 1
Ipsi 2
Contra 1
Contra 2
2 mV
5 s
e
NeuN tdTomato
Merged
200 µm
tdTomato
1000 µm
Bregma 0.86 mm
NeuN tdTomato
300 µm
Bregma 0.02 mm
NeuN
500 µm
Bregma -2.18 mm
f
MBP tdTomato
Merged
250 nm
10 µm
0.5 µm
tdTomato
MBP
g
NeuN tdTomato
Merged
MD
VL
VM
1000 µm
500 µm
tdTomato

Figure 5-1

Supplementary Figure 5-1. A) tdTomato expression in the corpus callosum of steel wire implanted mice without seizures immunolabeled for NeuN (green). B) tdTomato expression in the thalamus of steel wire implanted mice. Dotted lines indicate nuclear boundaries.

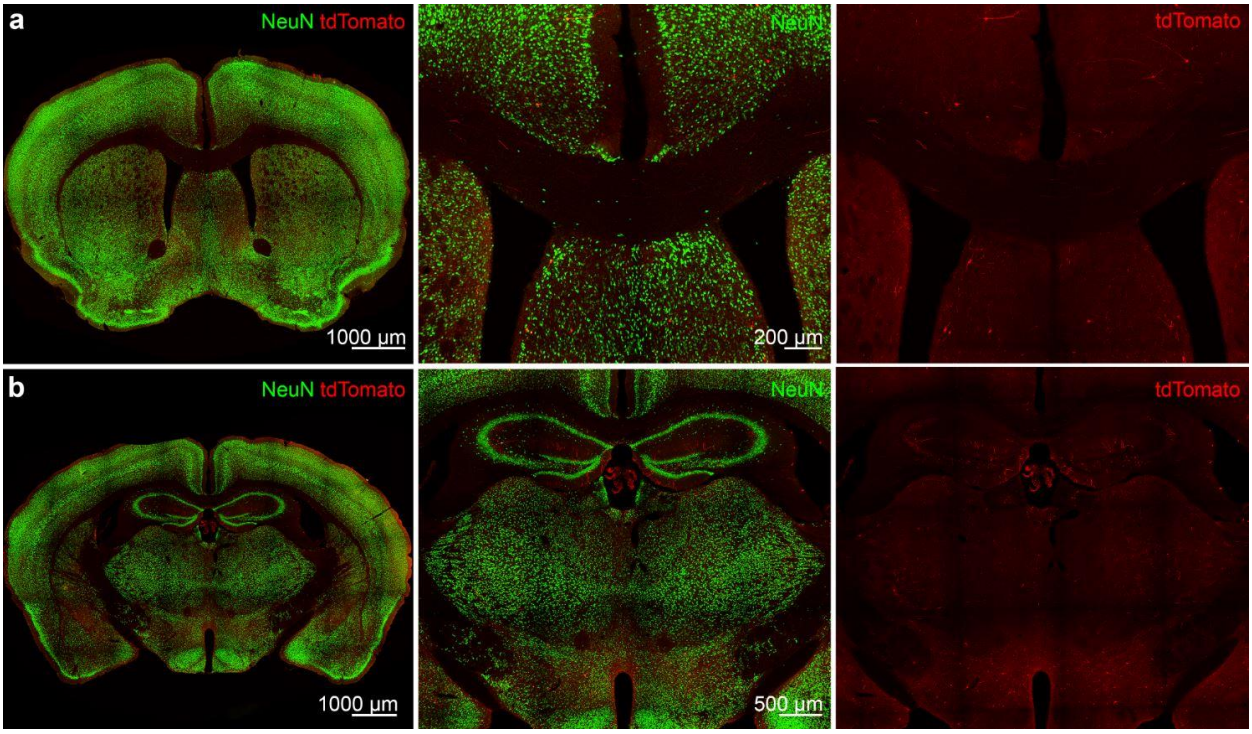

Supplementary Figure 5-1

easier electrode targeting. A current was applied at the end of the recordings to mark location of the electrode tips (Figure 5-2D). The data were analyzed only if the recording location was correct.

Surprisingly, we found that seizures spread faster to the contralateral cortex than to the contralateral thalamus (Figure 5-2A). Interestingly, some seizures required several tens of milliseconds to arrive to the contralateral thalamus (short latency < 200 ms), whereas others required several seconds to appear there (long latency > 200 ms). In the contralateral VL, 53% of all seizures were short latency, and 47% were long latency (Figure 5-2C). However, 100% of seizures arrived to the contralateral cortex within 200 ms (Figure 5-2B). Thus, in some seizures, contralateral seizure spread occurs without the engagement of the contralateral thalamus, supporting spread via the corpus callosum (Figure 5-1A).

Connectivity of excitatory neurons shapes seizure spread

In the previous paper, we showed that anatomical connections of the seizure focus are essential in shaping the subcortical seizure circuit (14). Here, we labeled anatomical projections of the seizure focus to determine if seizures utilize them to spread contralaterally. To trace efferent projections of the seizure focus, we injected AAV9 GFP virus (AAV9-CamKII0.4.eGFP.WPRE.rBG) in TRAP2 mice at the same coordinates in the premotor cortex two weeks before cobalt surgery and injected 4-OHT within 90 min after focal to bilateral tonic-clonic seizure.

The corpus callosum strongly expressed AAV9 GFP and tdTomato (Figure 5-3A), which indicates that seizures follow direct anatomical projections of the seizure focus across the corpus callosum to spread contralaterally. To further confirm that seizures used the corpus callosum, we injected Cre-dependent AAV9 virus (AAV9 pCAG-FLEX-EGFP-WPRE) in TRAP2 mice (which express Cre under the regulation of c-Fos), so that the virus would be expressed only in seizure-activated neurons and axons. The corpus callosum strongly expressed Cre-dependent GFP from the anterior to posterior sections, and the tdTomato positive axons of the corpus callosum colocalized with GFP (Figure 5-3B). We also found AAV9 GFP expression in the ipsilateral VL, VM, and MD, consistent with these receiving direct projections from the motor cortex (Figure 5-3C).

Figure 5-2. Seizures spread faster to the contralateral cortex than to the contralateral thalamus. A) Representative simultaneous LFP recordings from the bilateral premotor cortex and thalamic nucleus VL and the corresponding power spectrums. The seizure focus was in the ipsilateral premotor cortex. Red arrows indicate seizure onset time (twice the baseline); red bar in the contralateral VL indicates the delay of seizure onset. B) Seizure onset times (ms) in the contralateral cortex after seizure onset in the ipsilateral premotor cortex. Pie chart: 100% of seizures required < 200 ms to arrive to the contralateral premotor cortex from the ipsilateral premotor cortex (blue): 25.49 ± 3.00 ms, n = 64 seizures from 16 mice. C) Seizure onset times (ms or s) in the contralateral VL after seizure onset in the ipsilateral premotor cortex. Pie chart: 53% of seizures required < 200 ms to arrive to the contralateral VL from the ipsilateral premotor cortex (blue): 59.36 ± 5.61 ms, n = 34 seizures from 13 mice, and 47% required > 200 ms (red): 4.47 ± 0.65 s, n = 30 seizures from 11 mice. D) Lesions were done after the recordings to mark the location of the electrode tips in the VL on both hemispheres (red arrows).

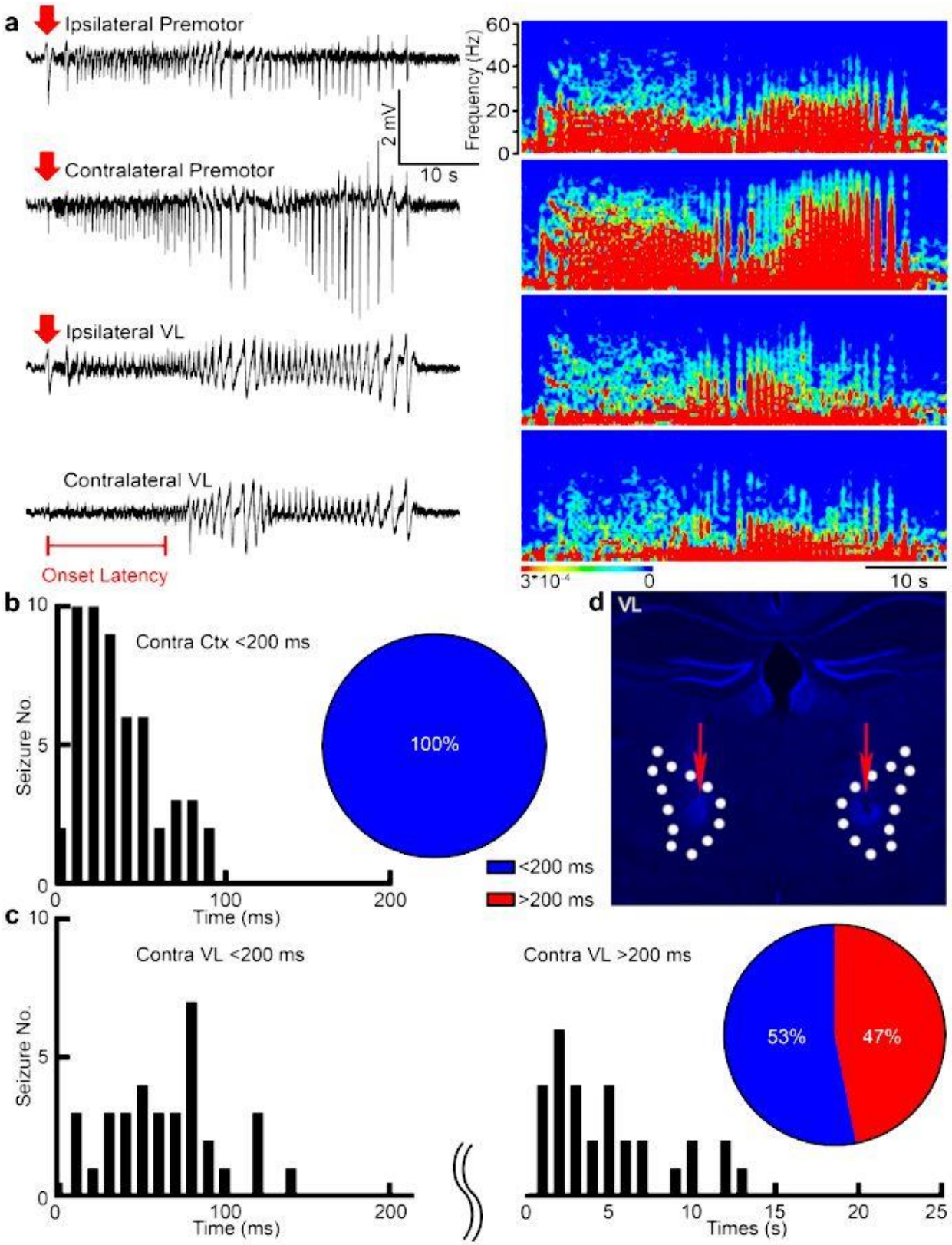
a
Ipsilateral Premotor
Contralateral Premotor
Ipsilateral VL
Contralateral VL
Onset Latency
2 mV
10 s
Frequency (Hz)
60
40
20
0
3*10-4
0
10 s
b
Contra Ctx <200 ms
Seizure No.
10
5
0
0
100
200
Time (ms)
100%
<200 ms
>200 ms
d
VL
c
Contra VL <200 ms
Contra VL >200 ms
53%
47%
0
5
10
15
20
25
Times (s)

Figure 5-2

Figure 5-3. Seizures utilize anatomical projections across the corpus callosum to spread contralaterally. A) A horizontal section shows AAV9 GFP injected in the right premotor cortex, labeling anatomical projections of the seizure focus, and tdTomato expression (red) after focal motor to bilateral tonic-clonic seizure with a magnified view. B) Top: a confocal image of Cre-driven AAV9 GFP expression in the corpus callosum of TRAP2 mice. Middle: super-resolution SoRa image of the callosal axons expressing Cre-driven AAV9 GFP with a magnified view. C) Viral expression in the ipsilateral thalamic nuclei MD, VL, VM after AAV9 GFP injection in the premotor cortex. Dotted lines indicate nuclear boundaries. Boxed insets: magnified views. D) Minimal anatomical connections between the ipsilateral and contralateral thalamus after AAV9 GFP injection on the ipsilateral side.

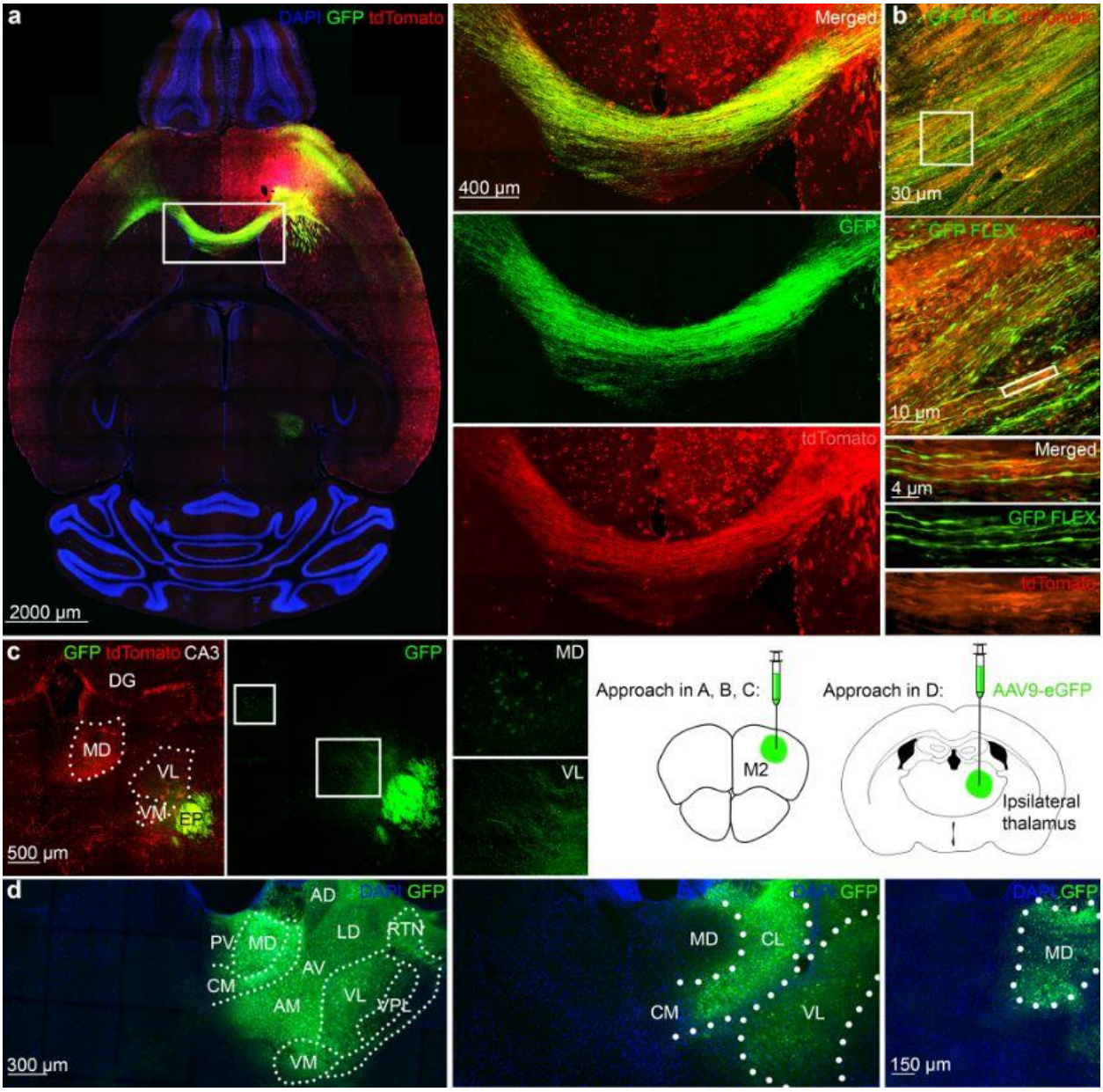
a
DAPI GFP tdTomato
2000 µm
Merged
400 µm
GFP
tdTomato
b
30 µm
10 µm
Merged
4 µm
GFP FLEX
c
GFP tdTomato CA3
DG
MD
VL
VM
EP
500 µm
GFP
MD
VL
Approach in A, B, C:
M2
Approach in D:
AAV9-eGFP
Ipsilateral thalamus
d
AD
DAPI GFP
PV
MD
LD
RTN
AV
CM
AM
VL
VPL
VM
300 µm
MD
CL
CM
VL
150 µm

Figure 5-3

Seizure onset delay that we find in the contralateral thalamus could be due to sparse anatomical projections from the ipsilateral thalamus, so we injected AAV9 GFP virus (AAV9-CamKII0.4.eGFP.WPRE.rBG) in the ipsilateral thalamus. CM, MD, VL, VM, and other ipsilateral thalamic nuclei were labeled with the virus. However, minimal viral expression was found in any of the nuclei in the contralateral thalamus (Figure 5-3D), which indicates that the ipsilateral thalamus is very weakly connected to the contralateral via direct monosynaptic connections, further supporting callosal spread (Figure 5-1A).

Contralateral seizure spread still occurs after chemogenetic inhibition of the ipsilateral thalamus, but seizure duration decreases

We inhibited ipsilateral motor thalamic nucleus VL to determine whether seizures would still spread to the contralateral hemisphere. We injected AAV8 hSyn-dF-HA-KORD-IRES-mCitrine and AAV9 CamKII.HI.GFP-Cre.WPRE.SV40 in 1:1 ratio in the ipsilateral VL of C57Bl/6 mice and allowed 2 weeks for expression (Figure 5-4A,B). We first confirmed the ability of KORD to generate SALB-induced hyperpolarization using whole-cell patch clamp recordings. Bath application of 100 nM SALB in DMSO led to hyperpolarization of transduced neurons with no effect after DMSO application alone (Figure 5-4C,D).

We next tested the effect of ipsilateral VL inhibition on seizure spread. KORD injected C57Bl/6 mice were implanted with cobalt and four LFP microelectrodes in the bilateral premotor cortex and VL and injected with salvinorin B (SALB, 10 mg/kg in DMSO), DMSO, or saline s.c. at 20 hours after cobalt insertion at the peak of seizures. Surprisingly, seizures still spread to the contralateral cortex after chemogenetic inhibition of the ipsilateral VL(Figure 5-4E). However, mean seizure duration decreased significantly (Figure 5-4E-H). Because not all mice started and finished seizing at the same time, we quantified seizure duration before the injection starting at 17 hours after cobalt, when 80% of mice developed seizures, and after the injection until 31 hours after cobalt (Figure 5-4H). The effect of SALB on the suppression of seizure duration was noticed for the next 7 hours following the injection. We also found that the overall seizure burden, defined here as the sum of seizure activity per hour (15), in SALB treated mice was similar to the saline treated control (Figure 5-4J). Thus, because

Figure 5-4. Chemogenetic inhibition of the ipsilateral VL decreases seizure duration but does not prevent contralateral spread. A) A schematic of KORD/CamKII.Cre injection in the ipsilateral VL. B) Confocal image of KORD expression in the ipsilateral VL. C,D) Membrane potential (mV) of transduced cells before and after SALB application (n = 1). E,F) A representative LFP recording of a seizure after SALB or saline injection. G) Mean seizure duration (s) after SALB (green) or saline (red) injection done at 20 hours after cobalt insertion (black arrow). H) % of mice starting to have seizures at specified number of hours after cobalt insertion, where green line indicates a mouse group destined for SALB treatment and red line for saline. I) Mean seizure duration before SALB (green) or saline (red) injection (17-20 hours after Co), following the injection (20-27 hours after Co), and after the injection (27-31 hours after Co). H) Seizure burden (sum of seizure durations per hour) in SALB (green) and saline (red) groups.

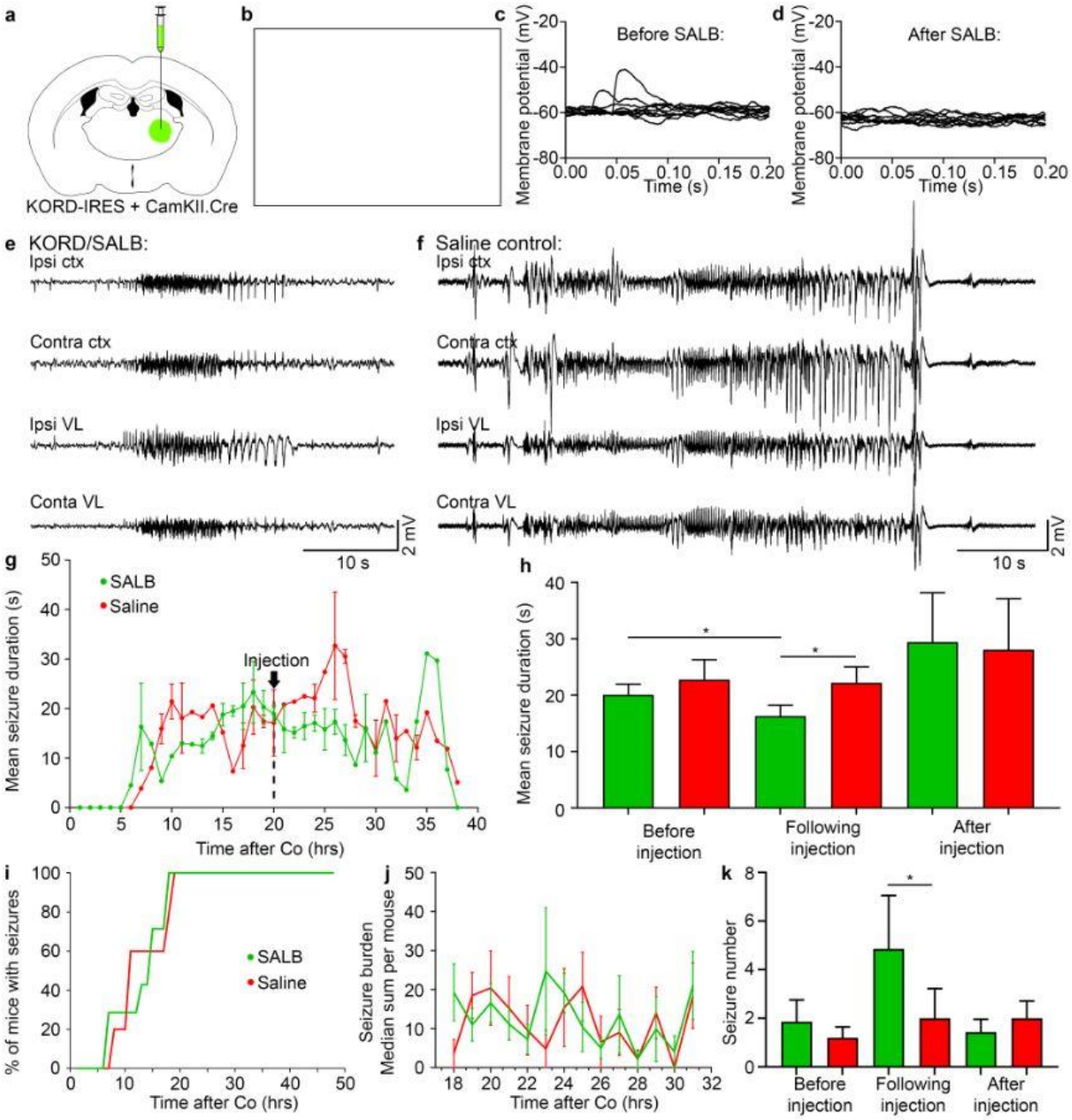
a
KORD-IRES + CamKII.Cre
b
c
Before SALB:
Membrane potential (mV)
Time (s)
d
After SALB:
e KORD/SALB:
Ipsi ctx
Contra ctx
Ipsi VL
Conta VL
10 s
2 mV
f Saline control:
Ipsi ctx
Contra ctx
Ipsi VL
Contra VL
10 s
2 mV
g
SALB
Saline
Injection
Mean seizure duration (s)
Time after Co (hrs)
h
Mean seizure duration (s)
Before injection
Following injection
After injection
i
% of mice with seizures
SALB
Saline
Time after Co (hrs)
j
Seizure burden
Median sum per mouse
Time after Co (hrs)
k
Seizure number
Before injection
Following injection
After injection

Figure 5-4

seizure duration decreased, but seizure burden stayed similar to the control, we find an increase in seizure number after ipsilateral VL inhibition (Figure 5-4K), suggesting that the thalamus amplifies seizures.

Closed-loop optogenetic inhibition of the ipsilateral thalamus

Because the duration of SALB inhibition is limited by its metabolism, we used closed-loop optogenetics to inhibit ipsilateral VL. We injected AAV9 CamKII-ArchT-GFP, which allows hyperpolarization when illuminated with 540 nm green light, or CamKII-driven GFP alone in the ipsilateral VL (Figure 5-5A,B). After two weeks, we inserted cobalt, four LFP microelectrodes in the bilateral premotor cortex and VL, and optic fiber in the ipsilateral VL.

Anterior callosotomy prevents contralateral seizure spread during initial seizures

We next cut the corpus callosum to determine if it would stop contralateral seizure spread. A knife was inserted in the posterior contralateral cortex, avoiding damaging the superior sagittal sinus (Figure 5-6A). The genu and body of the corpus callosum were cut as the knife was removed, cobalt was inserted, and the mice were monitored for seizures. After successful genu cuts, initial seizures either did not spread contralaterally or weakly appeared there only at the end of a seizure (Figure 5-6B). However, as the seizure number a mouse experienced increased, subsequent seizures reached the contralateral side faster, with shorter onset delay (Figure 5-6C,F), but the seizure amplitude was diminished. Faster seizure arrival to the contralateral cortex could be due to developed plasticity after repeated seizures that induce circuit changes. Seizures could form stronger networks via the posterior cortex and the splenium of the corpus callosum to spread contralaterally or via the anterior commissure.

In the instances where the genu was not cut but the body of the corpus callosum was, mice experienced immediate contralateral seizure onset just like the mice without callosotomy (Figure 5-6E,F), suggesting that it is the genu that is important for immediate focal to bilateral spread.

Figure 5-5. Closed-loop optogenetic inhibition of the ipsilateral VL. A) A schematic of optic fiber location in the ipsilateral VL. B) Confocal image of Arch GFP expression in the ipsilateral VL. C) Representative example of LFP recording from the bilateral premotor cortex and VL before and after 540 nm light delivery in the ipsilateral VL.

Figure 5-6. Anterior callosotomy prevents the contralateral spread of initial seizures. A) A schematic of the sagittal view during callosotomy. A curved knife (red) was advanced from the posterior contralateral cortex at 52° until the genu of the corpus callosum (gcc) was reached; the splenium of the corpus callosum (scc) was left uncut. B) A representative first seizure after callosotomy (with cut genu). C) A representative later seizure after callosotomy (with cut genu). D) Sequential light images of the callosotomy from the anterior to posterior brain sections, where red arrow indicates the lesion on the contralateral side (magnified images). E) Representative light image of the callosotomy where the genu was not cut (red arrow, magnified view) and the first seizure with immediate contralateral seizure onset. F) Onset seizure delay (s) in the anterior contralateral premotor cortex after callosotomy in mice with cut genu (green) and without cut genu (red). As the seizure number increased, onset delay decreased. The data for a separate mouse with cut genu is represented by a different shade of green.

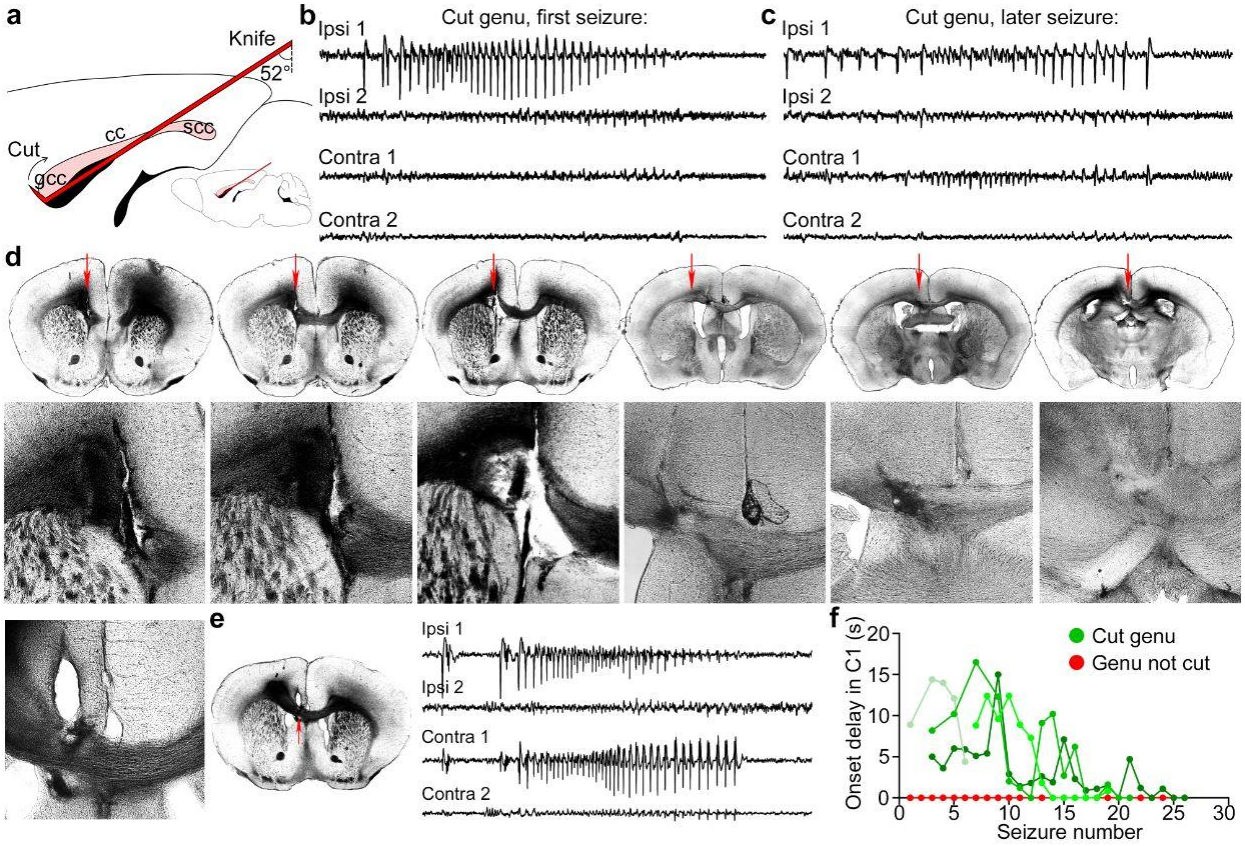
a
Knife
52°
Cut
cc
scc
gcc
b
Cut genu, first seizure:
Ipsi 1
Ipsi 2
Contra 1
Contra 2
c
Cut genu, later seizure:
Ipsi 1
Ipsi 2
Contra 1
Contra 2
d
e
Ipsi 1
Ipsi 2
Contra 1
Contra 2
f
Onset delay in C1 (s)
0
5
10
15
20
0
5
10
15
20
25
30
Seizure number
Cut genu
Genu not cut

Figure 5-6

DISCUSSION

We show that the thalamus amplifies frontal lobe motor seizures, whereas the corpus callosum allows spread to the contralateral hemisphere.

The choke point hypothesis indicates that the thalamus is essential for seizure maintenance and generalization. However, seizure spread from the seizure focus to the contralateral cortex has not been delineated. Several famous models of seizure generalization indicate that spread to the contralateral cortex occurs via commissural connections between the two thalami or through bilateral spread from the thalamus via the brainstem. We looked at the connectivity, and our findings support the model in which seizure spread to the contralateral cortex occurs through the corpus callosum.

Our new methods allowed us to both track and stop seizure spread to investigate the roles of the thalamus and corpus callosum. We selected novel kappa-opioid based DREADD over chemogenetics based on CNO to precisely inhibit the thalamus, without increasing susceptibility to seizures. Clozapine N-oxide is reverse metabolized to clozapine (16), which, as a D2 antagonist, exerts a pro-convulsant effect (17,18) compared to inert salvinorin B. We also developed a deep convolutional neural network-based automated seizure detection model in MATLAB for closed-loop optogenetics to inhibit ipsilateral thalamus in a fully automated way. Also, we lesioned the genu of corpus callosum during focal to bilateral seizures to determine its role in secondary generalization. Although corpus callosotomy surgeries are done to improve the outcome of intractable primarily generalized seizures, the role of the corpus callosum in secondarily generalized seizures has not been delineated to allow a confident clinical strategy.

Our studies demonstrate that the connectivity of excitatory neurons shapes the seizure spread. Thus, extensive direct anatomical projections from the seizure focus across the corpus callosum and lack of monosynaptic projections from the ipsilateral thalamus to the contralateral allow seizures to spread faster to the contralateral cortex than to the contralateral thalamus. We find that chemogenetic and closed-loop optogenetic inhibition of the ipsilateral thalamus still allowed contralateral seizure spread, whereas lesioning of the corpus callosum prevented it during initial seizures.

REFERENCES FOR CHAPTER 5

1. Falco-Walter, J. J., Scheffer, I. E. & Fisher, R. S. The new definition and classification of seizures and epilepsy. *Epilepsy Res.* **139**, 73–79 (2018).
2. Westbrook, G. L. Seizures and epilepsy. in *Principles of neural science* (eds. Kandel, E. R., Schwartz, J. H., Jessell, T. M., Siegelbaum, S. A. & Hudspeth, A. J.) 1116–1139 (New York: McGraw-Hill, 2013).
3. Blumenfeld, H. *et al.* Cortical and subcortical networks in human secondarily generalized tonic-clonic seizures. *Brain* **132**, 999–1012 (2009).
4. Englot, D. J., Morgan, V. L. & Chang, C. Impaired vigilance networks in temporal lobe epilepsy: Mechanisms and clinical implications. *Epilepsia* **61**, 189–202 (2020).
5. Paz, J. T. *et al.* Closed-loop optogenetic control of thalamus as a new tool to interrupt seizures after cortical injury. *Nat Neurosci* **16**, 64–70 (2013).
6. Paz, J. T. & Huguenard, J. R. Microcircuits and their interactions in epilepsy: Is the focus out of focus? *Nat Neurosci* **18**, 351–359 (2015).
7. Lothman, E. W. & Collins, R. C. Kainic acid induced limbic seizures: metabolic, behavioral, electroencephalographic and neuropathological correlates. *Brain Res.* **218**, 299–318 (1981).
8. Penfield, W. & Jasper, H. H. *Epilepsy and the functional anatomy of the human brain*. (Little, Brown, 1954).
9. Faingold, C. L. & Penfield, J. *Brainstem Networks Reticulo-Cortical Synchronization in Generalized Convulsive Seizures*. (2012).
10. Iadarola, M. J. & Gale, K. Substantia nigra: site of anticonvulsant activity mediated by γ-aminobutyric acid. *Science* **218**, 1237–1240 (1982).
11. Guenthner, C. J., Miyamichi, K., Yang, H. H., Craig Heller, H. & Luo, L. Permanent genetic access to transiently active neurons via TRAP: Targeted Recombination in Active Populations. *Neuron* **78**, 773–784 (2013).
12. Allen, W. E. *et al.* Thirst-associated preoptic neurons encode an aversive motivational drive. *Science* **357**, 1149–1155 (2017).
13. Singh, T., Joshi, S., Williamson, J. M. & Kapur, J. Neocortical injury–induced status epilepticus. *Epilepsia* **61**, (2020).

14. Brodovskaya, A., Shiono, S. & Kapur, J. Activation of the basal ganglia and indirect pathway neurons during frontal lobe seizures. *Brain* (2021).
15. Pressler, R. M. *et al.* The ILAE classification of seizures and the epilepsies: Modification for seizures in the neonate. Position paper by the ILAE Task Force on Neonatal Seizures. *Epilepsia* **00**, 1–14 (2021).
16. Manvich, D. F. *et al.* The DREADD agonist clozapine N-oxide (CNO) is reverse-metabolized to clozapine and produces clozapine-like interoceptive stimulus effects in rats and mice OPEN. **8**, 3840 (2018).
17. Koch-Stoecker, S. Antipsychotic drugs and epilepsy: indications and treatment guidelines. *Epilepsia* **43**, 19–24 (2002).
18. Alper, K., Schwartz, K. A., Kolts, R. L. & Khan, A. Seizure incidence in psychopharmacological clinical trials: an analysis of Food and Drug Administration (FDA) summary basis of approval reports. *Biol Psychiatry* **62**, 345–354 (2007).

CHAPTER 6

LONG RANGE SEIZURE PROPAGATION THROUGH CORTICAL LAYERS

SUMMARY AND CONCLUSIONS

1. We find stronger activation of the superficial cortical layers 2/3 than deep layers 5/6 after frontal lobe focal to bilateral tonic-clonic seizures.
2. Seizures spread faster posteriorly through the superficial layers and arrive to posterior deep layers with a delay.
3. We find stronger AAV9 GFP labeling of the posterior superficial layers compared to deep layers, indicative of more direct monosynaptic projections across layers 2/3 than layers 5/6.

INTRODUCTION

Focal to bilateral seizures manifest in many behaviors, including auras, motor activity, and altered consciousness because they travel long distance in the brain from the onset zone. Local spread of seizures has been investigated intensively by in vivo and in vitro imaging techniques (1,2). These studies in the hippocampus and the neocortex demonstrate a strong role for inhibition in shaping seizure spread. Propagation of seizures through the hippocampus is gated by strong inhibition of the dentate gyrus (3). Similarly, in the neocortex, the inhibitory surround shapes the seizure spread (4).

These studies however do not explain how seizures spread over a long distance. A recent study of seizure spread from the visual cortex, combining in vivo imaging with electrophysiology demonstrated that seizures follow the anatomical connections of the visual cortex (5). We also recently reported that seizures originating from the premotor cortex, activate anatomically connected structures: the striatum, globus pallidus, subthalamic nucleus, substantia nigra, and thalamus (6). These studies suggest that the connectivity of excitatory neurons drives seizure spread.

Superficial layers of the cortex play an important role in cortical connectivity. The superficial layers of the premotor cortex contain intratelencephalic (IT) neurons that have long-range intracortical projections, whereas deep layers contain pyramidal type (PT) neurons that project subcortically (7). The premotor cortex also receives long-distance connections from the somatosensory cortex and other cortical areas. Previous literature indicates that deep cortical layers such as layer 4 are necessary for seizure generation and propagation (8,9), but the motor cortex does not contain layer 4 (1). The corpus callosum allows the contralateral spread of frontal lobe seizures, and 80% of its axons arise from the superficial layers (10). The connectivity hypothesis would suggest that the cortical spread of seizures would engage the layer 2/3 of the cortex. Some recent studies indicate that superficial layers 2/3 are recruited ahead of deep layers 5/6 during acute seizures (1,2). However, they did not investigate long-range layer recruitment during spontaneous seizures away from the seizure onset zone. We studied seizure spread away from seizure focus in the premotor cortex intracortically, to test whether spread can be predicted by connectivity.

METHODS

Animals

Experiments were approved by the University of Virginia Animal Care and Use Committee. Mice expressing Cre-ER under the regulation of c-Fos promoter (Fos$^{2A\text{-}ICreERT2}$, #030323, Jackson Laboratories) were crossed to mice expressing tdTomato from Rosa locus (Ai9, #007909, Jackson Laboratories) to generate TRAP2 mice. TRAP2 and C57Bl/6 (Charles River) mice (7-12 weeks) of both sexes were maintained on a 12-hour light/dark cycle and had *ad libitum* food and water. For genotyping, KAPA Biosystems kit was used.

Seizure induction, electrophysiology, and virus injections

To induce frontal lobe focal to bilateral tonic-clonic seizures, TRAP2 or C57Bl/6 mice were placed under isoflurane anesthesia, and 1.7 mg of cobalt wire was inserted into the right premotor cortex (AP +2.6 mm, ML -1.8 mm) along with four bilateral subdural EEG electrodes and a reference as described previously (6). Mice were monitored for seizures via continuous video/EEG. 4-hydroxytamoxifen (4-OHT, 50 mg/kg s.c.) was injected in TRAP2 mice within 90 of a secondarily generalized tonic-clonic seizure. Animals were perfused 5 days after 4-OHT injection to allow tdTomato expression. 1.7 mg of steel wire was used as control and implanted instead of cobalt. Mice were monitored via continuous video/EEG and developed no seizures. 4-OHT was injected 18 hours after steel implantation.

Local field potentials (LFPs) were recorded with a custom-made array of microelectrodes with 60-70 kΩ resistance and 10 kHz sampling rate as described previously (6). For the activities to be considered independent, we coordinated the distance between each microelectrode so that the cross-correlation coefficient was less than 0.7 between each electrode. Fast Fourier Transform with a Cosine-Bell window was used to analyze LabChart 8 LFP data as we described before (6). To record seizures, the first electrode (E1) was implanted on the ipsilateral side 400 µm behind cobalt and subsequent electrodes separated from each other by 750 µm (E2-E5). E1 was located in the premotor cortex, E2 in the motor cortex, and E3-E5 in the somatosensory cortex. In double-layer recording electrodes, electrodes were inserted 200 µm below dura to record from layer 2/3 and 700 µm below dura to record from layer

5/6. Seizure start was defined as a deflection of voltage trace at least twice the baseline. After recordings, the electrode position was marked by applying a single 40 µA, 0.75 msec monophasic square wave pulse at 50 Hz for 30 sec using a constant current stimulator (Model 2100, A-M Systems). The brains were sectioned 40 µm thick on a cryostat (CM1900, Leica), stained with DAPI (0.02% in PBS), and imaged on Nikon Eclipse Ti-S, 2x/0.45 NA. If the electrode position was incorrect, the data were excluded.

Because CAG Double flox Synaptophysin-EGFP WPRE (#73816, plasmid, Addgene) was too large for efficient packaging into a virus, we replaced 1300 bp 3'UTR with a minimal version developed by Choi et.al.[11]. Minimal WPRE was PCR amplified with added HindIII and SphI sites and ligated to the original cut plasmid. Miniprep (Qiagen), sequencing, and maxiprep were carried out, and the plasmid was packaged into AAV9 virus through Vigene Biosciences (Titer >$1x10^{13}$ GC/ml).

AAV9 CamKII0.4.eGFP.WPRE.rBG (#105541-AAV9, Addgene), Cre-driven AAV9 pCAG-FLEX-EGFP-WPRE (#51502-AAV9, Addgene), or Cre-driven AAV9 CAG Double flox Synaptophysin-EGFP WPRE (described above) were injected in the right premotor cortex of TRAP2 or C57Bl/6 mice (AP +2.6 mm, ML -1.8 mm, DV -0.5 mm; 100 nl) with Hamilton syringe (#7634-01), and 2 weeks were allowed for the viral expression before proceeding with cobalt insertion.

Immunohistochemistry

Mice were deeply anesthetized with isoflurane and perfused with 4% paraformaldehyde, sliced at 40, and placed in a blocking buffer as described before (6). The primary antibodies used were rabbit anti-NeuN (1:500, #24307, Cell Signaling), rabbit anti-TBR1 (1:500, #ab31940, Abcam), rat anti-CTIP2 (1:300, #ab18465, Abcam), mouse anti-Bassoon (1:500, #ab82958, Abcam). The secondary antibodies (1:500, Invitrogen) were 405 goat anti-mouse, 488 goat anti-rabbit, 488 goat anti-mouse, 488 goat anti-rat, and 594 goat anti-rabbit.

Image acquisition and analysis

Confocal images were done on Nikon Eclipse Ti-U with NIS-Elements software at 10x/0.45 NA, 20x/0.95 NA, or 40x/1.80 NA, oil, 1024x1024 or 512x512 frame size, and 5 µm z-interval. Synapses were imaged on CSU-W1 SoRa Yokogawa Spinning Disk

Confocal, Nikon at 100x/1.35 NA, silicon, or 60x/1.49 NA, oil, 2304x2304, 0.5 µm step size. Excitation lasers were 405, 488, and 561. Imaris .3.0 (Bitplane) was used for visualization and Adobe Photoshop CC for figure display.

To count % of active cells in the cortical layers, the number of tdTomato positive cells in either layer 2/3 or 5/6 was counted in ImageJ and divided by the total number of neurons (NeuN positive cells) in either layer 2/3 or 5/6. Cortical layers were identified by TBR1 or CTIP2 stain.

Statistics

All statistical analysis was performed in Prism 8. Unpaired t-test was used for normally distributed data. Kolmogorov-Smirnov test was used for not normally distributed data. Results were considered statistically significant for $p < 0.05$. Data are presented as mean ± SEM, where n is the number of animals or the number of seizures followed by the number of animals.

RESULTS

Seizures activate superficial layers stronger and spread along them intracortically faster compared to deep layers

We induced frontal lobe focal motor to bilateral tonic-clonic seizures by placing 1.7 mg of cobalt in the right premotor cortex as described previously. To visualize activated neurons, we used activity reporter TRAP2 mice that express Cre under the regulation of c-Fos promoter (12,13). Injection of 4-hydroxytamoxifen (4-OHT, 50mg/kg) translocates Cre inside a nucleus and relieves repression from tdTomato to label only seizure-activated cells. The brains were then slices, and the pattern of tdTomato expression was investigated.

We found that superficial cortical layers contained more activated tdTomato positive cells than did deep layers (Figure 6-1A-D). We used cortical layer markers TBR1, which labels layers 2/3 and 5/6, and CTIP2, which labels 5/6, to delineate layers. Because superficial layers have higher cellular density per unit area than do deep layers, we expressed layer activation as the number of tdTomato positive cells divided by the total number of NeuN positive neurons in that layer, to obtain % activation. Overall, superficial layers 2/3 had on average 12.66 ± 1.038% more activated cells than deep layers 5/6 across frontal and parietal lobes on the contralateral hemisphere (Figure 6-1B). Anterior to posterior analysis across bregma revealed that the anterior frontal lobe cortex had the largest difference between activated cells in layer 2/3 versus 5/6 (Figure 6-1C) because that area was closer to the seizure focus. Frontal lobe cortical layers overall had more tdTomato expression than parietal lobe cortical layers (Figure 6-1C). We used anti-CaMKII antibody to confirm that activated tdTomato positive cells in the cortex were excitatory pyramidal neurons (Figure 6-1E).

To gain temporal resolution of seizure spread across the layers from anterior to posterior cortex, we recorded LFPs using an array of five microelectrodes placed on the ipsilateral hemisphere to the seizure focus with the first electrode 400 μm behind cobalt and each subsequent electrode 750 μm behind the previous one, recording from the premotor, motor, and somatosensory cortices simultaneously (Figure 6-2A). In one set of animals, all five microelectrodes were inserted in layer 2/3 (200 μm below dura) and in another set of animals in layer 5/6 (700 μm below dura). Seizure onset latency was

Figure 6-1. Superficial layers are more activated during seizures than deep layers. A,D) Superficial layers 2/3 expressed more tdTomato compared to deep layers 5/6. Cortical layers were determined by immunolabeling for TBR1 (green). B) % Activated cells (number of tdTomato cells divided by the total number of NeuN positive neurons in a layer) in layer 2/3 (blue) and 5/6 (red) from frontal to parietal lobe, (n = 3 mice) (unpaired t test). C) % Activated cells in layer 2/3 (blue) and 5/6 (red) from anterior (3.0 mm bregma) to posterior contralateral cortex (-4.0 mm bregma), (n = 3 mice). E) tdTomato positive cells (red) in the cortex are pyramidal neurons as indicated by CaMKII immunolabeling (green). Boxed inset: magnified view of the pyramidal neurons. Data are mean ± SEM, **** $p < 0.0001$.

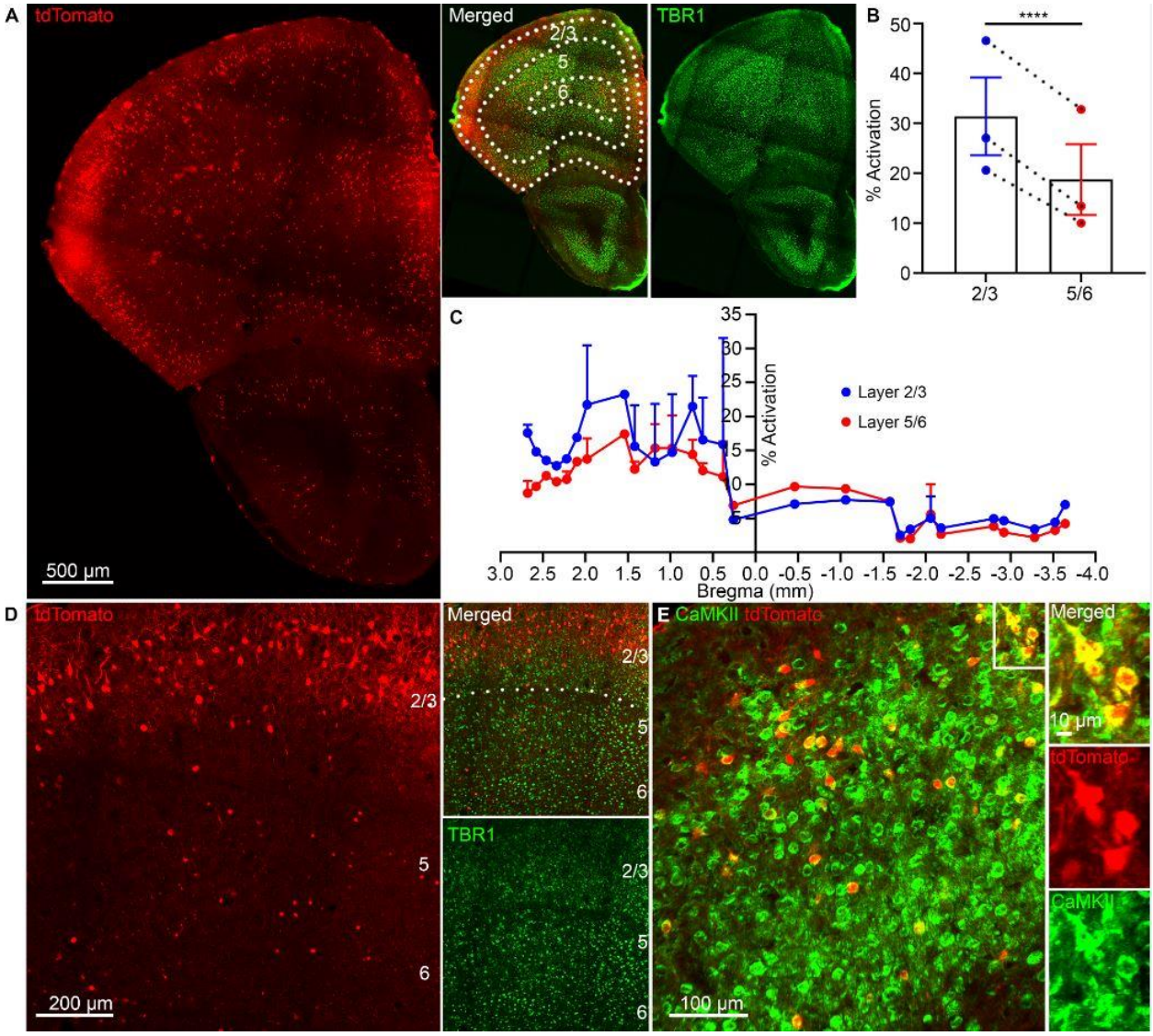
A
tdTomato
500 µm
Merged
2/3
5
6
TBR1
B
****
% Activation
50
40
30
20
10
0
2/3
5/6
C
% Activation
Layer 2/3
Layer 5/6
3.0 2.5 2.0 1.5 1.0 0.5 0.0 -0.5 -1.0 -1.5 -2.0 -2.5 -3.0 -3.5 -4.0
Bregma (mm)
D
tdTomato
2/3
5
6
200 µm
Merged
TBR1
E CaMKII tdTomato
100 µm
Merged
10 µm
tdTomato
CaMKII

Figure 6-1

determined from the time seizures start at the seizure focus. Microelectrode setup prevents recording from more than five LFP microelectrodes at the same time. In the second animal cohort, we carried out LFP recordings from layers 2/3 and 5/6 simultaneously. To establish that the source of electrical activity from one microelectrode was independent of that from a neighboring microelectrode, we analyzed the cross-correlation of activities from two neighboring electrodes, which had to be less than 0.7 for the activities to be considered independent. Microelectrodes with 60-75 kΩ resistance and 2 cm length yielded recording without significant cross-contamination (Figure 6-2B).

Seizures spread faster posteriorly through the superficial layers and slower through the deep layers (Figure 6-2C). 55% of all seizures reached superficial layers in less than 200 ms in the posterior parietal cortex, whereas only 7% of seizures could reach deep layers within 200 ms, and the rest (93%) took longer (Figure 6-3A,B). LFP recordings show an example of seizure onset latency in the posterior cortex (Figure 6-2E,F). Also, spikes in the posterior superficial layers had a higher frequency, whereas spikes in the posterior deep layers had slower frequency (electrodes E4 and E5, Figure 6-2D).

We hypothesized that the immediate seizure onset in the superficial posterior layers was due to more direct anatomical projections from the seizure focus, whereas deep posterior layers could have fewer direct connections and more synapses necessary to reach them, which would increase the chance of failures and cause seizure onset delay. We injected CamKII-driven AAV9 (AAV9-CamKII0.4.eGFP.WPRE.rBG) at the seizure focus to trace its efferent anatomical connections along the cortex. Layer 1 and cell bodies in layer 2/3 in the posterior parietal cortex extensively expressed AAV9 GFP, whereas deep layer 5 had only sparse dendritic GFP expression (Figure 6-2G). Although only a small number of viral particles could be transported transsynaptically in a Cre-independent AAV9 (14), labeling of cell bodies with GFP in the posterior layer 2/3 and 4 could indicate some transsynaptic or retrograde AAV9 spread. However, none of the cell bodies were labeled in the posterior layer 5/6, which indicates that passage of more synapses is necessary to reach them from the seizure focus compared to the superficial layers.

Figure 6-2. Seizures spread faster across superficial layers and slower through deep layers. A) Schematic placement of five LFP electrodes behind cobalt. In one group of animals, E1-E5 electrodes targeted superficial layers (200 µm below dura), and in another group all five electrodes targeted deep layers (700 µm below dura). Image of a custom-made array of microelectrodes. B) A correlation matrix plots the correlation coefficients (from 1.0 to 0) for each pair of microelectrodes, which were calculated based on the LFP time lags between the microelectrodes. E1 corresponds to 0 µm away from cobalt, and E5 corresponds to 3000 µm away from cobalt. C) Seizure beginning latency (s, median with 10-90% tile) in E1-E5 and one contralateral electrode (Contra) across from E1 in layers 2/3 (blue) and 5/6 (red) (n = 29-34 seizures from 7-8 mice, Contra 2/3: 0.020 ± 0.019 s; Contra 5/6: 0.023 ± 0.014 s; E1 2/3: 0.00 ± 0.00 s ; E1 5/6: 0.00 ± 0.00 s; E2 2/3: 0.00 ± 0.00 s; E2 5/6: 0.23 ± 0.92 s; E3 2/3: 0.87 ± 2.06 s; E3 5/6: 1.92 ± 3.36 s; E4 2/3: 1.13 ± 2.80 s ; E4 5/6: 3.99 ± 4.52 s; E5 2/3: 1.44 ± 2.88 s; E5 5/6: 6.61 ± 4.79 s). D) Spike frequency (spikes per minute, median ± IQR) at E1-E5 from superficial (blue) and deep layers (red) (E1 2/3: 0.17 ± 0.12 Hz; E1 5/6: 0.13 ± 0.053 Hz; E2 2/3: 0.17 ± 0.042 Hz; E2 5/6: 0.13 ± 0.053 Hz; E3 2/3: 0.083 ± 0.083; E3 5/6: 0.11 ± 0.053 Hz; E4 2/3: 0.033 ± 0.083 Hz; E4 5/6: 0.033 ± 0.025; E5 2/3: 0.017 ± 0.17; E5 5/6: 0.017 ± 0.025). E,F) Examples of short latency seizures without onset delay in the posterior ipsilateral cortex (E5) and long latency seizures with onset delay in the electrode E5. G) GFP AAV9 expression (AAV9-CamKII0.4.eGFP.WPRE.rBG) on the ipsilateral side to the seizure focus. Layers 1,2/3, and 4 have stronger cellular expression, whereas deep layers 5/6 exhibit only sparse dendritic labeling.

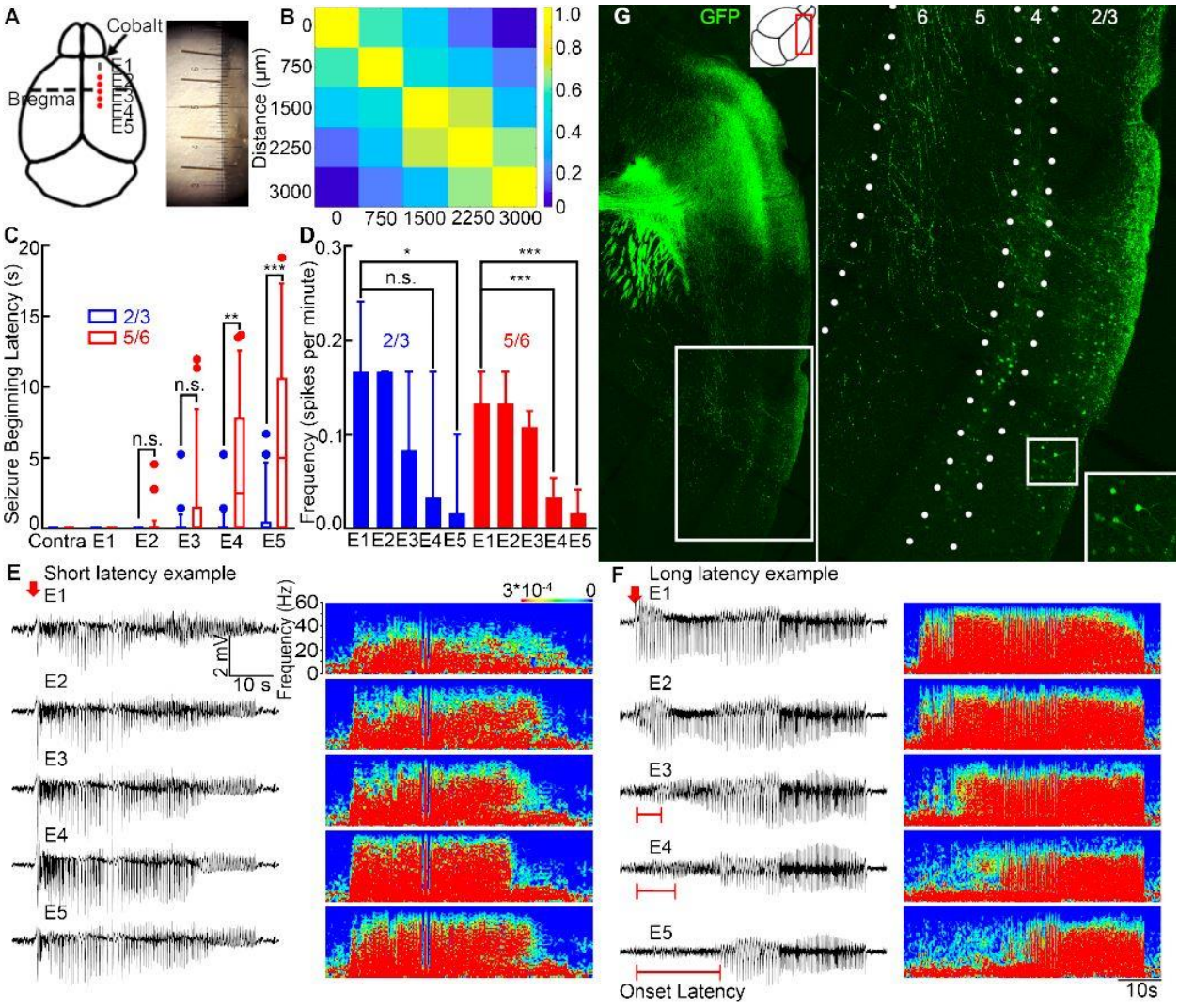
A
Cobalt
Bregma
E1
E2
E3
E4
E5
B
Distance (µm)
0
750
1500
2250
3000
1.0
0.8
0.6
0.4
0.2
0
C
Seizure Beginning Latency (s)
2/3
5/6
n.s.
n.s.
**
***
Contra E1
E2
E3
E4
E5
D
Frequency (spikes per minute)
n.s.
*
***
***
2/3
5/6
E1E2E3E4E5 E1E2E3E4E5
G
GFP
6
5
4
2/3
E
Short latency example
E1
2 mV
10 s
E2
E3
E4
E5
Frequency (Hz)
3*10-4
0
F
Long latency example
E1
E2
E3
E4
E5
Onset Latency
10s

Figure 6-2

Figure 6-3. Short latency and long latency seizures in the superficial and deep layers. A) Seizure onset times (ms or s) in superficial layers from the anterior premotor cortex (E1) to the posterior parietal cortex (E5) ipsilateral to the seizure focus. Pie charts indicate % of seizures that arrived to the corresponding electrodes in < 200 ms (blue) or > 200 ms (red). B) Seizure onset times (ms or s) in deep layers. Pie charts indicate % of seizures that arrived to the corresponding electrodes in < 200 ms (blue) or > 200 ms (red).

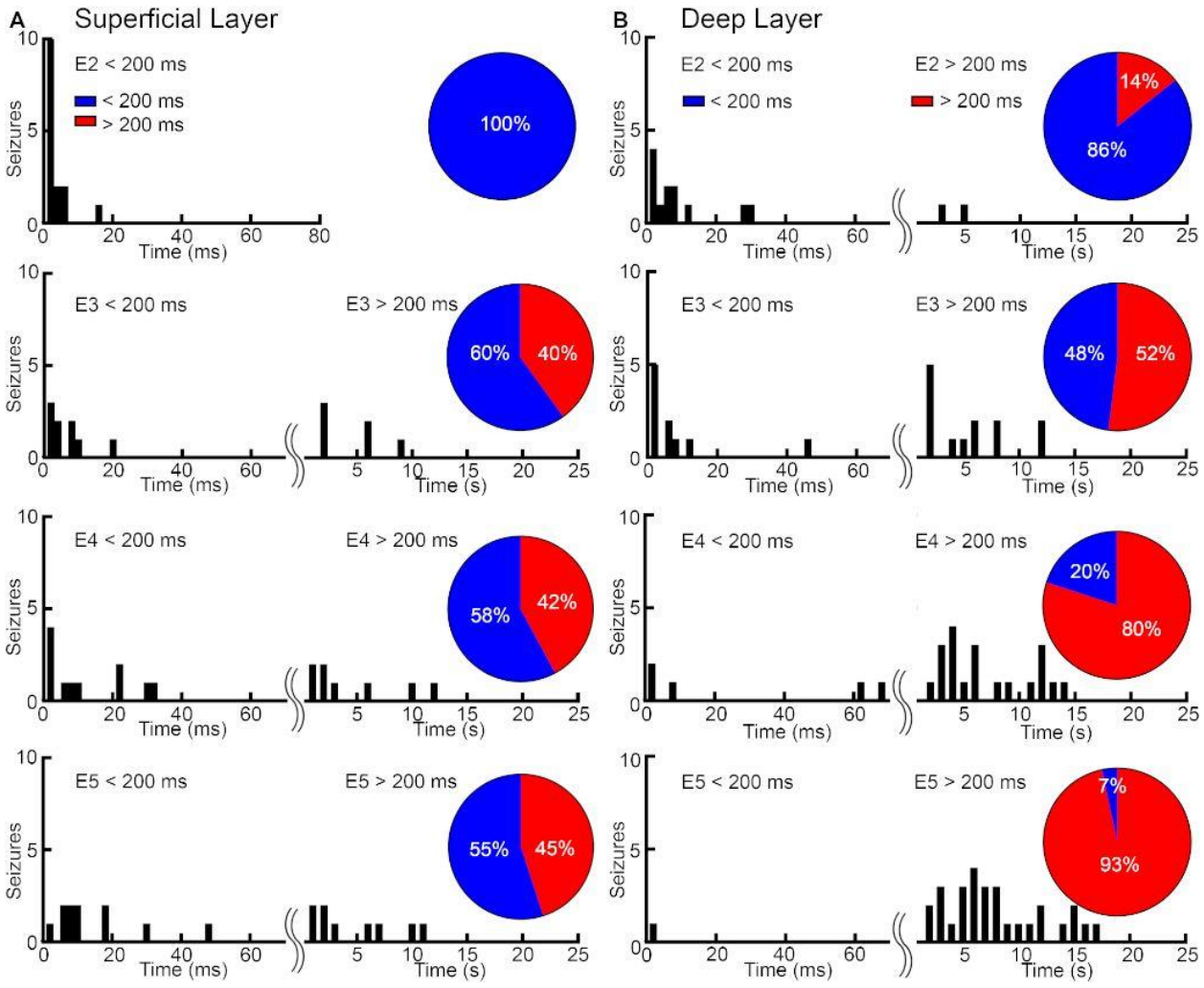
A
Superficial Layer
B
Deep Layer
E2 < 200 ms
< 200 ms
> 200 ms
100%
E2 > 200 ms
14%
86%
E3 < 200 ms
E3 > 200 ms
60%
40%
48%
52%
E4 < 200 ms
E4 > 200 ms
58%
42%
20%
80%
E5 < 200 ms
E5 > 200 ms
55%
45%
7%
93%
Seizures
Time (ms)
Time (s)

Figure 6-3

We also found extensive AAV9 GFP-labeled anatomical projections on the contralateral motor cortex as they arrived from the seizure focus across the corpus callosum (Figure 4A). Areas with stronger GFP expression, especially in the superficial layers, coincided with areas with more tdTomato positive cells, which further supports the connectivity hypothesis of seizure spread rather than seizure spread through the ephaptic connectivity or calcium waves through glia.

Next, we used Cre-dependent AAV9 (AAV9 pCAG-FLEX-EGFP-WPRE) to trace cortico-cortical connections active during seizures. Injecting Cre-dependent AAV9 GFP in TRAP2 mice that express Cre under the c-Fos promoter leads to GFP expression only in seizure active cells. We found that superficial layers on the ipsilateral side had denser GFP expression compared to deep layers (Figure 4B). tdTomato positive neurons had GFP puncta around them (Figure 4B), which is indicative of dendritic terminals from the seizure focus synapsing on the cell bodies to active them.

To confirm that these were synapses, we used Cre-dependent AAV9 GFP synaptophysin virus (CAG Double flox Synaptophysin-EGFP WPRE), which is expressed only in the activated synapses monosynaptically connected to the seizure focus, and anti-bassoon antibody, which marks presynaptic terminals (Figure 5A). Synaptophysin (green) colocalized with bassoon (blue) around tdTomato positive activated cells in the posterior ipsilateral cortex (Figure 5B), which confirms that direct anatomical projections of the seizure focus drive seizure spread. However, not all neurons that received direct projections from the seizure focus became tdTomato positive, which might suggest that those neurons were electrophysiologically different to begin with.

Figure 6-4. The connectivity of excitatory neurons drives seizure spread. A) Horizontal image of GFP AAV9 expression (AAV9-CamKII0.4.eGFP.WPRE.rBG) of the anatomical projections on the contralateral side that arrived from the seizure focus as they traveled across the corpus callosum. Areas with stronger GFP expression have more tdTomato cell labeling. B) Coronal image of Cre-driven GFP AAV9 expression (AAV9 pCAG-FLEX-EGFP-WPRE) in the posterior ipsilateral cortex with stronger AAV9 labeling in the superficial layers.

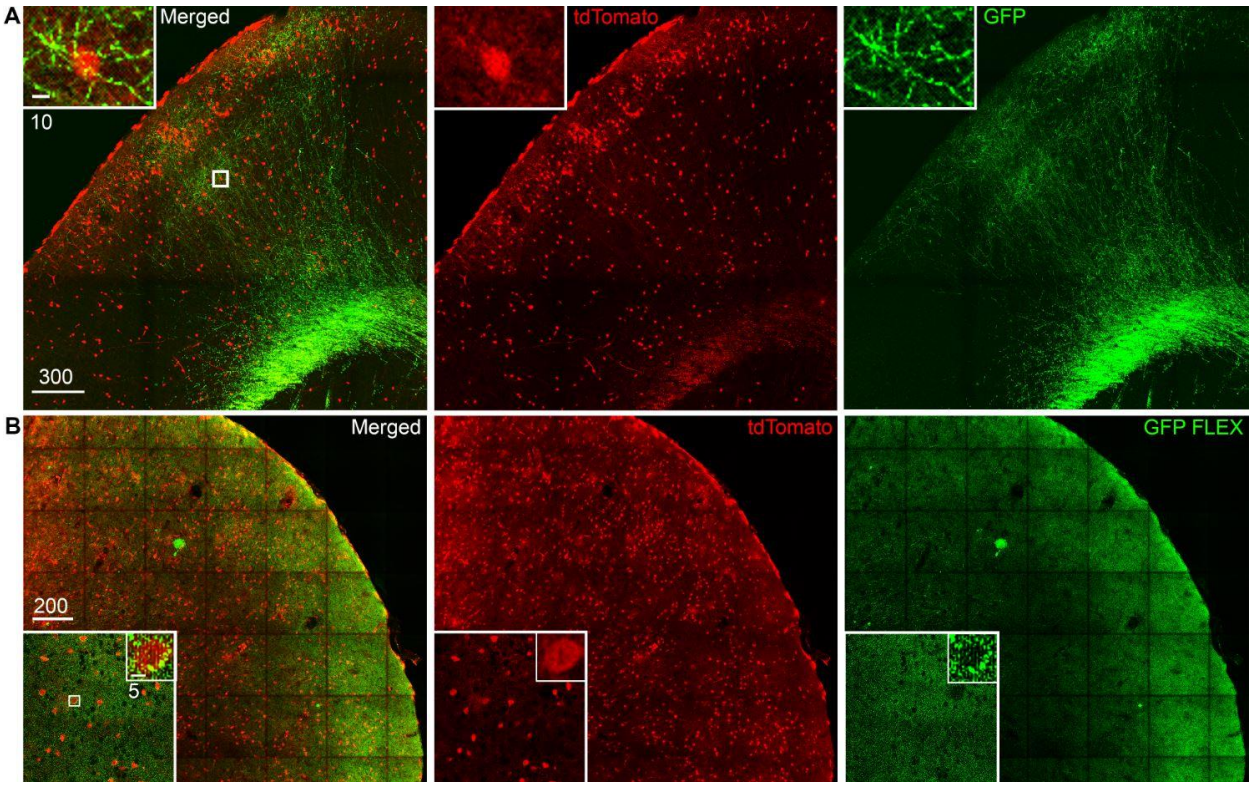

Figure 6-4

Figure 6-5. Direct synaptic connectivity drives seizures spread in the posterior cortex. A) Cre-driven GFP AAV9 synaptophysin expression (AAV9 CAG Double flox Synaptophysin-EGFP WPRE) in the posterior superficial cortical neurons on the ipsilateral side. B) Cre-driven synaptophysin (green) is colocalized with pre-synaptic marker Bassoon (blue) in activated tdTomato positive neurons.

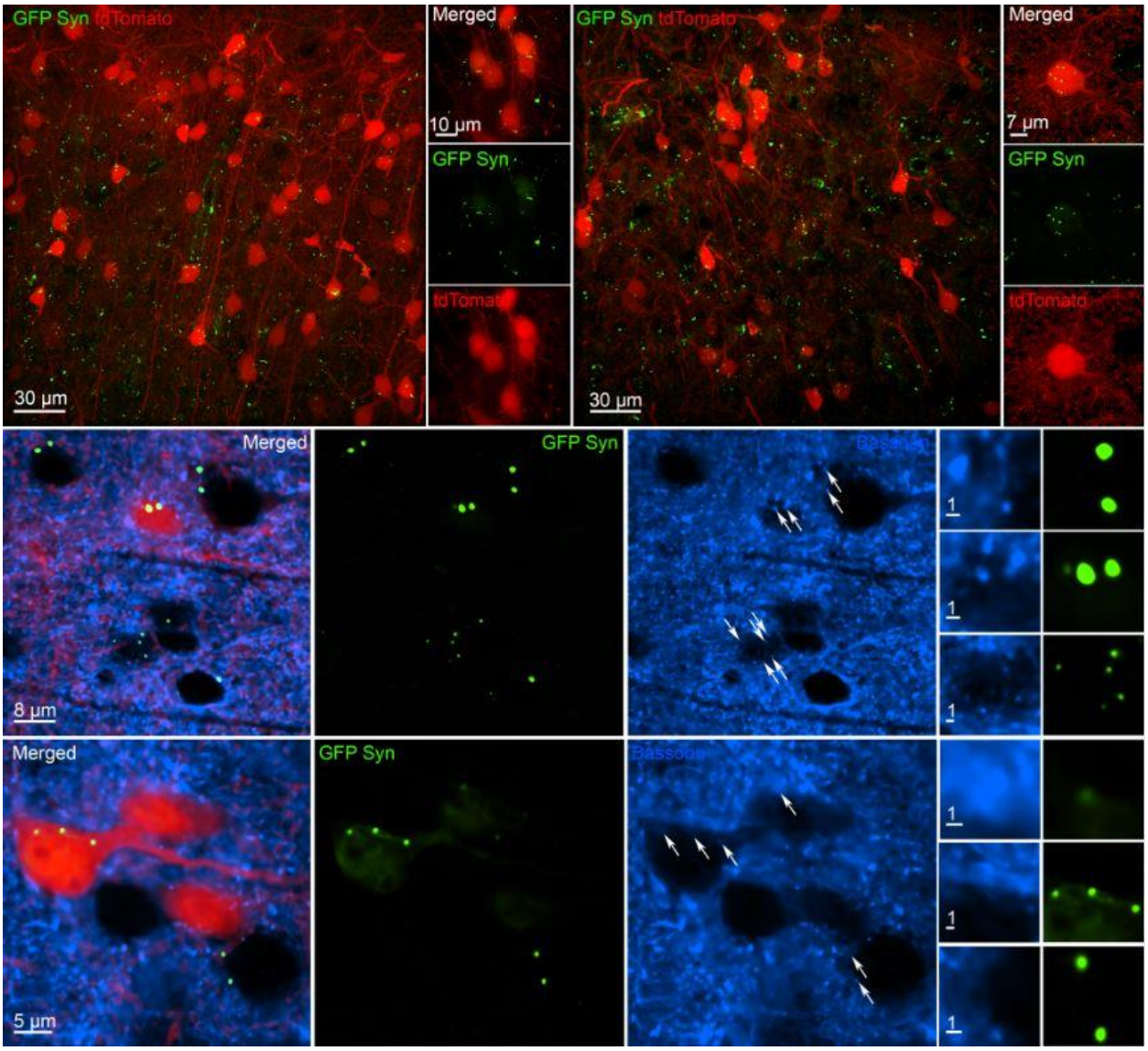
GFP Syn tdTomato
Merged
10 µm
GFP Syn
tdTomato
30 µm
GFP Syn tdTomato
Merged
7 µm
GFP Syn
tdTomato
30 µm
Merged
GFP Syn
Bassoon
8 µm
1
1
1
Merged
GFP Syn
Bassoon
5 µm
1
1
1

Figure 6-5

DISCUSSION

We find stronger activation of the superficial layers compared to deep during focal motor to bilateral tonic-clonic seizures. Our findings are consistent with recent studies that show that superficial layers are recruited ahead of the deep layers. However, previous studies used two-photon microscopy that images only through a small window[2], and dual patch clamp recordings have limitations as well[1]. We recorded LFPs from superficial and deep layers in awake mice during spontaneous seizures from the motor to parietal cortex, showing, for the first time, long-range cortico-cortical seizure spread through the layers.

Seizures spread faster to posterior superficial layers from the seizure focus and arrived to posterior deep layers with a delay. Yuste and colleagues also found similar temporal variation during ictal network recruitment locally in acute seizures and concluded that ictal progression is determined by interneuron activity. However, in our recent studies quantifying PV interneuron activation from anterior to posterior cortex after secondarily generalized seizures we did not find stronger PV activation posteriorly (cite PV paper). In fact, more PV interneurons were active closer to the seizure focus.

We discovered stronger AAV9 GFP labeling of posterior superficial layers and weak sparse dendritic labeling of deep layers. We found similar results using Cre-driven AAV9 GFP virus. Thus, superficial posterior layers receive more direct projections from the seizure focus compared to posterior deep layers, which could be due to IT-type neurons in layers 2/3 having more direct intracortical projections than deep layers that project subcortically. Thus, more synapses are necessary to reach posterior deep layers, which increases the chance of synaptic propagation failures. This further supports that direct connectivity of the seizure focus drives seizure spread, and neurons that are synaptically stronger connected to the seizure focus are more likely to be activated during a seizure.

REFERENCES FOR CHAPTER 6

1. Weiler N, Wood L, Yu J, et al. Top-down laminar organization of the excitatory network in motor cortex. Nat Neurosci. 2008; 11(3):360–6.
2. Wenzel M, Hamm JP, Peterka DS, et al. Reliable and Elastic Propagation of Cortical Seizures In Vivo. Cell Rep. 2017; 19(13):2681–93.
3. Krook-Magnuson E, Armstrong C, Bui A, et al. In vivo evaluation of the dentate gate theory in epilepsy. J Physiol. 2015; 593(10):2379–88.
4. Schevon CA, Weiss SA, McKhann G, et al. Evidence of an inhibitory restraint of seizure activity in humans. Nat Commun. 2012; 3.
5. Rossi LF, Wykes RC, Kullmann DM, et al. Focal cortical seizures start as standing waves and propagate respecting homotopic connectivity. Nat Commun. 2017; 8(1).
6. Brodovskaya A, Shiono S, Kapur J. Activation of the basal ganglia and indirect pathway neurons during frontal lobe seizures. Brain. 2021; .
7. Yamawaki N, Shepherd GMG. Systems/Circuits Synaptic Circuit Organization of Motor Corticothalamic Neurons. 2015; .
8. Connors BW. Initiation of synchronized neuronal bursting in neocortex. Nature. 1984; 310(5979):685–7.
9. Telfeian AE, Connors BW. Layer-specific pathways for the horizontal propagation of epileptiform discharges in neocortex. Epilepsia. 1998; 39(7):700–8.
10. Fame RM, Macdonald JL, Macklis JD. Development, Specification, and Diversity of Callosal Projection Neurons.
11. Choi J-H, Yu N-K, Baek G-C, et al. Optimization of AAV expression cossettes to improve packaging capacity and transgene expression in neurons. Mol Brain. 2014; 7(17).
12. Guenthner CJ, Miyamichi K, Yang HH, et al. Permanent genetic access to transiently active neurons via TRAP: Targeted Recombination in Active Populations. Neuron. 2013; 78(5):773–84.
13. Allen WE, DeNardo LA, Chen MZ, et al. Thirst-associated preoptic neurons encode an aversive motivational drive. Science. 2017; 357(6356):1149–55.

14. Zingg B, Chou X-L, Zhang Z-G, et al. AAV-mediated anterograde transsynaptic tagging: mapping corticocollicular input-defined neural pathways for defense behaviors. Neuron. 2017; 93(1):33–47.

CHAPTER 7

DISCUSSION

DISCUSSION

The findings of this dissertation support the main hypothesis that anatomical connections of the seizure focus and properties of excitatory neurons determine seizure circuits. Ephaptic connectivity and calcium waves through glia are the alternative hypotheses to explain long-distance communication in the brain. Our studies support that seizure spread can be predicted by direct connectivity.

We show, for the first time, a neuronal activation map of the basal ganglia during frontal lobe focal motor to bilateral seizures with unprecedented spatial resolution. We show activation of the striatum, globus pallidus externus, subthalamic nucleus, and substantia nigra pars reticulata. Seizures preferentially activate the indirect pathway over direct because D2 neurons are more excitable than D1 receptor-expressing neurons (1,2).

D2R agonists are anticonvulsants in limbic seizures, but their effectiveness in frontal lobe seizures was not tested (3,4). We show that direct infusion of D2 agonist into the striatum is anticonvulsant in frontal lobe seizures. We also show that systemic D2 agonist injection is anticonvulsant as well. D2 agonist activates parvalbumin interneurons in the cortex and striatum ipsilateral to the seizure focus, which could potentially explain the anticonvulsant effect of D2 agonists.

The thalamus is thought to be essential for seizure maintenance and spread to the contralateral hemisphere (5-7). Previous studies indicate that it is a choke point (8). However, seizure spread from the seizure focus to the contralateral cortex has not been directly traced. In some famous illustrations, seizures spread from the seizure focus to the contralateral cortex via commissural connections between two thalami (5,6,9) or through the bilateral thalamus via the brainstem (10-13). We show that seizures utilize the corpus callosum to spread contralaterally, whereas the thalamus amplifies frontal lobe seizures.

We also show for the first time long-range seizure propagation through the cortical layers during spontaneous seizures. We find that superficial layers are activated more and faster compared to deep layers throughout the whole cortex. Our findings support previous studies that superficial layers are activated ahead of the deep layers, which has been shown locally during acute seizures or in vitro (14,15). We also show

that activated cells in the parietal cortex receive direct synaptic projections from the seizure focus; however, not all cells that receive direct projections become activated, suggesting that these cells could be electrophysiologically different to begin with compared to activated cells, which further supports the hypothesis that properties of neurons also determine seizure spread.

In this dissertation, frontal lobe seizure circuits were mapped subcortically, contralaterally, and intracortically. Surprisingly, inhibition of the ipsilateral thalamus did not stop seizures. Although anterior callosotomy prevented contralateral seizure spread during initial seizures, as an animal experienced more seizures, new network formation occurred that still allowed seizures to spread contralaterally, so surgery alone would probably not be effective in achieving seizure freedom. Indeed, it has been shown that a combination of surgery with antiepileptic drug (AED) therapy was more effective to improve the outcome of refractory seizures than surgery and discontinuation of AEDs (17). The main hypothesis of this dissertation could have a direct clinical impact on pre-surgical mapping, surgical planning, and therapies. For example, a recent study shows that patients with refractory focal motor seizures significantly benefit from subthalamic nucleus stimulation (16). Therefore, it is very important to precisely map seizure circuits for more effective surgical interventions or neuromodulation.

REFERENCES FOR DISCUSSION

1. Gertler TS, Chan CS, Surmeier DJ. Dichotomous anatomical properties of adult striatal medium spiny neurons. J Neurosci. 2008; 28(43):10814–24.
2. Kreitzer AC, Malenka RC. Endocannabinoid-mediated rescue of striatal LTD and motor deficits in Parkinson's disease models. Nature. 2007; 445(7128):643–7.
3. Turski L, Cavalheiro EA, Bortolotto ZA, et al. Dopamine-sensitive anticonvulsant site in the rat striatum. J Neurosci. 1988; 8(11):4027–37.
4. Wahnschaffe U, Löscher W. Anticonvulsant effects of ipsilateral but not contralateral microinjections of the dopamine D2 agonist LY 171555 into the nucleus accumbens of amygdala-kindled rats. Brain Res. 1991; 553(2):181–7.
5. Westbrook GL. Seizures and epilepsy. In: Kandel ER, Schwartz JH, Jessell TM, et al., editors. Principles of neural science. New York: McGraw-Hill; 2013. p. 1116–39.
6. Englot DJ, Morgan VL, Chang C. Impaired vigilance networks in temporal lobe epilepsy: Mechanisms and clinical implications. Epilepsia. 2020; 61(2):189–202.
7. Paz JT, Davidson TJ, Frechette ES, et al. Closed-loop optogenetic control of thalamus as a new tool to interrupt seizures after cortical injury. Nat Neurosci. 2013; 16(1):64–70.
8. Paz JT, Huguenard JR. Microcircuits and their interactions in epilepsy: Is the focus out of focus? Nat Neurosci. 2015; 18(3):351–9.
9. Lothman EW, Collins RC. Kainic acid induced limbic seizures: metabolic, behavioral, electroencephalographic and neuropathological correlates. Brain Res. 1981; 218(1–2):299–318.
10. Blumenfeld H, Varghese GI, Purcaro MJ, et al. Cortical and subcortical networks in human secondarily generalized tonic-clonic seizures. Brain. 2009; 132:999–1012.
11. Penfield W, Jasper HH. Epilepsy and the functional anatomy of the human brain. Boston: Little, Brown; 1954. 896 p.
12. Faingold CL, Penfield J. Brainstem Networks Reticulo-Cortical Synchronization in Generalized Convulsive Seizures. 2012.
13. Iadarola MJ, Gale K. Substantia nigra: site of anticonvulsant activity mediated by

γ-aminobutyric acid. Science. 1982; 218(4578):1237–40.

14. Weiler N, Wood L, Yu J, et al. Top-down laminar organization of the excitatory network in motor cortex. Nat Neurosci. 2008; 11(3):360–6.
15. Wenzel M, Hamm JP, Peterka DS, et al. Reliable and Elastic Propagation of Cortical Seizures In Vivo. Cell Rep. 2017; 19(13):2681–93.
16. Ren L, Yu T, Wang D, et al. Subthalamic Nucleus Stimulation Modulates Motor Epileptic Activity in Humans. Ann Neurol. 2020; 88(2):283–96.
17. Schiller Y, Cascino GD, So EL, et al. Discontinuation of antiepileptic drugs after successful epilepsy surgery. Neurology. 2000; 54(2):346–9.